Title

Looking for the Minimal Recipe for Spontaneous TC Genesis

Author

Ramirez Reyes, Argel

Publication Date

2023

Peer reviewed|Thesis/dissertation

Looking for the Minimal Recipe for Spontaneous TC Genesis

By

Argel Ramírez Reyes
DISSERTATION

Submitted in partial satisfaction of the requirements for the degree of

DOCTOR OF PHILOSOPHY

in

Atmospheric Science

in the

OFFICE OF GRADUATE STUDIES

of the

UNIVERSITY OF CALIFORNIA

DAVIS

Approved:

Da Yang, Chair

Shu-Hua Chen

Christopher Davis

Committee in Charge

2023

Contents

Abstract

Tropical cyclones (TCs) are among the world's most intense and feared storms. What physical processes lead to cyclogenesis remains the most mysterious aspect of TC physics. Uncertainties in understanding and forecast of TCs hinders effective planning and risk mitigation by society. This work explores the processes that organize random convection into a TC in Rotating Radiative-Convective Equilibrium (RRCE) simulations to try and gain insight into the processes that turn a pre-existing disturbance into a TC on Earth..

We first study spontaneous TC genesis in RRCE using cloud-resolving simulations over an f plane with constant sea surface temperature. Previous studies proposed that spontaneous TC genesis requires either radiative or surface-flux feedbacks. To test this hypothesis, we perform mechanism-denial experiments, switching off both feedback processes in numerical simulations. We find that TCs can self-emerge even without radiative and surface-flux feedbacks. Although these feedbacks accelerate the genesis and impact the size of the TCs, TCs in the experiments without them can reach similar intensities as those in the control experiment. We show that TC genesis is associated with increased available potential energy (APE) and that convective heating dominates APE production. Our result suggests that spontaneous TC genesis may result from a cooperative interaction between convection and circulation and that radiative and surface-flux feedbacks accelerate the process. Furthermore, we find that increasing the planetary rotation favors spontaneous TC genesis.

Second, we ask, why is TC genesis possible without radiative and surface-flux feedbacks? Thirteen 3D cloud-resolving simulations show that the moisture-convection (MC) feedback can effectively lead to spontaneous TC genesis and intensification without radiative and surface-flux feedbacks. In the MC feedback, a moister environment favors new deep convective events that further moisten the environment, leading to aggregation of deep convection. The impact of the MC feedback on TC genesis and intensification occurs in two distinct time scales: a short time scale set by detrainment moistening the environment (a few hours) and a long time scale (17 days) due to subsidence drying. The hours-long time scale of detrainment suggests that the MC feedback is an

efficient process relevant to TC genesis in the real world.

Finally, we implement a GPU-capable convective parameterization into a flexible high-performance shallow water model using open-source software tools. This system permits running economic simulations of convective systems with and without rotation with linear or non-linear dynamics. We show that this model is capable of reproducing features of organized convection in much more complex 3D models at a fraction of the cost. We further show that simple scaling arguments can predict some geometric characteristics of the organized steady state, showcasing the usefulness of simple models to improve our understanding of tropical convection.

Acknowledgments

I want to thank my therapist, Dr. Varinia Sánchez Ortiz, who has been by my side since the moment approaching my qualifying exam; my psychiatrist, Dr. René Claire (who has accompanied me since the first year of the COVID-19 pandemic) and Alejandra, my loving wife who has been by my side during all my Ph.D. process. They, together with, Héctor, Lucas, Seth, Alma, César, Raiza, and Bernie, together picked me up more times than I can count and helped me see how much I had learned and discovered at every step of this Ph.D. journey. Theirs were the voices telling me, "I am sure you can do this".

I thank the people of México whose taxes helped pay for my education from kindergarten until this post-graduate adventure.

The work presented in this dissertation was mainly funded by the Consejo Nacional de Ciencia y Tecnología de México (CONACYT) and the University of California Institute for Mexico and the United States (UC Mexus). My studies also received resources from the Atmospheric Science Graduate Group at UC Davis, the UC Davis Fellowship for continuing graduate students, and the International Centre for Theoretical Physics and the Earth Cube RCN in the form of travel awards. In addition, I worked with resources from the Lawrence Berkeley National Laboratory, the Department of Energy's National Energy Research Supercomputing Center (NERSC), and UCAR's Cheyenne Supercomputer.

List of Figures

List of Tables

Chapter 1 Introduction

1.1 Some open questions in TC research

A tropical cyclone(TC) is a warm-cored, cyclonically rotating vortex driven by moist convection. TCs usually form over tropical oceans. Despite decades of physically-based TC research, some basic questions remain unanswered. For example, what sets Earth's nearly constant emergence rate of 80 TCs per year? What sets the intensification rate of TCs? (Emanuel, 2018) and their counterparts concerned with the future climate: how will the frequency of TCs change in the future climate? (Lee et al., 2020). The uncertainty regarding these questions hinders effective planning by society because quantities like frequency and intensification rate are directly linked to societal risk (Sobel et al., 2021). Therefore, looking for the answers to these questions in the current climate is fundamental to building confidence about how these features may change.

It is natural to ask: why has the scientific community not yet answered these questions? The answer is that TCs are very complex phenomena. They comprise interactions between dynamics and thermodynamics across widely varying spatial and temporal scales. For example, a typical TC has a diameter of around 500 km. Still, its energetics and impacts cannot be understood without considering individual thunderstorms of a horizontal extent of merely tens of kilometers. In short, this complexity hinders our understanding. This chapter briefly describes a TC and introduces its basic elements in section 1.2. We then discuss in section 1.3 what, in the eyes of the author, are the essence of the two perspectives used when trying to understand TCs (comprehensive vs. simplified modeling). We will then introduce the current research and the modeling framework in which this dissertation is embedded (sections 1.4,1.5), and finally, in section 1.6, we will introduce the structure of the dissertation.

1.2 Brief introduction to TCs

A TC is a storm system in the form of a warm-cored, cyclonically rotating vortex driven by moist convection. Viewed from above, it has a typical extent of $\sim \mathbf{O}(500km)$. At maturity, an intense TC is characterized by the strongest cyclonic winds near the surface and the eyewall, which is a ring of very strong upward motion surrounding the eye (a region of quiescent winds). Seen as a cross-section that cuts a TC on the middle, the lower levels are characterized by entropy-rich air flowing inward toward the eyewall. This air interacts with the warm ocean surface, which transfers energy to the inflow. The inflow reaches the eyewall and ascends while nearly conserving its moist entropy. After ascending, air exits the cyclone in the upper troposphere. Tropical cyclones often emerge over the tropical oceans, where the water is warm, but not over the equator, where the Coriolis parameter is null. The regions where TCs typically appear are classified into basins (e.g., the North Atlantic or the East Pacific basin), with each basin having a strong seasonality. The pioneering work of Gray (1968) identified some conditions that appear necessary for the genesis (or emergence) of a TC, summarized as follows by Klotzbach et al. (2017):

1. cyclonic low-level vorticity (from a preexisting easterly wave, the monsoon trough, or an upper-level low/frontal boundary),
2. moist mid-troposphere,
3. conditional instability through a deep tropospheric layer,
4. warm and deep oceanic mixed layer,
5. weak tropospheric vertical shear of the horizontal wind, and
6. location of disturbance a few degrees poleward of the equator (i.e., a significant value of Coriolis force).

This list has been refined, but it continues to be relevant nowadays, and it gives the main ingredients used to predict the frequency of TCs by statistical methods (Lee et al., 2020; Sobel

et al., 2021). Although statistical methods have succeeded at this task, their utility in explaining the causes of TC frequency is still unclear (Sobel et al., 2021). Therefore, in this work, we attack the genesis problem from a physical perspective.

1.3 Comprehensive vs simplified modeling

Increased computational power and modeling techniques have allowed the routinary use of increasingly comprehensive models of the atmosphere and its interactions with the ocean. This allows, for example, global atmospheric simulations at a resolution of a couple of kilometers for a short period (Satoh et al., 2019), allowing to partially resolve phenomena of the scale of a single convective storm. Although increasingly complex models may better represent some features of atmospheric phenomena as TCs, it is not clear that they alone can provide a physical understanding of these phenomena, nor will sufficiently long simulation periods become affordable soon. Additionally, high-resolution simulations produce massive amounts of data whose processing represents a technical problem by itself. Considering these points, it is desirable to explore simplified frameworks instead of increasingly complex ones to understand the fundamental mechanisms that govern TCs (Emanuel, 2020) and to help improve the models that guide public policy.

1.4 What sets the frequency of TCs?

We call the frequency of TCs how many TCs appear in a given region in a given time period. For example, the number of TCs that occur yearly over the whole Earth. In the current climate, this number is around 80 (Schreck et al., 2014). This number appears to be very stable since the satellite era. However, there is no current theoretical understanding of what sets this number or why it is stable. Among the possible explanations for the frequency of TCs, it would be desirable to find that this number is set by a combination of current climate parameters (e.g., the solar constant, the Earth's rotation rate). A successful scaling theory in this regard would explain why the number does not appear to vary greatly year by year. However, there is not yet a satisfactory proposal for the parameters that set this number, and there are arguments about why this combination may not exist. For example, global climate models cannot reproduce the current climatology of TCs

without tuning certain non-physical parameters (e.g., Zarzycki, 2022; Zhao et al., 2012). However, quantities that depend on simple scaling laws of global climate parameters are robust to this kind of modeling choice. Also, simple theories that constrain the behavior of some features of the climate system rely on the importance of these features on global-scale budgets (for example, precipitation rate and its importance in the water vapor and latent heating of the atmosphere (Sobel et al., 2021)). On the other hand, TCs seem to play an unremarkable role in most global-scale climate characteristics.

Recent work has proposed that the rate of the genesis of TCs can be explained by the rate of emergence of "seeds", times the probability of the seeds becoming TCs (Hsieh et al., 2020). This seems consistent with the fact that most TCs are formed from a pre-existing disturbance (e.g., African easterly waves in the Atlantic), though most seeds do not become TCs. That result suggests that the rate of the genesis of TCs is linked with processes that set the frequencies of the preferred type of pre-existing disturbances. However, two modeling results seem to suggest that although pre-existing synoptic-scale disturbances may aid TC genesis, they are not essential in their formation. That is, the frequency of the pre-existing disturbance may not be essential to answering the frequency of TCs. The first of these results is that the climatology of TCs in the Atlantic is not significantly altered in a numerical simulation even after filtering out the African Easterly Waves of one TC season (Patricola et al., 2018). Secondly, a growing body of numerical studies has shown that TCs can spontaneously appear from random convection in idealized simulations of rotating radiative-convective equilibrium (RRCE, RCE is a balance between latent heating by convection and radiative cooling in the atmosphere. It approximately holds when considering large regions of the tropical atmosphere) (Carstens and Wing, 2020; Khairoutdinov and Emanuel, 2013; Muller and Romps, 2018; Nolan et al., 2007b; Ramírez Reyes and Yang, 2021; Wing et al., 2016). These results once more suggest that a pre-existing disturbance may be a shortcut to TC genesis in real life, but that its role may not be *essential* (Emanuel, 2018).

1.5 The rotating radiative-convective equilibrium framework

The RRCE framework has proven useful in explaining some features of TC genesis and intensification in several previous studies. For example, in investigating the factors that allow spontaneous TC genesis to occur, researchers highlighted the role of feedbacks between radiative cooling and moisture (Muller and Romps, 2018; Wing et al., 2016). This result was then measured in more realistic settings (Ruppert et al., 2020). These examples show that studying spontaneous TC genesis in RRCE is not merely a curiosity but that understanding the processes that dominate this phenomenon may have substantial applications to understanding TC genesis in real life.

In the RRCE setup, many of the complexities of the real atmosphere are avoided. For example, the enthalpy fluxes from the ocean to the atmosphere do not affect the sea-surface temperature, there is no large-scale background flow, nor are there synoptic-scale weather systems (e.g., African easterly waves) which are the main precursors for TC genesis in the Atlantic ocean (Montgomery, 2016; Tang et al., 2020). The fact that TCs nevertheless emerge results fascinating. It also presents an opportunity to explore the processes that help organize convection into a TC when an appropriate precursor is present in the atmosphere (Davis, 2015). In these simplified frameworks, the goal is not to propose a complete theory for TC genesis in the real world but to evaluate some of the processes that can help or accelerate TC genesis in real situations. Although TCs can self-emerge in RRCE simulations without the typical ingredients observed in the real atmosphere, an erroneous interpretation of these results would be that we would expect to see TCs appearing without the other ingredients. Instead, this framework can be used to evaluate and quantify some processes' contributions without the atmosphere's full complexity.

The overarching story of this work concerns the search for a simple recipe for the genesis of TCs. Looking for simplicity has two main goals: By removing parts from the complexity of the atmosphere and removing the variables at play, we expect to observe in closer detail some processes that in real Earth may contribute to genesis or intensification but whose role is completely obscured by the presence of other dominant processes. Additionally, a simple model which contains just a few variables may be a good candidate for analytical exploration that could yield simple scaling

laws that help clarify questions about the frequency or the role of TCs in climate.

1.6 Structure of this dissertation

In the rest of this document, we will exploit the RRCE framework to inquire into the fundamental behavior of convection and how it leads to its organization as a TC. In chapter 2, we explore whether radiative feedbacks and surface-flux feedbacks are essential for spontaneous TC genesis, and we find that spontaneous TC genesis can still occur without both feedbacks. In chapter 3, we show that when surface flux feedbacks and radiative feedbacks are absent, a feedback mechanism between environmental moisture and convection is necessary for spontaneous TC genesis. In chapter 4, we explore another flavor of minimal simulation: we build a 2D Shallow Water model with a parameterization of convection, and we show that when we run this model into an RCE state, convection can still self-aggregate when rotation is absent, but TCs do not form in a rotating setup. Finally, in chapter 5, we discuss the main results of this dissertation and how they contribute to our current understanding of TCs.

Chapter 2 Spontaneous TC genesis without radiative feedbacks and spatially varying surface fluxes

This chapter has been adapted from the peer-reviewed article:

Ramírez Reyes, A. and Yang, D.: Spontaneous Cyclogenesis without Radiative and Surface-Flux Feedbacks, Journal of the Atmospheric Sciences, 78, 4169–4184, doi: 10.1175/JAS-D-21-0098.1, 2021.

Abstract

Tropical cyclones (TCs) are among the most intense and feared storms in the world. What physical processes lead to cyclogenesis remains the most mysterious aspect of TC physics. Here, we study spontaneous TC genesis in rotating radiative–convective equilibrium using cloud-resolving simulations over an f plane with constant sea surface temperature. Previous studies proposed that spontaneous TC genesis requires either radiative or local surface-flux feedbacks, in which the spatial structure of energy fluxes promotes the organization of convection. To test this hypothesis, we perform mechanism-denial experiments, in which we remove the spatial structure of radiative and surface enthalpy fluxes in numerical simulations, thereby removing both "local feedbacks". We find that TCs can self-emerge even without radiative and local surface-flux feedbacks. Although these feedbacks accelerate the genesis and impact the size of the TCs, TCs in the experiments without them can reach similar intensities as those in the control experiment. We show that TC genesis is associated with an increase in the available potential energy (APE) and that convective heating dominates the APE production. Our result suggests that spontaneous TC genesis may result from a cooperative interaction between convection and circulation and that radiative and local surface-

flux feedbacks accelerate the process. Furthermore, we find that increasing the planetary rotation favors spontaneous TC genesis.

2.1 Introduction

A tropical cyclone (TC) is a rapidly cyclonically rotating storm system that typically forms over a tropical ocean. It is often characterized by a center of anomalously low surface pressure, a closed low-level atmospheric circulation, a warm core, and a spiral arrangement of thunderstorms. TCs are among the most intense and feared storms of the world, with torrential rains that can last for 0 (1 week) and destructive winds that span over O(500 km). Despite extensive theoretical developments and the ever-advancing observing capabilities, TC genesis remains the most mysterious aspect of TC physics (see (Emanuel, 2018)).

Observational studies suggested that TCs often form from a pre-existing mid-level cyclonic vortex (Bartels and Maddox, 1991; Davidson et al., 1990; Laing and Fritsch, 1993; McBride and Zehr, 1981; Velasco and Fritsch, 2012). Recent studies observed that a closed "pouch" associated with a tropical wave protects a region of deep convection from the intrusion of dry air, favoring the formation of a surface-concentrated vortex that then intensifies to a TC (Dunkerton et al., 2009; Raymond and López Carrillo, 2011; Smith et al., 2015; Wang, 2012; Wang et al., 2010). Although these studies have provided many insights, the high degree of complexity in the real atmosphere makes it difficult to distinguish what physical processes are essential to TC genesis. Here, idealized modeling studies are ideal complements to the observational studies.

Recent work has shown that TCs can spontaneously develop in rotating radiative-convective equilibrium (RRCE) simulations using both cloud-resolving models (CRMs) and general circulation models (GCMs) (Bretherton et al., 2005; Carstens and Wing, 2020; Chavas and Emanuel, 2014; Chavas and Reed, 2019; Davis, 2015; Held and Zhao, 2008; Khairoutdinov and Emanuel, 2013; Merlis and Held, 2019; Merlis et al., 2016; Muller and Romps, 2018; Nolan et al., 2007b; Reed and Chavas, 2015; Shi and Bretherton, 2014; Wing et al., 2016; Zhou et al., 2013). These studies suggest that initial disturbances may help TC genesis in the real atmosphere, but they are not essential.

Spontaneous TC genesis is considered as f-plane convective self-aggregation. Convective self-

aggregation is a phenomenon in which large-scale circulations and convective organization can self-emerge over uniform sea-surface temperatures (SSTs) and boundary conditions (Arnold and Randall, 2015; Bretherton et al., 2005; Muller and Held, 2012; Wing et al., 2018; Yang, 2018a,b). This process is associated with increasing variance of moist static energy (MSE, an approximation for the total energy contained in a moist air parcel), and increasing eddy available potential energy (APE, defined in section subsection 2.2.5). Wing et al. (2016) analyzed the MSE variance budget in spontaneous TC genesis and showed that radiative and surface flux feedbacks help increase MSE variance, consistent with non-rotating self-aggregation processes. In addition, the authors removed the radiative feedback by horizontally homogenizing radiative cooling rates and confirmed the results of Frisius (Frisius, 2006), who showed that spontaneous TC genesis was delayed in these conditions. Muller and Romps (2018) further showed that removing local surface-flux feedbacks significantly delays TC genesis and reduces the TC strength at the mature stage. These mechanism-denial experiments are consistent with the MSE analysis, showing that radiative and local surface-flux feedbacks contribute to increase MSE variance, favoring TC genesis. As the MSE variance increase is associated with radiative and local surface-flux feedbacks, the MSE analyses seem to suggest that spontaneous TC genesis would not occur in the absence of radiative and local surface-flux feedbacks. However, as MSE is approximately conserved for an undiluted air parcel undergoing moist adiabatic processes (Romps, 2015), the MSE analysis does not explicitly show the role of convective heating.

Evaporation of water from the ocean surface constitutes the most important source of energy for TCs (Emanuel, 2003, 2018). This energy, later released by condensation of water vapor, is key to TC development and maintenance: Convective heating can generate APE, which can subsequently convert to kinetic energy, providing energy for TC genesis and maintenance (Nolan et al., 2007a). Generation of APE is also associated with the development of a warm core, which is necessary to sustain the vortex in hydrostatic and gradient wind balances. Although an APE-centric framework has been widely used to understand convectively coupled tropical circulations (including non-rotating convective self-aggregation and TC genesis in axisymmetric models) (Anthes and Johnson, 1968; Emanuel et al., 1994; Kuang, 2008; Nolan et al., 2007a; Veiga et al., 2008;

Wong et al., 2016; Yang, 2018a), it has not been applied to understand spontaneous TC genesis. In contrast to MSE, increases in APE are led by APE production due to convection, radiation, and surface fluxes (e.g., Yang 2018a). Therefore, an analysis of the APE highlights the role of convection, complementing the MSE analysis.

In this paper, we combine the analysis of APE with mechanism-denial CRM simulations to address the question of what processes contribute to the spontaneous TC genesis, and what is the minimum recipe. This study aims to extend our understanding of spontaneous TC genesis, moist convection, and convective organization by expanding the parameter space used in previous studies to attack the question of whether convection can or cannot aggregate in the form of a TC without the action of radiative and local surface-flux feedbacks, which depend on the spatial structure of energy fluxes. This study is also relevant to the study of planetary atmospheres in which a larger parameter space of rotation rates can be expected. We describe our research methods in section section 2.2, present simulation results in section section 2.3, and expose the APE analysis in Section 2.2.5. In section 2.2.4 we show the sensitivity of our results to changes of the Coriolis parameter, resolution, initial conditions, temperature and parametrizations of radiation and microphysics. We conclude and discuss the implications of our findings in Section 2.6.

2.2 Methods

2.2.1 Available potential energy

APE is the amount of gravitational potential energy that can be transformed into kinetic energy by lowering the center of mass of the atmosphere (Vallis, 2017). APE is, therefore, an energy reservoir for atmospheric circulations (Lorenz, 1955). APE can be computed as the difference between the potential energy in the fluid and the minimum potential energy possible for the same system after an adiabatic rearrangement of mass. In a dry APE framework (one that externalizes convective heating), the APE of an anelastic atmosphere is given by (Yang, 2018a)

$$APE = \frac{1}{2}\int_0^z \rho_0(z')\frac{\bar{b^2}(z')}{N^2(z')}dz' \tag{2.1}$$

where $b = b(x, y, z, t)$ is buoyancy, $\rho_0(z)$ represents the reference density, $N^2(z) = g\frac{1}{\overline{\theta_v}}\frac{\partial\overline{\theta_v}(z)}{\partial z}$ is the Brunt-Väisälä frequency squared (a measure of stratification), z denotes the vertical coordinate, $\theta_v = T(1+\epsilon q)(\frac{p_0}{p})^{\left(\frac{R_d}{c_{pd}}\right)}$ is the virtual potential temperature where T is the temperature, q the specific humidity, p_0 and p are pressure and reference pressures, R_d and c_{pd} are the gas constant and specific heat capacity at constant pressure for dry air, respectively, and $\epsilon = \frac{M_{air}}{M_{water}} - 1 = 0.61$. In here and in the following, the horizontal bar represents horizontal averaging over the region considered, and a prime denotes departures from said average.

To obtain an evolution equation for the APE, we consider the buoyancy equation

$$b = g\frac{\theta_v'}{\overline{\theta_v}} \tag{2.2}$$

$$\partial_t b + u\partial_x b + v\partial_y b + wN^2 = S_b \tag{2.3}$$

where t is time, u, v, and w are the components of the velocity vector, b is the buoyancy computed in a moist atmosphere (Emanuel, 1994), and S_b represents buoyancy sources, including convective heating, radiative cooling, and surface fluxes. Equation (2.2) differs from SAM's formulation of buoyancy in that it does not consider the effect of condensate loading. However, this widely used approximation should not impact the computation of the slow-varying component of APE. Using (2.1), (2.2), and (2.3), Yang (2018a) obtained an evolution equation for the slowly varying component of the APE:

$$\overbrace{\frac{1}{2}\int_0^z \frac{\rho_0}{N^2}\partial_t\overline{\tilde{b}^2}dz'}^{\partial_t\widetilde{APE}} = \overbrace{\int_0^z \frac{\rho_0}{N^2}\overline{\tilde{b}\tilde{S}_b}dz'}^{Production} - \overbrace{\int_0^z \frac{\rho_0}{N^2}\left(\overline{\tilde{b}u\widetilde{\partial_x b}} + \overline{\tilde{b}v\widetilde{\partial_y b}}\right)dz'}^{Advection} - \overbrace{\int_0^z \rho_0\overline{\tilde{b}\tilde{w}}dz'}^{Conversion}, \tag{2.4}$$

where the first term on the right-hand side is the APE production term, the second and third are the advection terms, and the last term is the conversion to kinetic energy. The tilde represents the slow-varying component. We focus our study on the slow-varying component of APE, which we expect to be associated with TCs. According to Yang (2018a), buoyancy sources are computed by

$$S_b = g\frac{S_\theta}{\overline{\theta}} + g\frac{\epsilon S_q}{1+\epsilon\overline{q}} \tag{2.5}$$

where θ is potential temperature, q is specific humidity, g is the acceleration of gravity, S_q and S_θ are sources of humidity and heating, respectively. It is important to note from (2.4) that the production of APE and growth of its associated circulations occurs when the product bS_b is positive (when buoyancy and buoyancy sources are positively correlated); when the product is negative, APE is reduced and its associated circulations decay (Emanuel et al., 1994; Yang, 2018a). Because anomalies in convective heating, surface heat fluxes, and radiative heating are buoyancy sources, they contribute to the APE production.

2.2.2 Model and experiment setup

We perform rotating RCE simulations over an f-plane using the System for Atmospheric Modeling, SAM, version 6.10.10 (Khairoutdinov and Randall, 2003). SAM solves the anelastic system of equations and prognoses liquid water and ice moist static energy, total nonprecipitating water (vapor + cloud water + cloud ice), and total precipitating water (rain + snow + graupel). SAM has been widely used to study tropical convection (e.g (Bretherton et al., 2005; Khairoutdinov and Emanuel, 2013; Muller and Held, 2012; Wing et al., 2016; Yang, 2018a)). The radiation scheme is that of the Community Atmosphere Model 3 (Collins et al., 2004), which computes long-wave and the short-wave radiative heating rate at each level of each column every 15 time steps; the sub grid-scale scheme is the SAM Smagorinsky scheme, which is the stationary version of a prognostic scheme based on turbulent kinetic energy, the implementation of which is described in (Deardorff, 1980); and the microphysics scheme is the SAM single-moment microphysics (Khairoutdinov and Randall, 2003), which computes the sum of nonprecipitating liquid and ice water and water vapor mixing ratio and the total precipitation mixing ratio. The surface fluxes are computed with bulk formulae with exchange coefficients computed using the Monin-Obukhov theory, with code adapted from NCAR's Community Climate Model 3 (Kiehl et al., 1996). SAM does not have a parameterization scheme for the boundary layer.

The main four experiments are summarized in Table 2.1. They have a shared configuration consisting of a doubly periodic horizontal domain of 1024 km $\times$ 1024 km with a horizontal grid spacing of 2 km. The vertical domain has an extension of 34.8 km, and the vertical grid-spacing

is 50 m from $z = 0$ m to $z = 1050$ m, and then it increases gradually until it reaches 600 m at $z = 3000$ m. The integration timestep is 10 s but decreases when needed to prevent numerical instabilities. The simulations are run for 100 days, starting with an RCE profile produced as the mean potential temperature and humidity sounding from the last 20 days of a smaller 2D simulation. The sounding profiles are the same as those used in (Yang, 2018a). We save 3D variables every two hours and 2D variables every hour. Following (Khairoutdinov and Emanuel, 2013), we use a constant Coriolis parameter $f = 4.97 \times 10^{-4}\mathrm{s}^{-1}$. This value corresponds to 10 times the Coriolis parameter at 20 ° latitude. The large f helps shrink the horizontal scale of TCs and allows us to simulate TCs in a small domain. Although intuitively, a higher Coriolis parameter would also accelerate the TC genesis process (e.g., by increasing vorticity due to stretching), previous studies have not found a robust relation between time to genesis and rotation rate in f-plane simulations (Carstens and Wing, 2020; Nolan et al., 2007b), thus we don't expect this choice to have a leading order impact in the time to genesis in our simulations. Similar values have been used in other studies of spontaneous TC genesis (Chavas and Emanuel, 2014; Cronin and Chavas, 2019). The choices of *f*, domain size and resolution stem from a necessary compromise: using a realistic value of f with 2-km grid-spacing would require a much larger domain that becomes computationally prohibitive. On the other hand, a grid spacing of 2 km is desirable to have a good representation of some aspects of convection, for example, in-cloud downdrafts and updrafts and mid-troposphere entrainment (Nolan et al., 2007b). For consistency with previous studies of non-rotating convective aggregation in RCE using doubly periodic domains (Jeevanjee and Romps, 2013; Muller and Held, 2012; Yang, 2018a), the horizontally averaged wind speed is nudged to zero at all levels with a timescale of two hours. This prevents the emergence of wind shear, which in a rotating setup adds complexity to the study of TC formation (Nolan et al., 2007b). However, nudging the wind speed does not strongly affect our results (see Appendix 2.6). The sea surface temperature is held at 300 K. The diurnal cycle is turned off, and the solar insolation is a constant set to 685 W m^{-2}, with a solar zenith angle of 51.7 degrees, similar to the value used in (Tompkins and Craig, 1998). The model has a rigid lid, but SAM applies Newtonian damping to all the prognostic variables in the upper third of the domain to prevent gravity wave reflection.

2.2.3 Mechanism-denial experiments: turning off local feedbacks

Name	Feedbacks removed	Grid size	Domain size	Simulation length
Control	None	$512 \times 512 \times 80$	1000km $\times$ 1000km $\times$ 34.8km	100 days
HomoSfc	local surface-flux feedbacks removed	$512 \times 512 \times 80$	1000km $\times$ 1000km $\times$ 34.8km	100 days
HomoRad	Radiative feedbacks removed	$512 \times 512 \times 80$	1000km $\times$ 1000km $\times$ 34.8km	100 days
HomoAll	Radiative and local surface-flux feedbacks removed	$512 \times 512 \times 80$	1000km $\times$ 1000km $\times$ 34.8km	100 days

Table 2.1: Summary of simulation parameters in the mechanism-denial experiments.

We perform mechanism-denial experiments to investigate the sensitivity of TC genesis to the radiative and local surface-flux feedbacks. The radiation-moisture feedback appears when the atmosphere is organized in moist, convecting regions and dry, subsiding regions. In this case, radiative cooling leads to subsidence in the dry area, which promotes more radiative cooling and further dries the atmosphere. To disable this feedback, we follow Muller and Romps (Muller and Romps, 2018) in substituting the radiative cooling rate at each grid point with its horizontal average, as commonly done in similar studies of spontaneous TC genesis (Wing et al., 2016) and convective self-aggregation (Bretherton et al., 2005; Yang, 2018a). Substituting radiative fluxes by their horizontal mean removes horizontal radiative heating anomalies, so radiation cannot contribute to the generation of APE, effectively removing the feedback.

The local surface-flux feedbacks comprise two competing effects. The buoyancy fluxes from the sea-surface to the atmosphere depend on wind speed and sea-air differences in moisture and temperature through the latent and sensible heat fluxes. For example, the latent heat fluxes are computed as $LHF = \rho C_E L_v U \left(q^*_{T_s} - q_v\right)$, where ρ is the density of the air, C_E, an exchange coefficient, L_v, the latent heat of vaporization of water, U the air wind speed near the surface, and $q^*_{T_s}$, q_v, the saturation specific humidity and specific humidity, respectively. On a given location, an enhanced wind speed near the surface promotes moisture fluxes to the atmosphere, which in turn increases the overturning circulation and enhances surface wind speeds, closing the feedback loop. On the other hand, regions of enhanced air humidity have a decreased humidity difference. This acts to decrease the surface fluxes, weakening the convection and resulting in a negative feedback. A similar argument holds for the sensible heat flux, $SHF = \rho C_H C_p U \left(T_s - T_a\right)$ with C_p, C_H, T_s

and T_a are the dry air specific heat capacity at constant pressure, a transfer coefficient and the temperatures of the ocean surface and atmosphere, respectively. Following Muller and Romps (Muller and Romps, 2018), we remove the local surface-flux feedbacks by replacing the surface heat fluxes at each grid point with their horizontally averaged value, as in previous studies (Bretherton et al., 2005; Yang, 2018a). On a domain integrated sense, the homogenization of surface fluxes still allows the evolution of surface fluxes in response to increased winds and its corresponding influence in the convective activity. Therefore, it could be argued that "global surface-flux feedbacks" are still present. However, our main goal is to analyze the relation of the spatial structure of surface fluxes in the spatial distribution of convection. By destroying the spatial structure of surface fluxes, these "local" feedbacks are turned off. In this case, surface fluxes do not contribute to APE production.

We will present four sets of simulations: Control, where the interactive radiation and surface fluxes are not altered; HomoRad, where the radiative feedback is turned off; HomoSfc, where the local surface-flux feedbacks are removed, and HomoAll where both radiative and local surface-flux feedbacks are turned off (see Table 2.1).

2.2.4 Sensitivity experiments

We perform a suite of experiments to test the sensitivity of our results to changes in resolution, Coriolis parameter, initial conditions, sea-surface temperature and choices of radiation and microphysics schemes (Table 2.2). In the following we summarize the design of these sensitivity simulations, where we keep the domain and the rest of configurations unaltered with respect to the experiments in Table 2.1. a) Initial condition: We create two additional initial profiles that differ from each other and from the original sounding used to initialize the simulations of Table 2.1. Using these initial profiles, we run two 50-day simulations with each of the Control, HomoRad, HomoSfc and HomoAll configurations. To construct the two different initial conditions, we add random noise in the first five levels of the original potential temperature sounding, as done by Wing et al. (Wing et al., 2016). The temperature perturbation has an amplitude of 0.1 K in the first level and decreases linearly to 0.02K in the fifth level. b) Horizontal resolution: We perform a 30-day simulation with horizontal grid-spacing of 1 km in the HomoAll configuration to explore the sensitivity

of the results to changes in resolution. c) Coriolis parameter: We run 50-day simulations with $f = 3 \times 10^{-4}\text{s}^{-1}$ and $f = 1 \times 10^{-4}\text{s}^{-1}$ in the HomoAll configuration, respectively. d) Microphysics: We conduct a 50-day HomoAll simulation but with the Thomson microphysics scheme (Thompson et al., 2008) which is a one moment bulk parameterization that predicts the mixing ratios of cloud water, rain, cloud ice, snow and graupel, and also predicts the number concentration of cloud ice e) Radiation: We run a 50-day HomoAll simulation but with the RRTM radiation scheme (Mlawer et al., 1997).

	Parameter changed	Base configuration	Description of change	Simulation length
1	Sea surface temperature	HomoAll	297 K	50 days
2	Sea surface temperature	HomoAll	305 K	50 days
3	Initial conditions	Control, HomoSfc, HomoRad, and HomoAll	Changed initialization profile	50 days
4	Coriolis parameter	HomoAll	$f = 1 \times 10^{-4}\text{s}^{-1}$	50 days
5	Coriolis parameter	HomoAll	$f = 3 \times 10^{-4}\text{s}^{-1}$	50 days
6	Radiation scheme	HomoAll	Used RRTM radiation model	50 days
7	Microphysics scheme	HomoAll	Used Thompson microphysics scheme	50 days
8	Resolution	HomoAll	Grid spacing of 1 km	30 days

Table 2.2: Summary of simulation parameters in the sensitivity experiments.

2.2.5 APE computation and TC composite

We compute APE and APE budgets from Equations 2.1 - 2.4. Convective heating is not a standard output of SAM, which solves the conservation law of MSE. Therefore, to compute the contribution of convective heating to APE production, we diagnose convective heating from the buoyancy equation: we first calculate left-hand-side terms in (Equation 2.3); we then calculate convective heating as the residual of (Equation 2.3)—the left-hand-side terms minus radiative cooling and surface buoyancy fluxes. We compute the convective heating from the 3D output (every two hours) for the whole simulation. After computing convective heating, we have all the variables needed to compute APE and the APE budget using equation 2.4. Following Yang (2018a), to focus on the slow-varying component of APE evolution, we use a moving mean filter in the variables that enter the APE and

APE budget computation. The moving mean filter has a window size of 30km in the horizontal directions and 5 days in the time dimension, but other averaging windows show similar results.

To characterize basic TC features, we make an "average TC" using the last 50 days of each of the simulations shown in Table 2.1 (or 600 output times to match the bi-hourly frequency of the rest of the analysis, which uses 3D data). Similar to (Zhou et al., 2017), we identify TCs as the point of minimum surface pressure within regions of anomalously low surface pressure. We first find the departure of surface pressure from its horizontal mean ($P'_{sfc}(x,y,t) = P_{sfc}(x,y,t) - \overline{P_{sfc}}(t)$, where the overline denotes the horizontal mean). Because the scale of a tropical cyclone is of $\mathcal{O}$(500km), we smooth this pressure anomaly with a moving median filter to reduce the smaller scale features. We use a window size of 20 km for smoothing, and our results are robust over different choices of window sizes. We then identify contiguous regions of pressure anomaly less than -9 hPa. Next, we find the point of minimum pressure within this region, which we record as a TC. Identifying TC centers as a point of minimum pressure has been used in other studies (Reed and Chavas, 2015), so this method is adequate to build our composites. Having obtained the time and location of the TC centers (the minima of surface pressure perturbation), we then create the TC composite by aligning the centers of the identified TCs and taking the time average only over the time steps with identified TCs. This gives a composite of TC-associated variables, including surface pressure, surface winds, air temperature, and others. We then compute the azimuthal average of all the quantities in radial bins of 2km width starting at r=1km as done by (Cronin and Chavas, 2019). This process yields radial profiles of the characteristic features of the TC composite.

2.3 Results

TCs self-emerge in all four simulations. Movie S1 shows the time evolution of surface pressure and wind speed from a homogeneous state. Figure 2.1 shows contours of surface winds and surface pressure over a snapshot at day 70 for the Control, HomoRad, HomoSfc, and HomoAll experiments. All experiments simulate TC-like structures, featuring organized areas of low surface pressure ($<$ 990hPa to be noticeable in the Movie S1) and high wind speed ($>$ 10ms^{-1} to be noticeable in the Movie S1), with a clearly defined eye region in the center. In the Control simulation, regions of

enhanced wind speed and a center of low pressure occur after 7 days. By day 8, multiple centers of low pressure, and high wind speed have emerged. As time progresses, the low-pressure centers become centers of low wind speed surrounded by rapidly rotating wind, and a clear eye of low pressure surrounded by an eyewall of high wind speed is discernible by day 9. We consider at this point that TCs are developed. By day 15 we can observe up to 7 TCs in the domain with wind speeds as high as 50ms^{-1}. The multiple TCs merge. After 33 days, we can only observe three TCs, and only two TCs of greater horizontal extent exist from day 68 till the end of the simulation.

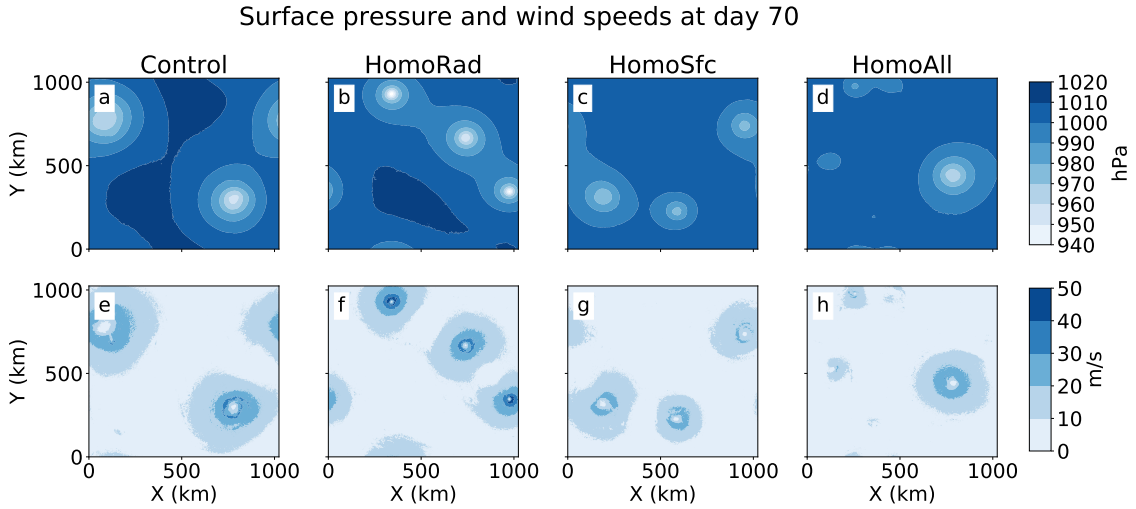

Figure 2.1: Map views of surface pressure and surface wind speed at t = 70 days (snapshot): contours of (top) surface pressure (hPa) and (bottom) surface wind speed (ms^{-1}) for the (a),(e) Control; (b),(f) HomoRad; (c),(g) HomoSfc; and (d),(h) HomoAll simulations with 2-km grid spacing.

In HomoRad, TC genesis is slower: the regions of enhanced wind speeds appear around day 10, and several clearly defined TCs are developed after 15 days. We observe up to 9 TCs coexisting in the same domain by day 16. Multiple TCs have merged by day 66, and only 3 TCs exist for the rest of the simulation. In HomoSfc, regions of low surface pressure appear by day 13, and one TC clearly formed by day 22. Notably, the closed region of maximum wind speed around the center is less well defined than in the previous two simulations, suggesting an important role of surface fluxes in maintaining the structure of the TCs. The genesis process is further delayed in HomoAll. The region of enhanced wind speeds can be first observed around day 22, and the first clearly defined

TC is developed by day 38. During the last 20 days of the simulation, two TCs coexist. They both have similar intensities, but one is notably smaller than the other.

TCs without radiative and local surface-flux feedbacks can reach the same intensity as those in the Control simulation. In Figure 2.1 and Movie S1, we observe TCs in all experiments, showing a similar intensity. Figure 2.2 shows the temporal evolution of maximum surface wind speed (Figure 2.2a) and minimum surface pressure (Figure 2.2b) in the domain of each experiment. The first 50 days of Figure 2.2 show a continuous line which is a mean of the 3-member ensemble (see Table 2.1 and Table 2.2) for each experiment, and the ribbon spans from the minimum to the maximum value of these 3 members. The next 50 days show only the values for the simulations described in Table 2.1. After an initial period of intensification, the maximum surface wind speed and minimum surface pressure in all the experiments oscillate around similar values. In the Control and HomoRad experiments, maximum surface wind speed and minimum surface pressure first reach a maximum and minimum value, respectively, after which the maximum wind speed and minimum surface pressure oscillate around a slightly lower wind speed and higher surface pressure for the rest of the simulation. It is interesting to note that after the first 50 days, the HomoRad experiments achieve the strongest wind speed (above 50ms^{-1}) and lowest surface pressure (around 920 hPa) among the 4 experiments of Table 2.1, suggesting TCs with the strongest intensity. However, during the first 50 days, the ensembles of Control and HomoRad overlap significantly. The fact that TCs in Control and HomoRad are of the same intensity to the leading order is consistent with previous studies (Muller and Romps, 2018). In all four experiments, the maximum wind speed does not vary significantly after the first 50 days. The standard deviation of the maximum wind speed in the last 50 days is about 12% in control, 7% in HomoRad, 15% in HomoSfc, and 15% in HomoAll, suggesting that the system has achieved a statistically steady state. When the grid spacing is reduced to 1 km in HomoAll, the intensity remains similar to that of the 2-km simulation (see Movie 2), suggesting that the intensity of the TCs converges with increased resolution.

Radiative and local surface-flux feedbacks accelerate spontaneous TC genesis (Fig. 2). We identify TC genesis as the period when the maximum surface wind speed first reaches 33ms^{-1}, similar to (Wing et al., 2016), and we mark this moment with a star on top of the line. This

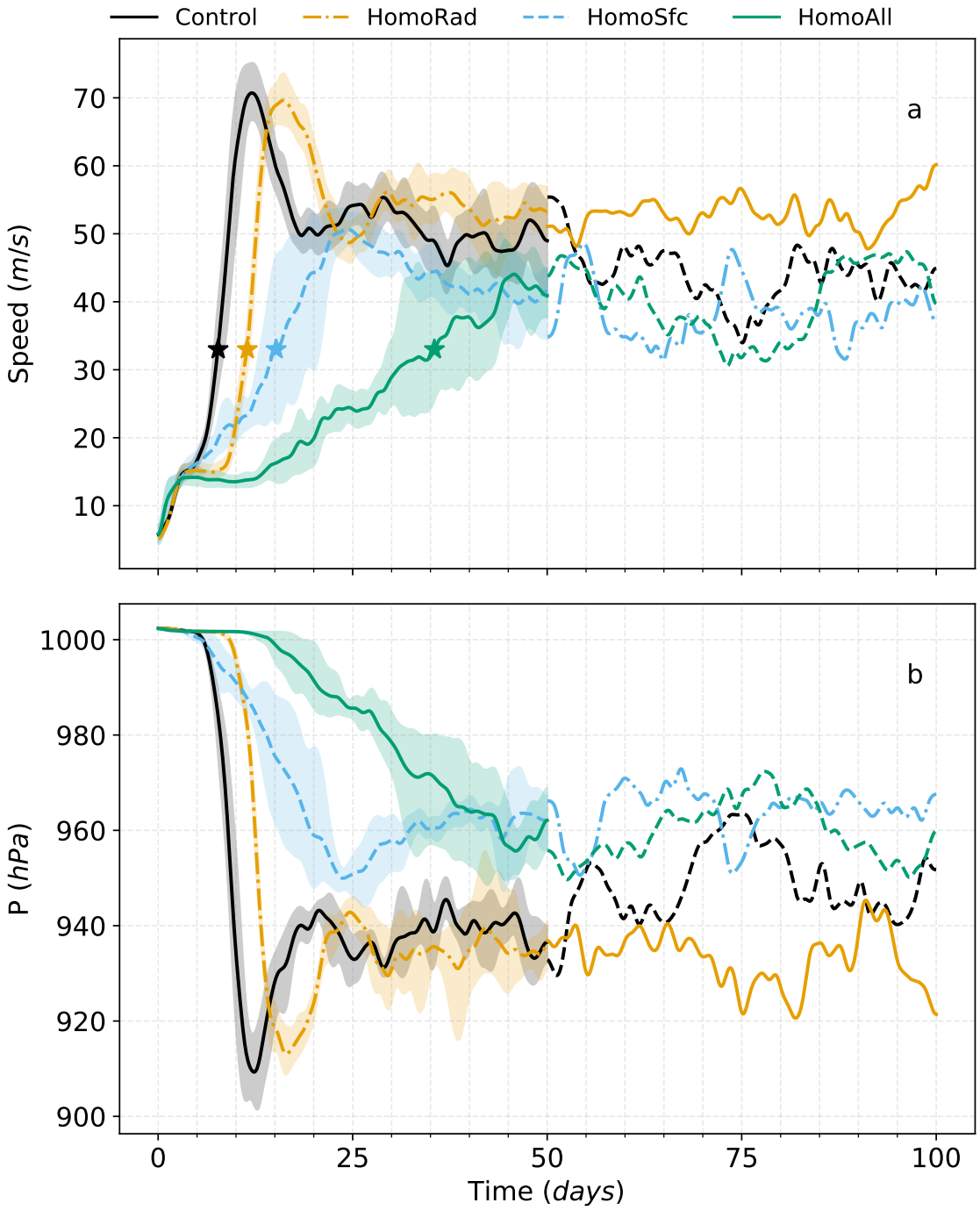

Figure 2.2: Time evolution of (a) maximum surface wind speed (ms^{-1}) and (b) minimum surface pressure (hPa). Hourly data are smoothed with a moving-average filter with window = 20 h.

moment occurs around day 7.6 in Control, day 11.4 in HomoRad, day 15 in HomoSfc and day 35.5 in HomoAll. This occurs around the time the rotation is noticeable in the Movie S1: around day 8 in the Control simulation, day 10 in HomoRad, day 13 in HomoSfc, and day 33 HomoAll, showing that genesis is also slower when removing both feedbacks. The order of emergence of TCs is consistent across ensemble members (first in Control, second in HomoRad, third in HomoSfc and fourth in HomoAll). The acceleration of TC genesis by radiative and local surface-flux feedbacks is consistent with the results of Muller and Romps (2018), Wing et al. (2016) and Zhang and Emanuel (2016).

TC composites show that the simulated TCs have horizontal structures that resemble observations of real TCs. Figure 2.3 shows the azimuthal average of surface wind speed (2.3a) and surface pressure (2.3b) of the composites. TCs in the four simulations are all characterized by a center of quiescent winds collocated with a well-defined eye of minimum surface pressure. Both the azimuthal averages of tangential and radial surface wind speeds have local extrema (minimum for the tangential component and maximum for the radial component) at the center of minimum pressure in the three cases. The mean tangential wind increases rapidly outward while the radial component decreases (Figure 2.3a). The mean tangential wind speed is around 24ms^{-1} at 40 km from the center in Control, 32ms^{-1} at 22 km from the center in HomoRad, 21ms^{-1} at 50 km in homoSfc, and 17ms^{-1} at about 20 km from the center in HomoAll. After reaching the maximum, the tangential wind speed then decreases with distance from the center, reaching 12ms^{-1} at 200 km in Control, at around 165 km in HomoRad and HomoSfc and at 100 km in HomoAll. This shows that the TCs in HomoAll have a smaller horizontal extent than the other three experiments. Our results are robust over different definitions on the size of the average storm, e.g., the radius of maximum azimuthally averaged tangential wind or the radius where tangential wind reaches 12ms^{-1} (Chavas et al., 2016). The radial wind speed has a similar structure, reaching a minimum and then increasing with radius. Similarly, the surface pressure has a local minimum in the center of the TC, and it increases with distance (Figure 2.5b). The mean surface pressure minimum is 958hPa in Control, 947hPa in HomoRad, 972hPa in HomoSfc and 977hPa in HomoAll, and the ambient surface pressure is around 1000hPa in all the experiments.

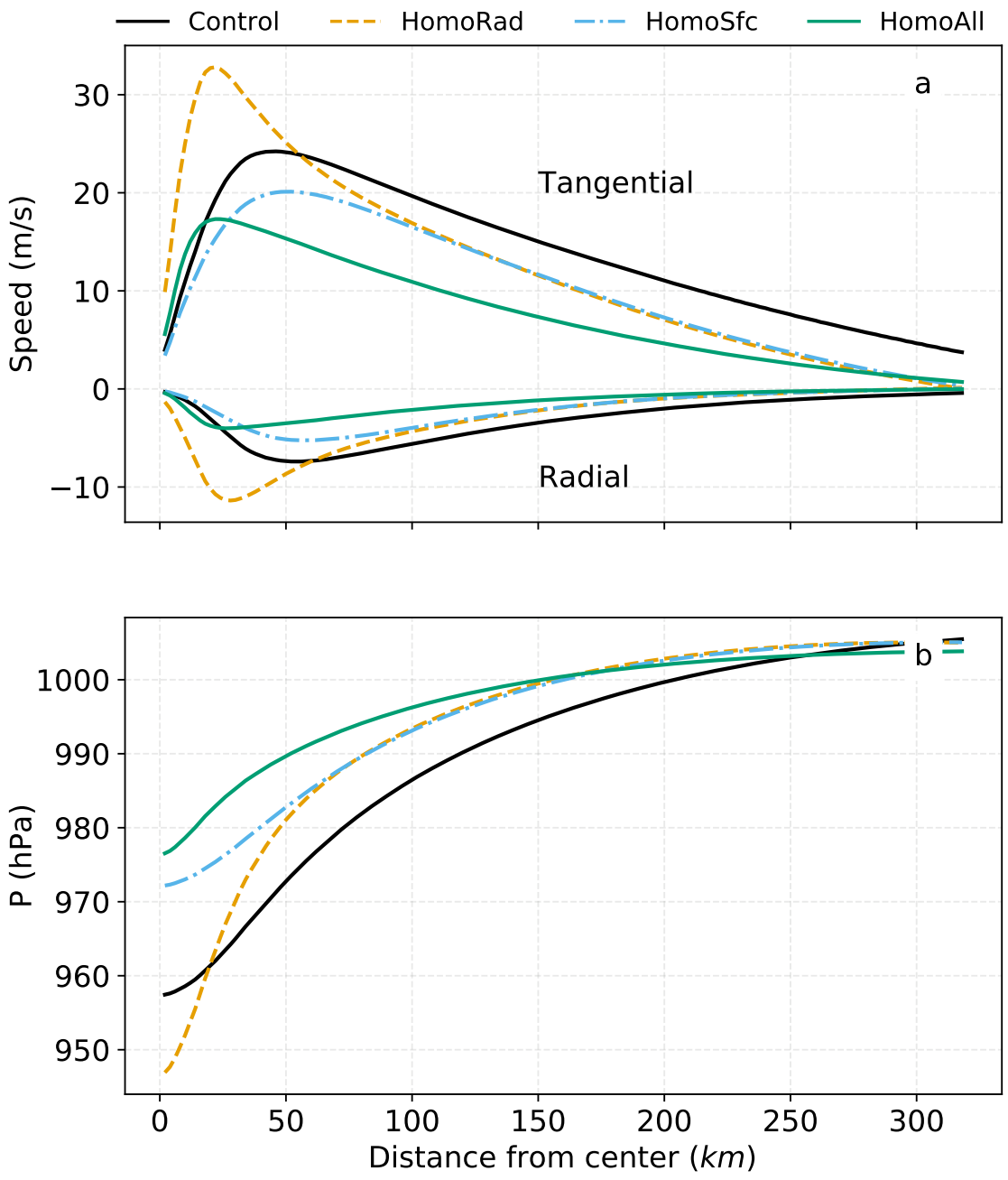

Figure 2.3: Azimuthal averages of (a) radial and tangential wind speed at the surface (ms^{-1}) and (b) surface pressure (hPa) in the composite TCs.

The vertical structures of the simulated TCs also are consistent with realistic TCs. Figure 2.4 shows azimuthal averages of tangential wind speed in shading and black contours of virtual potential temperature anomaly (2.4a-2.4d), and convective heating anomaly (2.4e-2.4h) with a horizontal red line denoting the radiative tropopause, computed using the last 50 days of simulations, as the height at which the horizontally averaged time-mean radiative cooling rate vanishes (Cronin and Chavas, 2018; Pierrehumbert, 2010; Seidel and Yang, 2020). The tangential wind speed is positive, indicating cyclonically rotating wind throughout much of the troposphere (Figure 2.4a – Figure 2.4d). Above this cyclonic wind, we observe tangential wind in the opposite direction in the four experiments. Additionally, Figures 2.4a-2.4d, show a buoyant (warm) core in the center of each TC, indicated by the contours of virtual potential temperature anomaly. The warm core extends vertically to the tropopause, which is at 15.7 km in Control ,16 km in HomoRad, 14.9 in HomoSfc and 14.4 km in HomoAll.

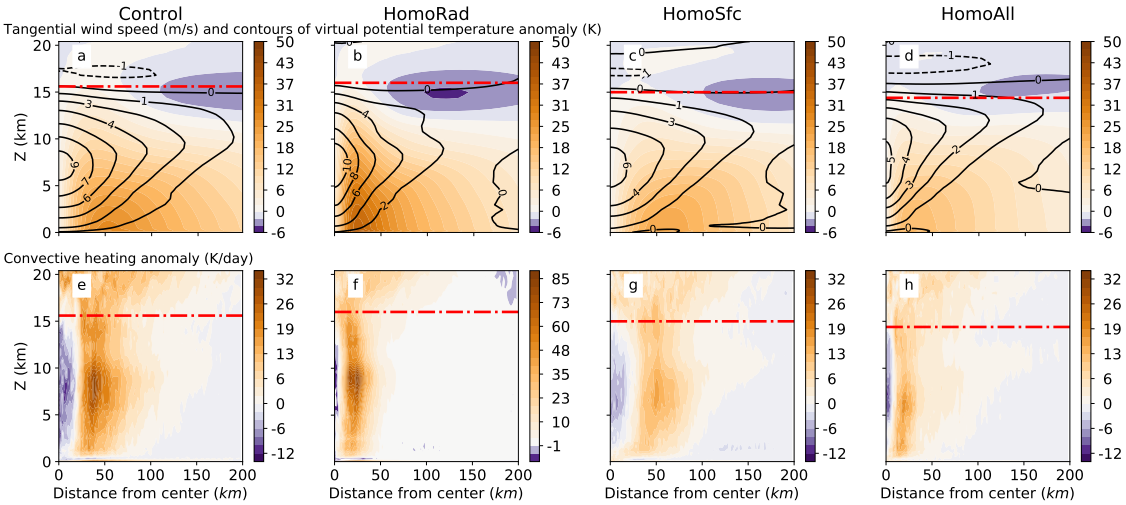

Figure 2.4: Azimuthal average of (top) tangential wind speed (shading; ms^{-1}) and virtual potential temperature anomaly (K), along with (bottom) convective heating rate anomaly (shading; $Kday^{-1}$) in the composite TC for the (a),(e) Control; (b),(f) HomoRad; (c),(g) HomoSfc; and (d),(h) HomoAll simulations. The horizontal dash-dotted red line indicates the height of the radiative tropopause defined by zero radiative cooling rate.

Positive convective heating anomalies extend from near the surface to the tropopause and are more intense in the eyewall, a narrow region relatively close to the center, (Figures 2.4e-2.4h). This region is partially collocated with the warm core of the simulated TCs. The deep heating structure

in the troposphere captures latent heat release in convective storms with maximum intensity in the middle troposphere, around 7.5 km in Control, around 8 km in HomoRad, around 6.5 km in HomoSfc and around 6 km in HomoAll. It is worth noting that all the simulations present negative convective heating anomalies at the center. The region of strong convective heating is wider in Control and in HomoSfc than in HomoRad and HomoAll. An interesting feature is that the convective heating in the HomoRad experiment is twice as strong as that in the rest of the simulations. In this case, the heating also coincides with a higher temperature perturbation than in the rest of the experiments due to the heating being concentrated in a thinner region than in the rest of the simulations. The spatial coincidence of positive convective heating and buoyancy anomalies seen in Figure 2.4, suggests positive APE production due to convection (as observed in subsection 2.2.5). To examine this hypothesis further, we now examine the time evolution of APE and APE budgets in the simulations.

2.4 Evolution of APE in the simulated TCs

TC development is associated with APE evolution. Figure 2.5a shows the time evolution of the total APE in the domain for the four experiments shown in Table 2.1. In all simulations, the APE grows initially with time (the genesis period) and reaches the first local maximum around days 12, 24, 28 and 20 for Control, HomoRad, HomoSfc and HomoAll, respectively. For reference, the time to genesis is marked with a star at the same position as in Figure 2.2. We can see that genesis is led by APE growth, and as time advances and more TCs appear and intensify, APE further increases. This suggests that diagnosing APE evolution may help understand TC genesis and intensification.

Figures 2.5b-2.5e show the APE budgets. In all simulations, convective heating dominates APE production, and the APE production by convective heating is mainly balanced by its conversion to kinetic energy ($-wb$), whereas the contribution of radiative and surface fluxes is modest. These results hold, in particular, for Control, HomoRad and HomoSfc, where radiative and/or local surface-flux feedbacks are active. The magnitude of the APE budgets is similar in all the simulations. This observation may help explain the occurrence of TCs in HomoAll after removing radiative and local surface-flux feedbacks.

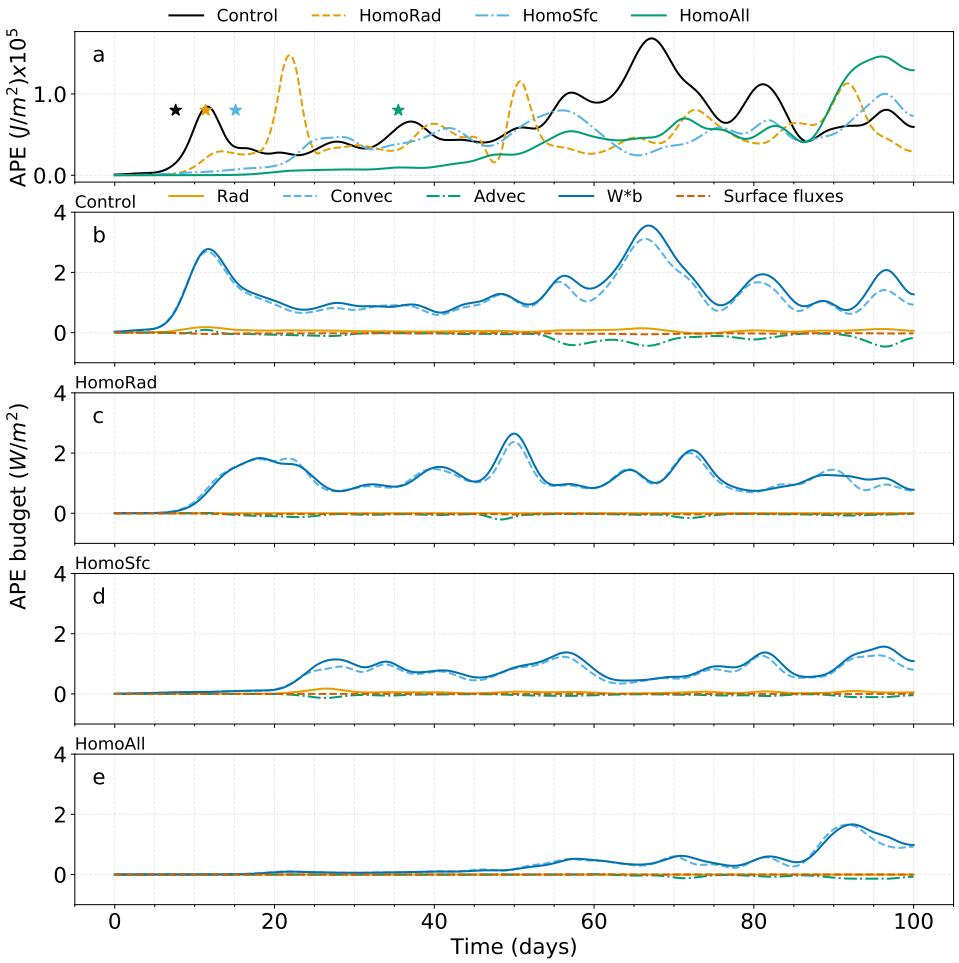

Figure 2.5: (a) The available potential energy (APE), integrated from the surface to the radiative tropopause, in the Control, HomoRad, HomoSfc, and HomoAll experiments, and its budget, integrated from the surface to the radiative tropopause, in the (b) Control, (c) HomoRad, (d) HomoSfc, and (e) HomoAll simulations. In (b)–(e), the orange solid line represents the radiation term, the light-blue dashed line represents the convection term, the green dash–dotted line represents the advection term, the dark-blue solid line represents the conversion to kinetic energy which is multiplied by -1, and the red dashed line represents the surface fluxes term. Data are smoothed with a moving-average filter with window width = 20 h.

Spontaneous TC genesis without radiative and local surface-flux feedbacks challenge the prevailing theory of spontaneous TC genesis. Previous studies regarded local surface-flux or radiative feedbacks as essential ingredients in the spontaneous TC genesis process (Muller and Romps, 2018; Wing et al., 2018). However, we found that TCs can self-emerge without radiative and local surface-flux feedbacks (Figures 2.1 and 2.2). Additionally, our analysis of APE budgets shows that convective heating dominates APE production (Figure 2.5) in all the experiments, and therefore may be determinant in the spontaneous TC genesis.

2.5 Sensitivity of spontaneous TC genesis without radiative and surface flux feedbacks

TCs self-emerge without radiative and surface flux feedbacks in 50-day-long simulations in a variety of configurations where we change the radiation scheme, microphysics scheme, sea-surface temperature, and resolution, while otherwise maintaining the HomoAll configuration. Movie S2 shows the time evolution of surface wind speed of the sensitivity experiments shown in Table 2.2. Regarding model physics, we observe clearly defined TCs by day 14 when using the Thompson Microphysics scheme, and by day 24 when using RRTM radiation. In the SST sensitivity experiments, TCs first appear by day 14 with a surface temperature of 305K and by day 21 with a surface temperature of 297K. When we set the Coriolis parameter to f=$3\times10^{-4}\mathrm{s}^{-1}$, TCs first appear by day 33, and when $f = 1 \times 10^{-4}\mathrm{s}^{-1}$, convection remains randomly distributed. Tcs do not emerge even when running the simulation to 100 days (not shown). This is consistent with the results of (Muller and Romps, 2018), who showed that spontaneous TC genesis does not occur when $f = 1 \times 10^{-4}\mathrm{s}^{-1}$ in a similar computation domain. In Movie S3, spontaneous TC genesis occurs by day 16 when the horizontal grid-spacing is reduced to 1km in the HomoAll configuration.

Figure 2.6 shows the minimum surface pressure and maximum surface wind speed in the domain for the sensitivity experiments shown in Table 2.2. We observe maximum surface wind speeds greater than 20 m s^{-1} and decreasing minimum surface pressure in all of the simulations except with $f = 1 \times 10^{-4}\mathrm{s}^{-1}$, where the wind speed and surface pressure remain relatively flat, consistent with the random convection shown in Movie S2. It is important to note that the minimum surface

pressure shows a decreasing trend accompanied by the increase in maximum surface wind speed by the end of the simulation period in the sensitivity experiments for radiation physics, $f = 3\times10^{-4}\mathrm{s}^{-1}$, and the experiment with a surface temperature of 297K, suggesting that the TCs in these sensitivity experiments have not yet finished intensifying. However, this trend is not observed in the experiment with $f = 1 \times 10^{-4}\mathrm{s}^{-1}$. In the experiment with 1-km grid-spacing, TCs reach similar intensities as those of the experiments in Table 2.1 by day 30 (Movie S3). The sensitivity study shows that our results are robust over different choices of model physics.

Here, we speculate on potential explanations for the dependence of spontaneous TC genesis on the value of f. The spatial scale of TCs may be approximately proportional to $1/f$ (Chavas and Emanuel, 2014; Zhou et al., 2013), so TCs in the simulations with $f = 1 \times 10^{-4}\mathrm{s}^{-1}$ would have 3 times larger spatial scale than in the case with $f = 3 \times 10^{-4}\mathrm{s}^{-1}$ if all other factors are equal. Therefore, using the same computing domain, the $f = 1 \times 10^{-4}\mathrm{s}^{-1}$ simulation may not be able to accommodate a TC. Another plausible explanation is that increasing the rotation rate reduces the scale separation between the convective organization and the deformation radius ($R = NH/f$ where N is the Brunt-Väisälä frequency and H the height of the tropopause), favoring TC genesis (Ooyama, 1982). The deformation radius is roughly the minimum spatial scale that is affected by the rotation and is often much larger than the scale of individual convective storms. Increasing the rotation rate would reduce the deformation radius and, thereby, the scale separation between convective storms and the deformation radius. This makes it easier for organized convection to be affected by the planetary rotation, favoring TC genesis. In Table 2.3, we show the value of the deformation radius. We compute the deformation radius using the mean sounding of the last 50 days of the simulations shown in Table 2.1. We observe that in contrast to the cases with $f = 5 \times 10^{-4}\mathrm{s}^{-1}$ and $f = 3 \times 10^{-4}\mathrm{s}^{-1}$, the deformation radius of the case with $f = 1 \times 10^{-4}\mathrm{s}^{-1}$ becomes larger than the simulated domain in all the cases of Table 2.1, making this a plausible explanation for why we do not observe spontaneous TC genesis in this case. A detailed investigation of the hypotheses requires large-domain simulations and is left for future work.

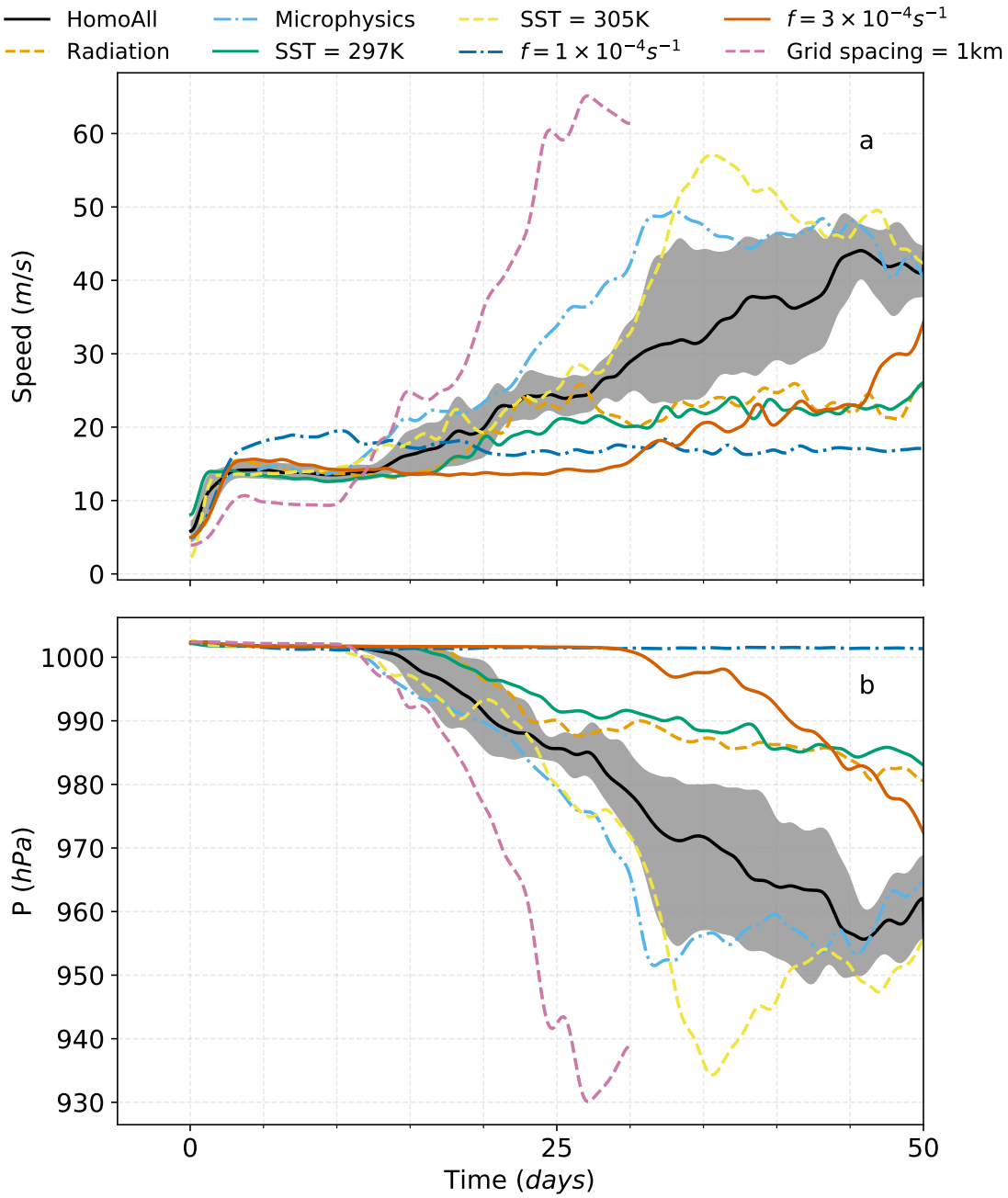

Figure 2.6: Time evolution of (a) maximum surface wind speed (ms^{-1}) and (b) minimum surface pressure (hPa) for simulations at 2-km grid spacing. Different lines correspond to different experiments, as described in the legend. Hourly data are smoothed with a moving-average filter with a window = 20 points.

	Control	HomoRad	HomoSfc	HomoAll
$f = 4.97 \times 10^{-4}\text{s}^{-1}$	**386.1**	**397.1**	**335.7**	**399.0**
$f = 3 \times 10^{-4}\text{s}^{-1}$	639.6	657.8	556.1	509.4;697.6*
$f = 1 \times 10^{-4}\text{s}^{-1}$	1919.0	1973.5	1668.4	1528.2;1957*

Table 2.3: Deformation radius NH/f (km) for different values of the Coriolis parameter using the mean sounding of last 50 days of the simulations in Table 2.1 to compute N (the Brunt–Väisälä frequency) and H (the height of the tropopause). The values marked with an asterisk are the deformation radii computed using the mean sounding from the sensitivity simulations with different f (see Table 2.2). The values in bold face correspond to the simulations of Table 2.1

2.6 Main findings and implications

This paper, for the first time, shows that spontaneous TC genesis can occur after turning off both radiative and local surface-flux feedbacks in f-plane CRM simulations. The simulated TCs in all of our experiments have realistic horizontal and vertical structures. Our simulation results are robust to varying horizontal resolutions, initial conditions, and a wide range of model physics. This result challenges our previous understanding that spontaneous TC genesis requires either radiative or local surface-flux feedbacks (Muller and Romps, 2018; Wing et al., 2018).

We find that a high Coriolis parameter favors spontaneous TC genesis. In our computing domain of 1024 km $\times$ 1024 km, the minimum f that allows TCs to self-emerge in HomoAll is $f = 3 \times 10^{-4}\text{s}^{-1}$, which has been used before in studying spontaneous TC genesis. A plausible explanation for this dependence suggests that our simulation domain may be too small to accommodate spontaneous TC genesis in the HomoAll simulations when the Coriolis parameter becomes smaller. Another explanation suggests that as the Rossby radius of deformation and the convective scales become closer, the probability of convecting regions becoming controlled by the background rotation increases. Another hypothesis considers that a high Coriolis parameter accelerates spontaneous TC genesis by increasing the effect of planetary rotation on the production of vorticity by stretching. Therefore, this dependence of TC genesis on the Coriolis parameter deserves further exploration that considers a larger computation domain or even a different geometry, as recent studies have found that the minimum Coriolis parameter needed for TC genesis depends on the

Rhines scale, which on an f-plane becomes infinite (Chavas and Reed, 2019). In all these further explorations, the APE framework offers an opportunity to re-examine the role of convective heating in the TC genesis process. Therefore, our results contribute to our understanding of the nature of convection and TC genesis and show that, even in earth-like conditions, a cooperative intensification between convective heating and the overturning circulation may contribute to the organization of a TC through its role in APE production, a possibility that had been disregarded in recent studies. Further exploration of the role of convective heating in the production of APE in under Earth-like conditions is desirable to pursue in the future.

Our results are consistent with the broadly defined conditional instability of the second kind (CISK), if we define CISK as a cooperative instability between atmospheric flows and convection that does not require local surface-flux feedbacks or radiative feedbacks (Bretherton, 2003). Conventional CISK studies mainly focused on linear stability analysis or computer simulations with parameterized convection (Montgomery and Smith, 2014; Ooyama, 1982; Smith, 1997). These studies are, therefore, subject to criticisms on assumptions in the representation of dynamics or convection. Their simulated TCs often have a much smaller spatial scale than the observed TCs. To our knowledge, this paper presents the first 3D nonlinear CRM simulations showing that TC genesis can result from interactions between convection and atmospheric circulations. This result is, therefore, a significant advancement in our understanding of TC genesis.

Can convection drive large-scale circulations without radiative and local surface-flux feedbacks (e.g., (Emanuel et al., 1994; Ooyama, 1982)?) This is a central question in tropical atmospheric dynamics. This paper and recent research show that cooperative interactions between convection and atmospheric circulations can lead to a wide spectrum of convectively coupled circulations, including convective self-aggregation (Muller and Bony, 2015; Yang, 2018a, 2021), TCs (Montgomery and Smith, 2014; Ooyama, 1982), convectively coupled equatorial waves (Andersen and Kuang, 2008; Kuang, 2008; Mapes, 2000) and the Madden-Julian Oscillation (MJO) (Wang et al., 2016; Yang and Ingersoll, 2013, 2014). These studies suggest that convection can indeed drive large-scale circulations without radiative and local surface-flux feedbacks.

We use an APE-centric framework (Yang 2018a), which complements the widely used MSE

analysis. Our APE analyses show that convective heating coincides with positive buoyancy anomalies (Figure 2.4) and dominates APE production during both the genesis and mature stages of TC development (Figure 2.5). The fact that convection dominates the APE production even in the full-physics simulation may help explain why spontaneous TC genesis can exist without the radiative and local surface-flux feedbacks. The computation of APE requires defining the atmosphere state of minimal potential energy after adiabatic rearrangement of air mass. The minimal potential energy state may be sensitive to the choice of methods. This challenge is particularly notable when accounting for the phase changes of atmospheric water vapor—a moist APE framework (Lorenz, 1978; Randall and Wang, 1992; Wong et al., 2016). It is important to note that we use a "dry" APE framework, which treats convective heating as an external heat source. In future studies, we should analyze our experiments using "moist" variables, including the MSE and moist APE, which may provide additional insights into the spontaneous TC genesis. Aside from an approach centered in thermodynamics, future work focusing on spontaneous TC genesis dynamics (e.g., analysis of vorticity) is necessary. The dynamic and thermodynamic approaches are complementary, and a complete picture of the TC genesis should consider both.

The energy that powers TCs ultimately comes from the ocean (Emanuel, 1986, 2003), which transfers energy to the atmosphere primarily through surface sensible and latent heat fluxes. Our experiments are not exceptions, as the surface energy fluxes are key to sustaining a moist convecting atmosphere. However, our experiments show that when radiative or local surface-flux feedbacks are not active, convective heating may be capable of producing horizontal pressure perturbations, allowing spontaneous TC genesis to occur.

This paper aims to understand TC genesis by studying it in RRCE. In RRCE simulations, TCs can self-emerge, but this process often takes $10 - 30$ days (Carstens and Wing, 2020; Emanuel, 2018; Muller and Romps, 2018; Wing et al., 2016). This timescale is long compared to that of synoptic-scale disturbances in the tropical atmosphere: physical processes leading to TC genesis in RRCE might be less efficient than synoptic-scale weather systems. Therefore, other physical processes likely promote TC genesis in the real atmosphere. In future studies, it would be useful to repeat our simulations using a hierarchy of numerical models, including aqua-planet GCMs with uniform

SSTs, aqua-planet GCMs with realistic SST distributions, and GCMs with realistic topography and SST distributions. This approach will not only test the robustness of our results but will also help bridge the gap between highly idealized studies and observation-based studies.

Appendix

Sensitivity of Spontaneous TC genesis and APE evolution to relaxation of mean wind speed.

Here we show the evolution of four 50-day simulations with no horizontal wind speed nudging. The simulations are otherwise identical to Control, HomoRad, HomoSfc, and HomoAll. Spontaneous TC genesis occurs in the Control, HomoRad, HomoSfc, and HomoAll configurations without relaxing the mean wind to zero at all levels. In Figure 2.7 and Movie S4 we show map views of the surface wind speed and surface pressure in simulations where we do not relax the mean wind speed to zero. The simulations are qualitatively similar to their counterparts with wind speed nudging, showing various vortices with maximum wind speeds around 50ms^{-1}. Figure 2.8 shows that the evolution of maximum wind speed and minimum surface pressure closely follows those of Control, HomoRad, HomoSfc, and HomoAll. Figure 2.9 shows that the APE and APE budgets are also qualitatively similar to the experiments with wind speed nudging for the first 50 days of the simulations.

Data and software availability

The namelist files to run the experiments and the analysis code is available at `https://github.com/aramirezreyes/RamirezReyes_Yang_2020_SpontaneousCyclogenesis`.

Acknowledgments

This work was supported by Laboratory Directed Research and Development (LDRD) funding from Berkeley Lab, provided by the Director, Office of Science, of the U.S. Department of Energy under contract DE-AC02-05ch21231. Argel Ramírez Reyes' doctoral studies are supported by Mexico's National Council for Science and Technology (CONACYT) and The University of California

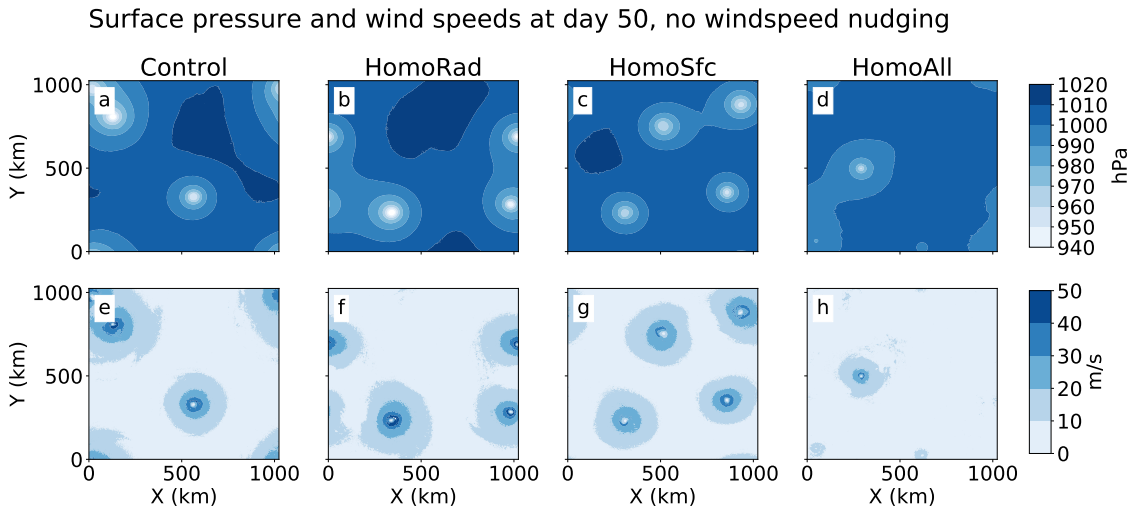

Figure 2.7: Map views of (top) surface pressure (shading; hPa) and (bottom) surface wind speed (shading; ms^{-1}) at t = 50days (snapshot) for the (a),(e) Control; (b),(f) HomoRad; (c),(g) HomoSfc; and (d),(h) HomoAll simulations with 2−km grid spacing without mean wind speed nudging.

Institute for Mexico and the United States (UC Mexus) through the CONACYT-UC Mexus doctoral fellowship. Computational resources were provided by the Department of Energy's National Energy Research Scientific Computing Center (NERSC) at Lawrence Berkeley National Laboratory. The computational model was kindly provided by M. Khairoutdinov and can be obtained through http://rossby.msrc.sunysb.edu/ marat/SAM.html. We thank T. Cronin, S. D. Seidel, D. Chavas and W. Zhou for helpful comments during the early stage of this work, D. Nolan for a helpful discussion at the AGU 2019 Fall Meeting.

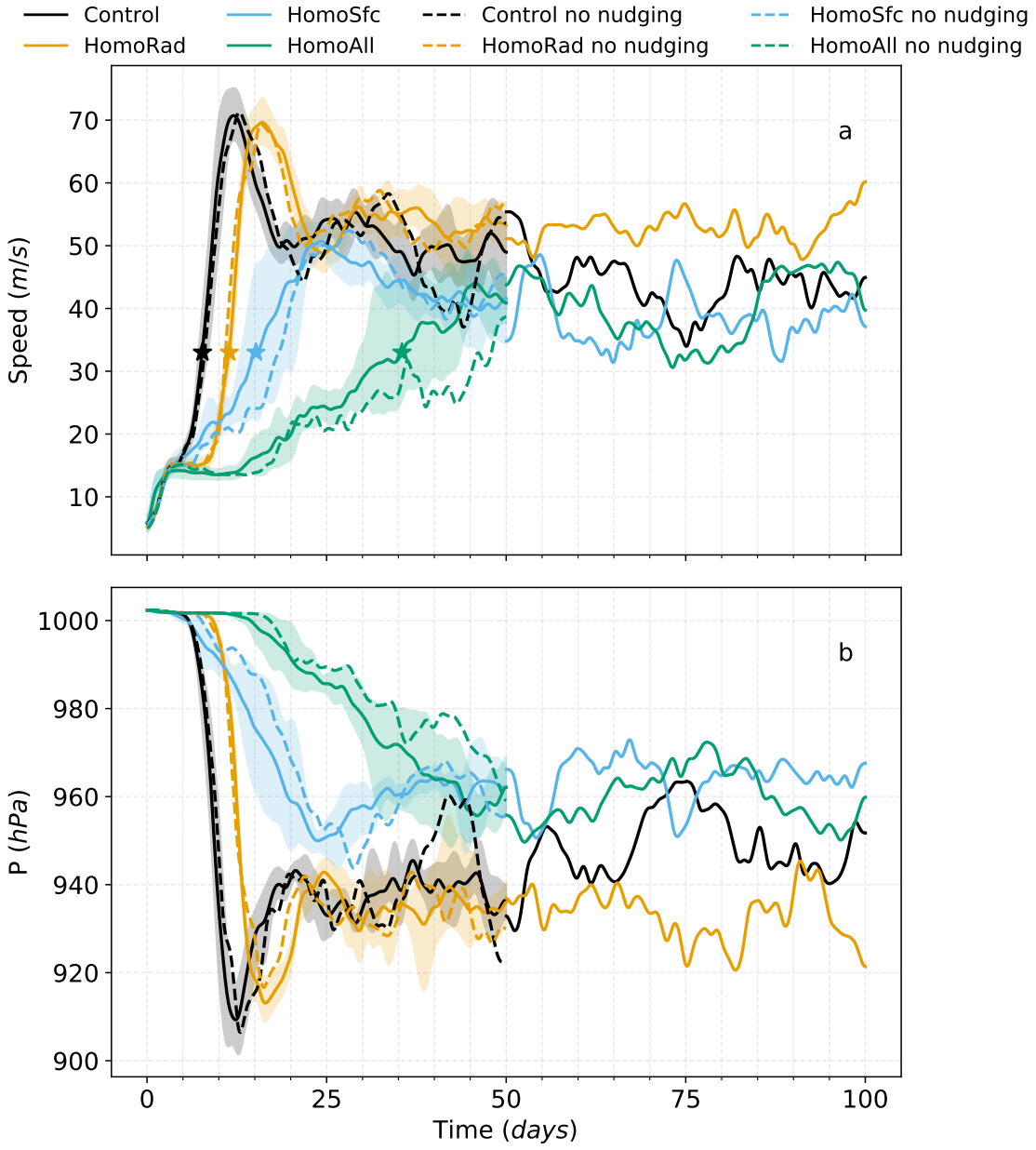

Figure 2.8: Time evolution of (a) maximum surface wind speed (ms^{-1}) and (b) minimum surface pressure (hPa) for simulations at 2-km grid spacing. Different lines correspond to different experiments, as described in the legend. Continuous lines show values in the simulations with mean wind speed nudging, and dashed lines show values in the simulations without mean wind speed nudging. Hourly data are smoothed with a moving-average filter with window = 20h.

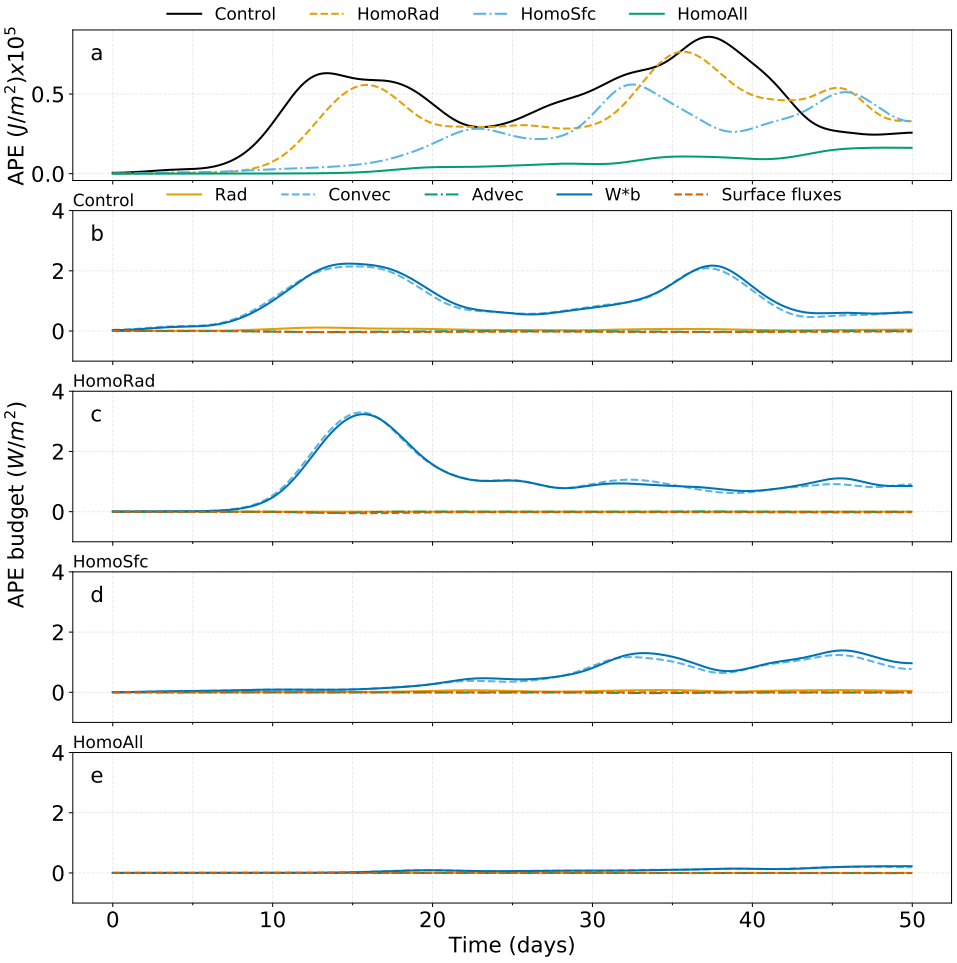

Figure 2.9: As in Figure 2.5, but for 50-day experiments without relaxation of the horizontal mean wind.

Chapter 3 The Moisture-Convection feedback can be sufficient for spontaneous TC genesis

This chapter has been adapted from the preprint of the same name that is stored in the ArXiV, and it is currently being consider for the journal Geophysical Research Letters after revisions. **Ramírez Reyes, A. and Yang, D.: The Moisture-Entrainment-Convection Feedback Can Lead to Spontaneous Tropical Cyclone Genesis, doi: 10.48550/arXiv.2208.11160, 2022b**

Abstract

In contrast to prevailing knowledge, Ramírez Reyes and Yang (2021) showed that tropical cyclones (TCs) can form spontaneously without moisture-radiation and surface-flux feedbacks in a cloud-resolving model (CRM) simulation. Here we ask, why? Thirteen 3D cloud-resolving simulations show that the moisture-convection (MC) feedback can effectively lead to spontaneous TC genesis and intensification in the absence of radiative and surface-flux feedbacks. In the MC feedback, a moister environment favors new deep convective events that further moisten the environment, leading to aggregation of deep convection. The impact of the MC feedback on TC genesis and intensification occurs in two distinct time scales: a short time scale set by detrainment moistening the environment (a few hours) and a long time scale (17 days) due to subsidence drying. The hours-long time scale of detrainment suggests that the MC feedback is an efficient process relevant to TC genesis in the real world.

Plain language summary

Computer simulations show that dispersed thunderstorms tend to self-organize into a tropical cyclone (TC) in idealized setups. This process occurs even in highly idealized climates without the most common processes that, in nature, are observed to aid TC formation (e.g., pre-existing disturbance or special spatial structure in ocean energy fluxes and radiative energy fluxes). What causes tropical cyclones to form in such an exotic atmosphere? We find, using computer simulations, that thunderstorms and environmental moisture reinforce one another, causing disorganized patches of storms to aggregate into a tropical cyclone. We call this the moisture-convection (MC) feedback. By varying our simulation parameters, we find that the MC feedback operates over periods of a few hours to several weeks. The MC feedback's fast (hours-long) component may be important for understanding and forecasting the genesis of real-world TCs.

3.1 Introduction

In Earth's atmosphere, there are around 90 tropical cyclones (TCs) every year. They are warm-cored, rapidly rotating storms with horizontal scales of the order of 500 km in maturity and are typically formed over tropical oceans. Despite extensive research and improved forecast techniques, uncertainties in forecasting TC genesis and intensification hinder safety and evacuation planning by policymakers. TC-associated intense rainfall, strong winds, and storm surges continue to cost lives and cause economic losses and other societal impacts. Therefore, improving our understanding of TC genesis and intensification is of primary importance in tropical meteorology and atmospheric science.

In computer simulations, TCs can self-emerge from random convection over uniform sea-surface temperatures on an f-plane (Bretherton et al., 2005; Carstens and Wing, 2020; Davis, 2015). This phenomenon is known as *spontaneous TC genesis*. On Earth, TCs often develop from a pre-existing disturbance, and a vast amount of literature has explored the leading-order processes that dominate typical TC genesis events (Dunkerton et al., 2009; Emanuel, 1986, 2018; Montgomery et al., 2006; Ooyama, 1982; Raymond et al., 2007). However, the processes that lead to spontaneous TC genesis

in these idealized setups are still present in the real atmosphere and may help the evolution of a pre-existing disturbance into a TC. Therefore, spontaneous TC genesis offers a simplified framework to understand some elements of TC genesis without the full complexity of the real atmosphere (Davis, 2015). Wing et al. (2016) showed that spontaneous TC genesis requires either radiative feedback or local surface-flux feedback. This result was then confirmed and recast by Muller and Romps (2018) using small-domain (1000 km x 1000 km) cloud-resolving simulations. However, Ramírez Reyes and Yang (2021) showed that TCs can self-emerge without radiative and local surface flux feedbacks using the same cloud-resolving model (CRM). A major difference is that Ramírez Reyes and Yang (2021) used a higher Coriolis parameter, making TCs smaller and easier to fit into a limited computing domain. This result challenges the prevailing understanding of spontaneous TC genesis.

What leads to spontaneous TC genesis and intensification without radiative and local surface flux feedbacks? Here, we test the hypothesis that the moisture-convection (MC) feedback leads to TC genesis and intensification in the study of Ramírez Reyes and Yang (2021). The moisture convection feedback requires horizontal moisture gradients which influence and are in turn influenced by the spatial distribution of deep convection. In the MC feedback, deep convection moistens its environment. The moister environment promotes new convective events in the same region, which further moisten the environment, promoting the next cycle of convection. The mutual reinforcement of convection and moisture could help TC genesis in more than one way. For example, it promotes the emergence of deep convective towers that amplify ambient vorticity by tilting and stretching (Montgomery et al., 2006), and because it can create a moistening tendency in the lower troposphere, which weakens the evaporation of rain and its associated divergence in the low levels (Nolan, 2007; Raymond et al., 2007; Wang, 2012). The MC feedback was first proposed by Scorer and Ludlam (1953), and it recently gained relevance from the thorough studies of Tompkins (2001). Since then, several authors have studied the impact of a MC feedback in organizing convection both in the small scales ($\tilde{5}$-50 km) and in the larger scales ($\tilde{5}$00 km and above) (Craig and Mack, 2013; Grabowski and Moncrieff, 2004; Kuang and Bretherton, 2006; Seeley and Romps, 2015; Tompkins and Semie, 2017; Waite and Khouider, 2010; Wang, 2014b; Yang, 2019).

In this work, we use a mechanism-denial experiment and high-resolution simulations to test the hypothesis that the MC feedback is responsible for spontaneous TC genesis and intensification without radiative and surface-flux feedbacks in the simulations of Ramírez Reyes and Yang (Ramírez Reyes and Yang, 2021). We also explore the time scales in which the components of this feedback operate, and we discuss if the MC feedback could be relevant to real TC genesis.

3.2 Hypothesis: the MC feedback leads to spontaneous TC genesis in the absence of radiative feedbacks and spatially-varying surface fluxes

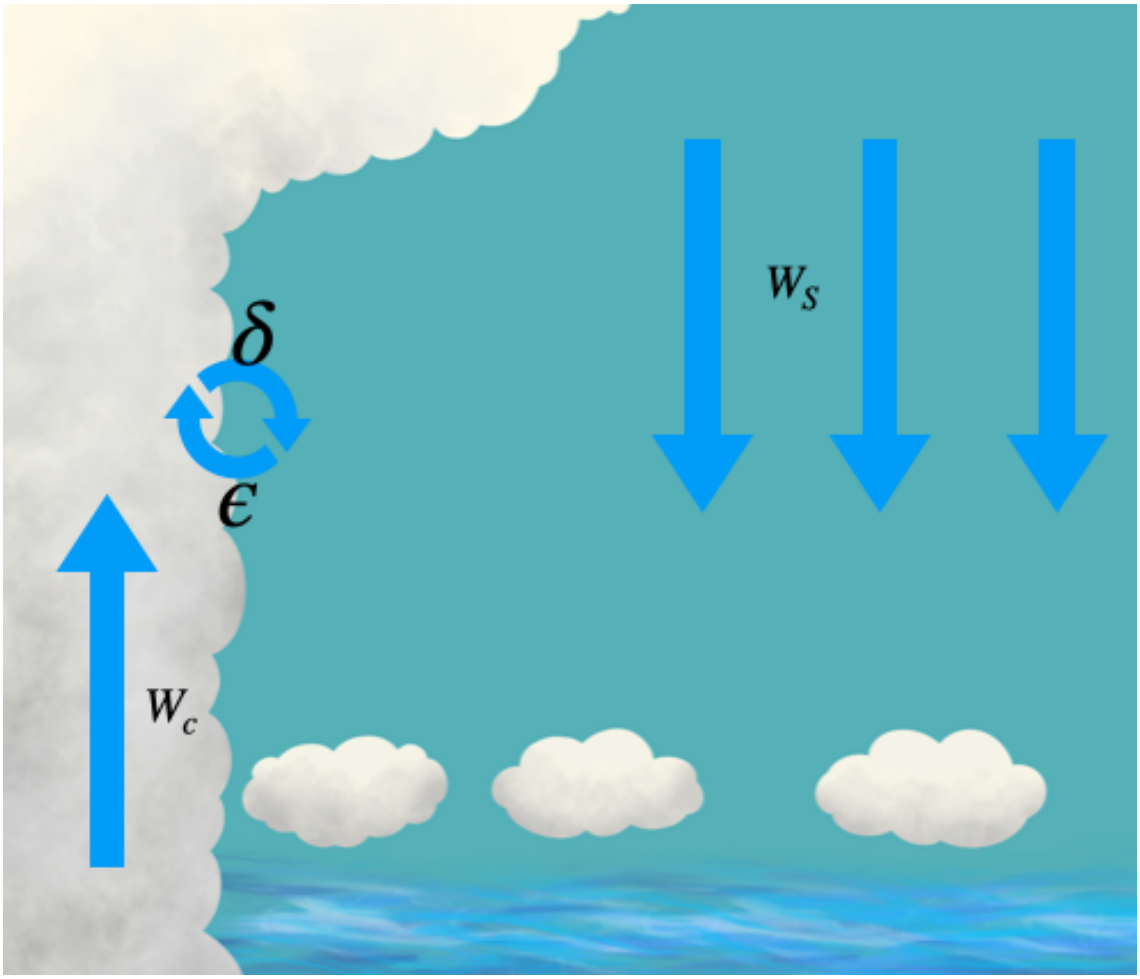

Figure 3.1: Schematic of the elements that interact in the MC feedback

3.2.1 The Moisture-convection feedback

Dry environments inhibit deep convection, and moist environments favor deep convection. Reciprocally, deep convection further moistens its environment, which favors new deep convective events, closing a feedback loop. This simple but intuitive statement summarizes the MC feedback on the mesoscales ($\tilde{5}$-50 km) and large scales ($\tilde{5}$00 km and above). The difference between the two cases resides in which processes dominate the transport of moisture in the free troposphere and what are their associated time scales. For example, close to the convective cloud, the mixing of cloudy air into the environment occurs on timescales associated with "fast" mixing processes, while in the larger scale moisture is transported via "slow" advective timescales (Grabowski and Moncrieff, 2004). Because we are trying to understand the up-scale organization of convection into a TC, both spatial scales and their associated time scales may be relevant for spontaneous TC genesis: the small-scale processes may be relevant during the genesis stage, and the large-scale processes will become relevant once the large-scale circulations of a TC are established.After giving an overview of the MC feedback, in the following paragraphs we will try to establish two relevant time scales (and their associated spatial scales) in which the interaction between moisture and convection may be relevant to spontaneous TC genesis.

A deep convective cloud that rises with vertical velocity W_c exchanges mass with its environment through mixing processes, by which environmental air flows into the cloud and cloudy air flows into the environment Figure 3.1.These mixing processes have diverse spatial scales, some are small scale eddies and others occur through larger scale flows. In the following, we will refer to these broadly defined mixing processes as entrainment and detrainment, acknowledging that their usage for an evolving convective plume may be subject to discussion (de Rooy et al., 2013; Yano, 2014). These mixing processes are characterized by fractional detrainment and entrainment rates of δ and ϵ, respectively. Mixing environmental air into convective updrafts reduces the buoyancy of the convecting parcels due to evaporative cooling (Tompkins and Semie, 2017) and the buoyancy effect of water vapor (Seidel and Yang, 2020; Yang and Seidel, 2020). This implies that mixing moist environmental air into the updrafts results in a smaller buoyancy reduction than it would if

the environmental air were drier. Through similar mixing processes (the turbulent eddies adding moisture to the immediate environment of the clouds and the mixing of the moisture of multiple convective plumes into the large scale by coherent large-scale flows), moist convection influences moisture in the environment. Moisture detrained from convective clouds into the environment creates an anomalously moist region that favors new deep convective events in the vicinity of existing convective clouds and around the location of recently extinct convective clouds. Outside of the deep convective clouds, where moisture is not added directly by detrainment and entrainment but is advected by large-scale flows, other slower processes affect moisture: In the clear-sky environment, air subsides with a characteristic vertical velocity W_s. This subsidence dries the atmosphere, inhibiting new deep convective events.

This reciprocal interaction of environmental moisture and convection constitutes a feedback process that promotes the organization of deep convection on the scale of a few convective storms and on large scales. To the best of our knowledge, this feedback was first proposed by Scorer and Ludlam (1953) and discussed by Randall and Huffman (1980). It has been thoroughly examined by Tompkins (2001); Tompkins and Semie (2017) in studies of convective self-aggregation; this feedback was then further developed and applied to study the convective organization of the tropical atmosphere in the scale of individual convective clouds (Waite and Khouider, 2010), in the large-scale (Grabowski and Moncrieff, 2004) and in the scales in-between (Craig and Mack, 2013; Kuang and Bretherton, 2006; Seeley and Romps, 2015; Yang, 2019) and by Wang (2014b) in the study of TC genesis in numerical models. Below we analyze two characteristic timescales associated with this feedback; both timescales contribute to generating horizontal moisture gradients in different scales.

3.2.2 Entrainment and detrainment timescale in the convective-cloud scale

The cloudy air ascending at vertical velocity W_c will exchange mass with the environment with a fractional detrainment rate δ (with units of m^{-1}). This detrainment rate corresponds to a vertical length $\mathrm{Length}_\delta \equiv 1/\delta$ over which convection moistens the environment. A typical value of the fractional detrainment rate of deep convection on Earth is $0.2\mathrm{km}^{-1}$ (Romps, 2014). We select

a characteristic vertical velocity of the convecting plume of 1ms^{-1} , which is approximately the mean updraft velocity from the Control simulation described below. This value is also close to the median vertical velocity of updrafts in some observations of tropical deep convection (Lucas et al., 1994). Another proposal would be to take the mean vertical velocity in the simulation (e.g., Fig 3 in (Wang, 2014a)). However, in RCE the value of this computation would be zero. Therefore, we consider that using only the upward motion represents well the role of convective updrafts in the moisture exchange. Using our selected vertical velocity, we find that the moistening time scale is

$$\tau_d = \frac{\text{Length}_\delta}{W_c} \approx \frac{5000\text{m}}{1\text{ms}^{-1}} \approx 1.38\text{hours}. \tag{3.1}$$

Here we assume that, in the leading order, the entrainment and detrainment rates are approximately equal (Romps, 2014). We expect this time scale to be more relevant in the small scale.

3.2.3 Subsidence timescale in the TC scale

In clear-sky regions away from organized convection, air subsides with a characteristic velocity W_s. This process dries the clear-sky region and tends to tends to promote the convective organization in longer temporal scales than the previously described detrainment processes. For our experiments, it is sensible to select the radiative subsidence associated with the outer region of a TC. In the outer region of a TC, subsidence has characteristic velocities of around 2mm s^{-1} (Chavas et al., 2015). A characteristic length of the problem is the scale height of water vapor which has values around 3000m (Romps, 2014). With these two ingredients, we can estimate the time scale of drying by subsidence:

$$\tau_s = \frac{\text{Water vapor scale height}}{W_s} \approx \frac{3000\text{m}}{0.002\text{ms}^{-1}} \approx 17\text{days}. \tag{3.2}$$

We note that τ_s is much longer than τ_d, suggesting that detrainment of water vapor is a more efficient process in creating horizontal moisture perturbations.

3.2.4 Expectations

We hypothesize that the MC feedback is responsible for spontaneous TC genesis in the absence of a pre-existing disturbance or other feedbacks. The moistening tendency from extinct convective events maker more likely the emergence of deep convective storms. Deep convection in a vorticity-rich environment would produce local vorticity anomalies by vortex tilting and stretching. These anomalies are then candidates for vortex merger (Montgomery et al., 2006). The same moistening tendency would also help create a thermodynamic profile that inhibits evaporation and it associated divergence in the lower levels of the troposphere (Raymond et al., 2007). Our hypothesis predicts that the homogenization of clear-sky water vapor on a shorter time scale than τ_d will effectively remove horizontal water vapor gradients, removing a factor that promotes the emergence of nearby deep convective events, and will thereby inhibit spontaneous TC genesis (P1).

Additionally, subsidence of dry air inhibits convection outside the core of a TC with a time scale of τ_s. Inhibiting convection outside the core allows convection to be concentrated near the core, favoring the intensification of TCs. Therefore, we expect that moistening the descending branch on a time scale faster than τ_s will prevent the intensification of the spontaneously formed TCs (P2).

3.3 Methods

3.3.1 The cloud-permitting model and simulation details

We run 3D simulations using the *System for atmospheric modeling* (SAM, version 6.10.10) (Khairoutdinov and Randall, 2003). SAM solves the anelastic equations of motion using a finite-difference numerical scheme in an Arakawa-C grid. Regarding thermodynamics, SAM solves the conservation equation for frozen moist static energy. We use the CAM radiation scheme for long-wave and short-wave fluxes (Collins et al., 2004), and the default SAM single-moment bulk microphysics scheme. The latent and sensible heat fluxes are computed using a bulk formulation where the transfer coefficients are computed using the Monin-Obukhov theory with code adapted from the Community Climate Model 3 (Kiehl et al., 1996). We used the SAM Smagorinsky SGS parameterization described in (Deardorff, 1980). One difference between SAM and other models like WRF (Skamarock

et al., 2021) is that SAM does not employ a specific parameterization for the boundary layer. Instead, the sub grid-scale fluxes in the boundary layer are computed by the same SGS scheme. To prevent erroneous values near the model surface, only the vertical grid scale is used on the SGS grid length when the horizontal grid spacing is much larger than the vertical (Khairoutdinov and Randall, 2003). We output 3D fields every two hours and 2D fields every hour.

The simulation domain is a square of 1024 km x 1024 km in the horizontal dimensions and 34.8 km in the vertical. Grid spacing is 2 km in the horizontal direction and stretched in the vertical direction: it is 50 m from z = 0 m to z = 1050 m. Then, the vertical grid spacing increases gradually until z = 3000 m, where it becomes 600 m. The boundary conditions are periodic in the horizontal directions. The bottom boundary is an ocean with a fixed surface temperature of 300 K, and the upper 30 levels are a sponge layer to prevent the reflection of gravity waves. We use a constant Coriolis parameter of $f = 5 \times 10^{-4}\mathrm{s}^{-1}$. This value is ten times that of 20 deg latitude on Earth. A similar value has been used before (Cronin and Chavas, 2019; Khairoutdinov and Emanuel, 2013; Ramírez Reyes and Yang, 2021). The increased Coriolis parameter is necessary for spontaneous TC genesis without radiative and surface flux feedbacks in this domain with a grid spacing of 2 km (Ramírez Reyes and Yang, 2021), and it also allows for the reduction of the size of individual TCs, allowing several TCs to exist in this domain (Khairoutdinov and Emanuel, 2013). While in real Earth, radiative and surface-flux feedbacks may be necessary for TC genesis to occur, turning them off allows us to explore in detail the role of the MC feedback. The knowledge gained from this framework can then be compared to more realistic simulations. We initialize the simulations using a sounding from the last days of a non-rotating RCE simulation, the same profile used in (Yang, 2018a). In all the simulations, we disable the radiative and surface-flux feedbacks by substituting surface heat fluxes and radiative fluxes with their horizontally averaged value before applying them (Muller and Romps, 2018; Ramírez Reyes and Yang, 2021; Wing et al., 2016). By removing the spatial variation of surface fluxes, we prevent surface fluxes from creating and intensifying moisture gradients, which effectively disables the surface-flux feedbacks, especially the so-called WISHE mechanism (Montgomery and Smith, 2014).

3.3.2 Experiment design: Weakening the MC feedback

We design experiments to test P1 and P2 by homogenizing clear-sky water vapor. We run in total 13 simulations. Our Control simulation is similar to the HomoAll experiment of Ramírez Reyes and Yang (Ramírez Reyes and Yang, 2021), where radiative and surface-flux feedbacks are disabled by substituting radiative heating rate and surface fluxes with their horizontal averages before applying them (Muller and Romps, 2018; Ramírez Reyes and Yang, 2021; Wing et al., 2016). Although we expect the buoyancy effect of water vapor on buoyancy of the convecting cloud to be small when compared to the effects of energy released by phase changes (Yang, 2018a), we turn off the buoyancy effect of water vapor as in (Yang, 2019) to further simplify the system. We then setup our mechanism-denial experiment.

This experiment consists of a set of simulations that differ from Control by relaxing (nudging) the clear-sky (unsaturated grid points) water vapor toward its horizontal average. In the anomalously moist regions, homogenizing clear-sky water vapor means drying; in the anomalously dry regions, it is moistening. To homogenize clear-sky water vapor, we add a relaxation term to the water vapor field in the unsaturated grid points as done by Yang (Yang, 2019).

$$(\widetilde{\delta r}(i,j,k,t_i))\Delta t = \begin{cases} \delta r(i,j,k,t_i)\Delta t, & \text{if } r_{cond}(i,j,k,t_i) > 0.01 g kg^{-1} \\ \delta r(i,j,k,t_i)\Delta t + \overline{r}(k,t_i) - r(i,j,k,t_i))\Delta t/\tau_r, & \text{otherwise} \end{cases} \tag{3.3}$$

where i,j,and k represent the grid indices in the space dimensions and t_i represents the time index. δ_r is the original tendency of the water vapor field computed by SAM and multiplied by the timestep Δt. r_{cond} is the total condensate mixing ratio. The overbar represents an average over all the points that fulfill the same criterion of low condensate. τ_r is the relaxation time scale. We let τ_r take 12 values: 0.5 h, 1h, 3h, 5h, 8h, 12h, 1 day, 2 days, 5 days, 8 days, 10 days and 15 days. This method resembles the relaxation done by Seeley and Romps (Seeley and Romps, 2015), except that they nudged the relative humidity field. Like the method employed by Seeley and Romps, our method effectively reduces moisture gradients (Figure 3.2).

3.3.3 Detection and characterization of TC-associated inflow and updrafts

To characterize the location of convective updrafts relative to the TC centers and the intensity of the inflow we first identify TC centers as local minima of surface pressure at each time step during each 10-day period of each simulation. Next, we compute the total number of updrafts (defined as grid points where the vertical velocity exceeds 2 ms^{-1},) that occur at each distance from the center (using 2-km bins starting in $r = 1$km) and divide it by the number of points that fall within said bin (a measure of the area of the region that falls between said bins). Finally, we divide the total number of updrafts that occur between $r = 3r_{max}$ and $r = 6r_{max}$ by those that appear between $r = 0$ and $r = 6r_{max}$. This quantity, which we call the "updraft ratio" shows how concentrated convection is near the radius of maximum winds. We selected the region between $r = 3r_{max}$ and $r = 6r_{max}$ somewhat arbitrarily. However, we tested other choices of radii, and the results remain robust. TCs that have most of their convective events near the radius of maximum winds would have an updraft ratio close to zero, and TCs that have as many updrafts close to the radius of maximum winds as far from it would have an updraft ratio close to 0.5. To compute the inflow we create an "average" TC by aligning each center and averaging the velocity fields, as in (Ramírez Reyes and Yang, 2021). We then compute the mean radial velocity in a region bounded by the radius of maximum winds (r_{max}) and $6r_{max}$ in the radial direction and from the surface to 6 km height. We perform the calculation for all the experiments with TCs for 10-day periods between day 60 and 100 (e.g., day 60 to 70, 70 to 80, 80 to 90 and 90 to 100).

3.4 Results

Relaxation of clear-sky water vapor to its horizontal average has little effect on the domain-mean specific humidity ($\sim$ 16g/kg in Control vs 14g/kg in the experiment with $\tau_r = 0.5$h) but a larger effect in the standard deviation of specific humidity (2.1 g/kg in Control vs 1.2 g/kg in the experiment with $\tau_r = 0.5$h) (Figure 3.2). This smaller standard in the experiments with nudging implies a more homogeneous water vapor field. Furthermore, as the nudging becomes faster, the standard deviation becomes smaller.

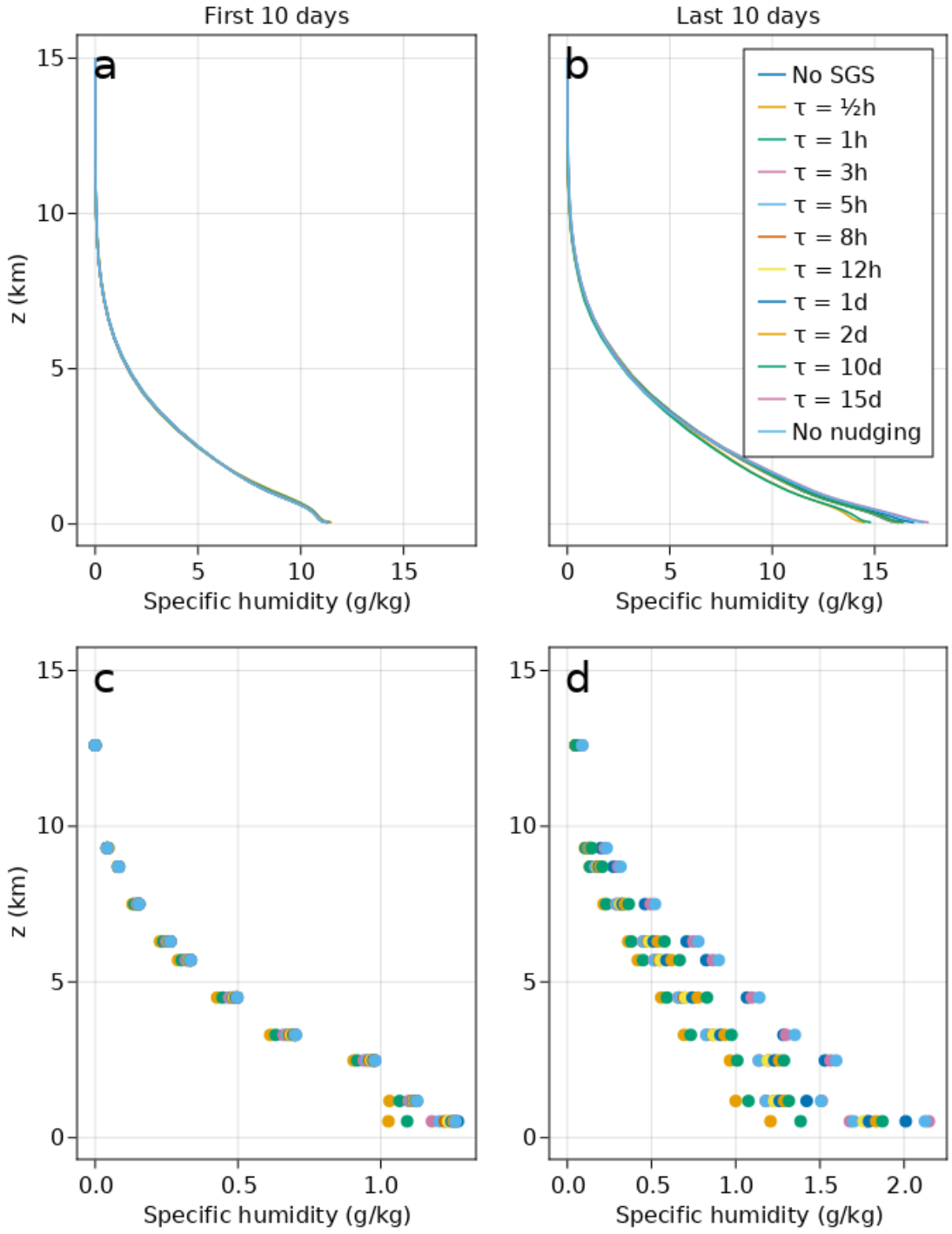

Figure 3.2: Mean profile of specific humidity averaged over the first 10 days of the simulation (a) and the last then days of the simulation (b). The standard deviation of specific humidity averaged over the first 10 days of the simulation (c) and the last ten days of the simulation (d). See section 3.5 for a note on the experiment NoSGS.

Homogenizing clear-sky water vapor on a timescale shorter than τ_d prevents spontaneous TC genesis (P1). TCs spontaneously emerge in Control and in simulations with nudging timescale τ_r between 2 hours and 15 days. However, no TCs form in simulations with nudging timescales smaller than 2 hours. In Figure 3.3 we show snapshots of precipitable water (PW), surface wind speed, and surface pressure at day 95 for a selected subset of simulations (see also Movie S1). We observe that the PW shows negligible spatial variance for the short relaxation time scales (e.g., $\tau_r = 0.5$hours or $\tau_r = 1$hour), which increases as τ_r becomes longer. In Control and $\tau_r = 15$days, there are distinct large-scale high PW regions that coincide with the TCs, which is surrounded by low PW regions. For relaxation time scales below 2 hours, we observe randomly distributed winds with maximum speeds of around 10ms^{-1}. When τ_r increases above 2 hours, we observe regions of increased surface wind speed around the eye. TCs in the experiments with τ_r between 3 hours and 5 days show modest intensities by day 60, while experiments with relaxation time scales above 10 days show similar intensities to TCs in Control.

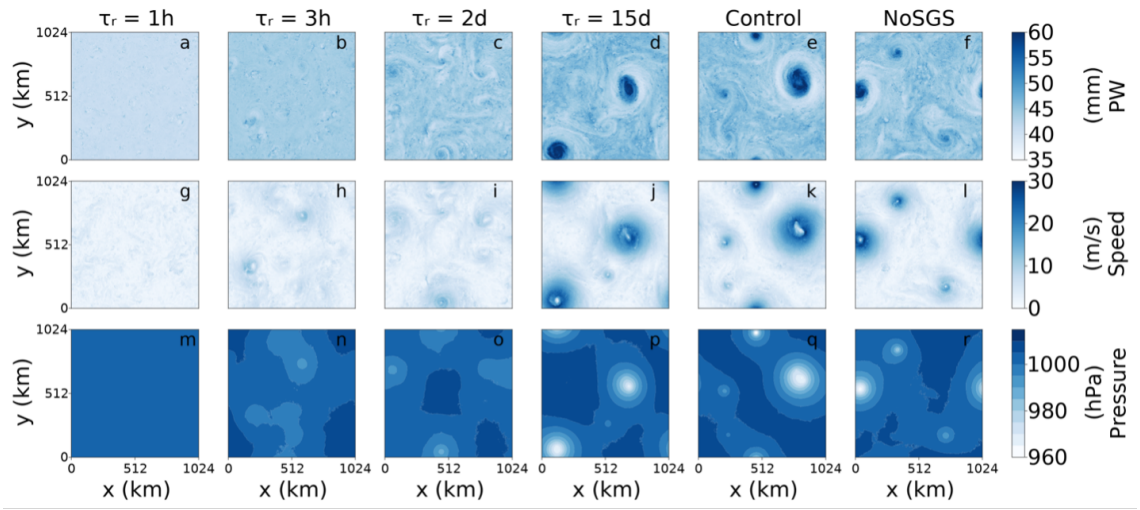

Figure 3.3: Map views of precipitable water, surface pressure, and surface wind speed at t = 95 days (snapshot). (a-f) precipitable water (mm), (g-l) surface wind speed (ms^{-1}), and (m-r) surface pressure (hPa). Columns 1-4 correspond to experiments with water vapor relaxation time scales of 1 h, 3 h, 2 days, and 15 days respectively, and the fifth column is the Control experiment and the sixth column is the NoSGS experiment (see section 3.5). Simulations with 2-km grid spacing.

Our experiments also support P2 and show that homogenizing clear-sky water vapor on a multi-day time scale prevents the intensification of spontaneously formed TCs. The behavior of

simulations can be described as three distinct regimes: No TCs, weak TCs, and intense TCs (similar in intensity to those in Control).Figure 3.4 shows the maximum surface wind speed and minimum surface pressure in the domain versus time for a selected subset of experiments (see Figure 2.8) for all the experiments). The experiments with τ_r below 2 hours show almost constant maximum wind speeds of around 15 ms^{-1} (corresponding to random wind gusts) and nearly constant minimum surface pressures of around 1000 hPa. These simulations show random convection. Experiments with τ_r higher than 2 hours show stronger wind speeds and lower pressures at the surface: after an initial intensification period, simulations with τ_r between 3 hours and 5 days show surface wind speeds and surface pressures fields that oscillate around 20 ms^{-1} and 990 hPa, corresponding to weak TCs. Finally, the experiment with τ_r equal to 15 days mimics the Control simulation, with maximum wind speeds oscillating around 40ms^{-1} and minimum surface pressures that oscillate around 960 hPa after an intensification period. These three regimes ("short" relaxation time scales with no organization, "moderate" relaxation time scales with weak TCs and "long" relaxation time scales with strong TCs) suggest that the coupling between environmental water vapor and convection may operate in two different mechanisms in TC genesis and TC intensification. A fast process is instrumental for initial convective organization and spontaneous TC genesis, and a slower process helps TC intensification. These results are consistent with P2. We note though, that the simulations with $\tau_r = 5$ days and $\tau_r = 10$ days reach similar intensities to Control by the end of the 100-day period (Figure 2.7). This suggests that the transition between the no non-intensifying and the intensifying regime may not be abrupt. A more detailed study of the transition would require a substantial increase in computational expense and is left to future work.

Here we speculate about how clear-sky water vapor homogenization on a multi-day time scale prevents the intensification of TCs. Intensification of TCs requires a strong inflow to bring air parcels closer to the eyewall while nearly maintaining their angular momentum. This amplifies the tangential wind speeds and intensifies the TC (Montgomery and Smith, 2014). Meanwhile, drying by subsidence beyond the eyewall opposes the appearance of convection beyond the TC eyewall. In our experiments, homogenizing water vapor leads to the moistening of the subsiding areas, allowing deep convective events beyond the radius of the eyewall. This increased convection

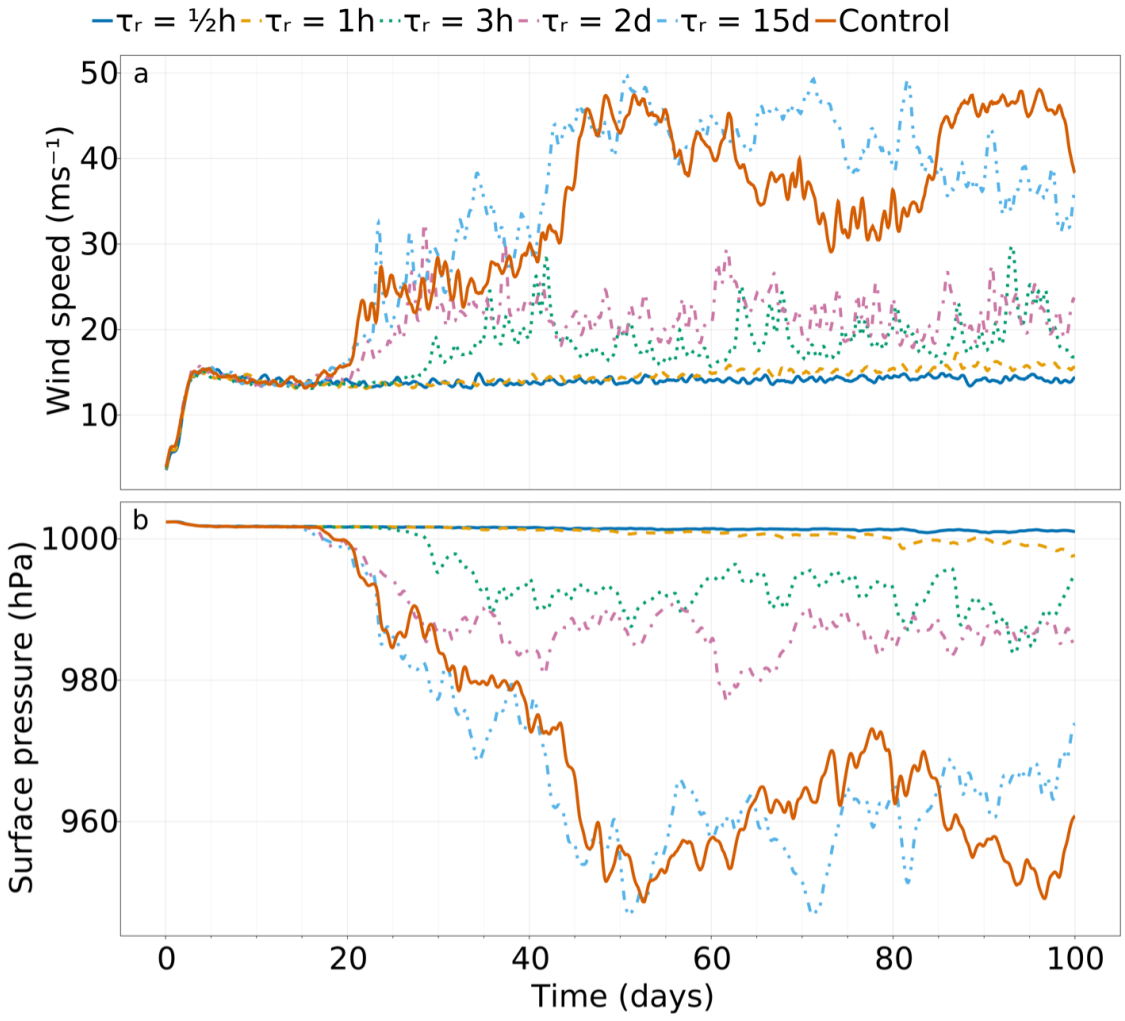

Figure 3.4: Time evolution of the maximum surface wind speed (ms^{-1}) (a) and minimum surface (hPa) (b). Hourly data is smoothed with a moving average filter with window = 12hours.

beyond the eyewall reduces the inflow to the eyewall and therefore opposes the intensification of the TCs.

To test this hypothesis, Figure 3.5 shows the relationship between mean inflow and updraft ratio, which measures how concentrated updrafts are near the radius of maximum tangential winds (a value close to 0.0 shows that convection is concentrated near the radius of maximum winds and a value of 0.5 shows that convection is uniformly distributed). In our experiments, the updraft ratio is related to the mean inflow approximately by $\log(inflow) = -2.77 * \text{updraft ratio}$ (correlation coefficient $= -0.77$), showing that TCs with most updrafts concentrated near r_{max} have a stronger inflow than those where convection is uniformly distributed at all radii, which is consistent with our hypothesis. However, we note that this is a diagnostic result and does not indicate causality. For example, it does not prove that the reduced inflow is caused by the uneven distribution of convection. Furthermore, another study found that moistening of the subsidence region of TCs with a long time scale results in a larger steady-state intensity than in a simulation with no moistening in an axisymmetric model (Rousseau-Rizzi et al., 2021). Thus, a reduction in the moisture at large radii would have two competing effects: it promotes convective organization by suppressing convection outside of the core, but it also reduces the moisture supply to the storm, which is important for development (Fritz and Wang, 2014). Other plausible explanations include that asymmetries in convection outside the eyewall may lead to the weakening of the TCs (Nolan et al., 2007a) or that the environmental maximum potential intensity of TCs is reduced by modification of the moisture field (Bister and Emanuel, 1998). However, computation of the potential intensity with the routine provided by Bister and Emanuel (Bister and Emanuel, 2002) does not support this hypothesis (see Figure 3.6). A conclusive investigation of the causes for the different intensities when weakening the MC feedback on the "long" timescales would require a deeper study.

3.5 Main findings and implications

This work answers what process is responsible for spontaneous TC genesis in the absence of radiative and surface-flux feedbacks in the simulations of Ramírez Reyes and Yang (2021). We perform mechanism-denial experiments using cloud-permitting simulations to test the hypothesis

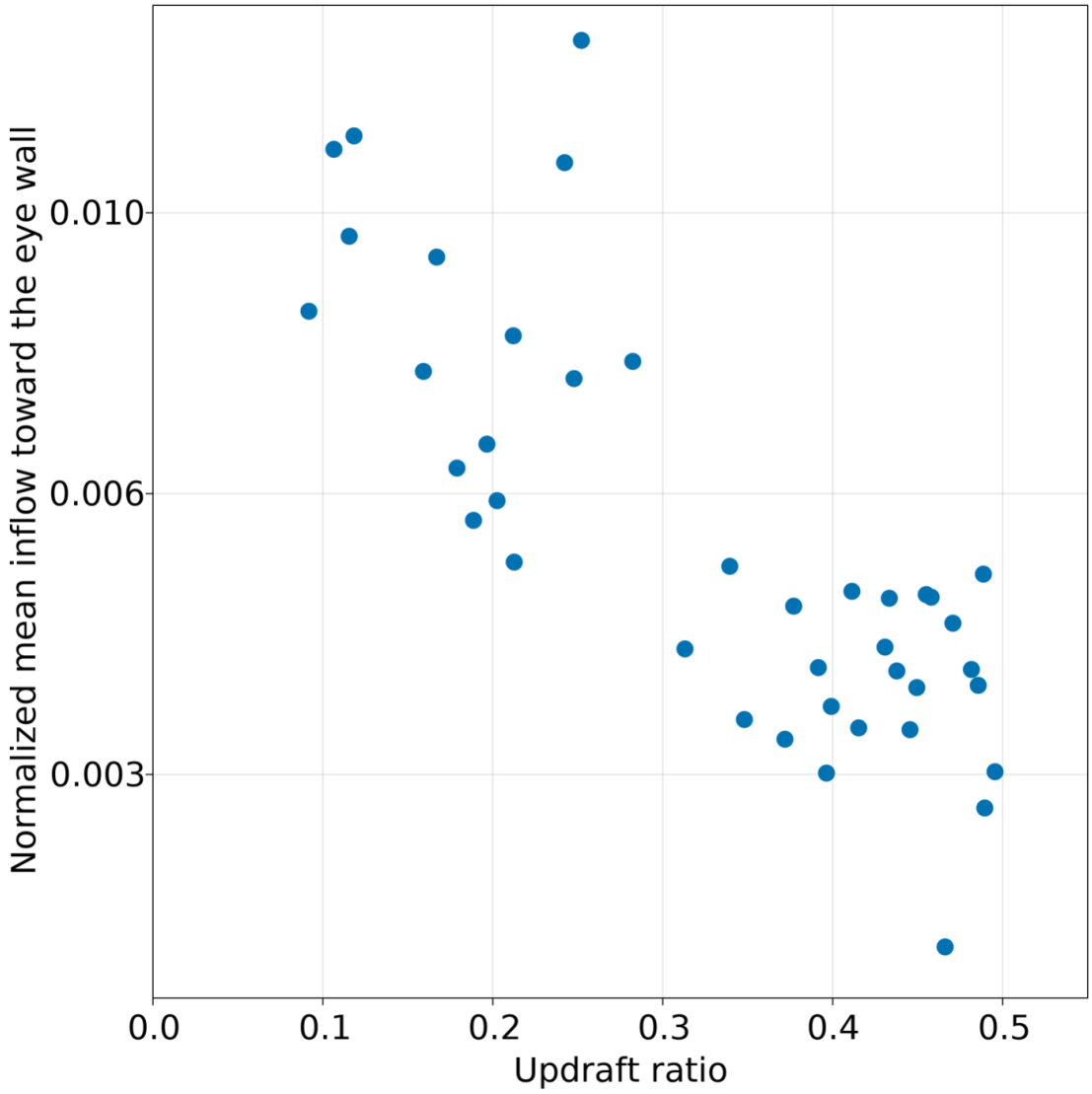

Figure 3.5: The absolute value of mean radial velocity from $r = 0$ to r_{max} and from surface to $z = 6$km, normalized by the maximum tangential wind speed vs. the updraft ratio. The vertical axis has a logarithmic scale.

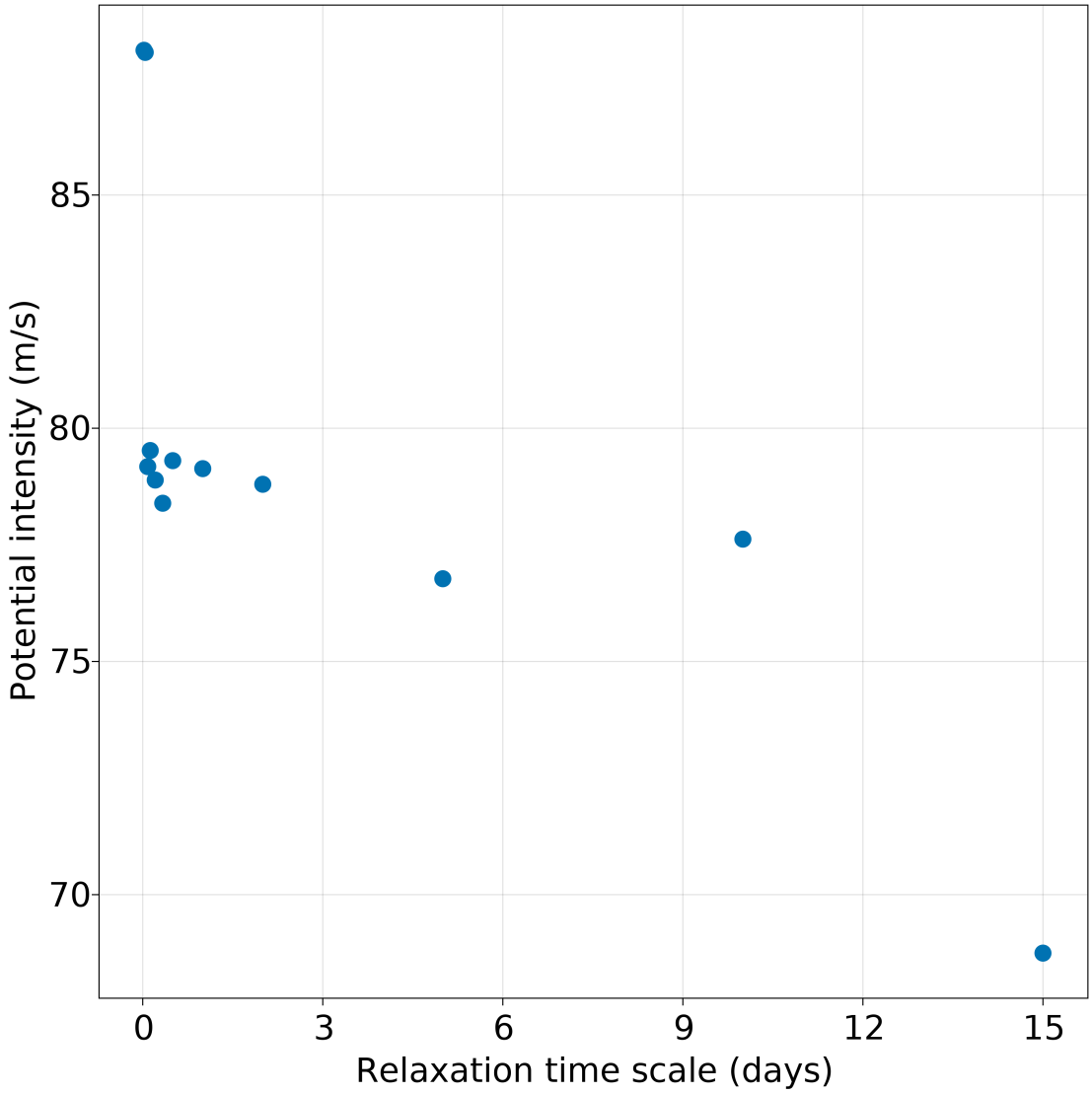

Figure 3.6: The potential intensity of simulations vs relaxation time scale

that the MC feedback is responsible for spontaneous TC genesis and intensification in the absence of radiative and surface-flux feedbacks. In the MC feedback, moisture detrained from convective clouds moistens the environment and makes it favorable for new convective clouds, and drying by subsidence inhibits convection in the region. Both processes can lead to the convective organization (Tompkins, 2001). We find that the moisture gradients created by the MC feedback lead to spontaneous TC genesis and intensification in the absence of radiative and surface-flux feedbacks.

The MC feedback influences spontaneous TC genesis and intensification in two different time scales. Using dimensional analysis, we estimate that the entrainment and detrainment time scale is about a few hours, setting the short time scale of the MC feedback. We test this prediction by weakening the MC feedback across different time scales. We observe that using a time scale shorter than 2 hours, spontaneous TC genesis is inhibited, which corroborates our hypothesis. This "fast" time scale should not be mistaken to indicate the time to genesis. Instead, this fast time scale suggests that the MC feedback is efficient and relevant for real-world TC genesis as an aide to the process of converting a pre-existing disturbance into a Tropical Cyclone. For example, this result seems consistent with the real case study of Wang (2014b), who pointed out that repeated congestus convection moistens the lower troposphere, leading to organized convection and to TC genesis. This result and previous literature highlight the importance of continuing to evaluate and improve the representation of moisture and its interaction with convection, especially in general circulation models (GCMs), which remain a primary tool for TC genesis forecasting and do not explicitly resolve convection (Halperin et al., 2020).

Subsidence drying sets a time scale of $\tilde{1}7$ days. We propose that subsidence drying promotes intensification of the TC by preventing the appearance of new convective events far from the radius of maximum winds, which would reduce the radial advection of angular momentum required for intensification of the TC (Montgomery and Smith, 2014). When we homogenize clear-sky water vapor on a multi-day time scale, we observe more frequent updrafts far from the eyewall of incipient TCs. This is accompanied by reduced inflow and lower TC intensity when compared with experiments with longer relaxation time scales or with no relaxation. This result again is consistent with our hypothesis. However, there are other possible explanations for the decreased

TC intensity when using shorter water vapor-nudging timescale. For example, vertical wind shear (Alland et al., 2017), advection of dry environmental air (Wu et al., 2015), and moisture-radiation feedbacks (Ruppert et al., 2020) can all affect TC intensity. Examining these mechanisms in our modeling framework will require future research.

Data and software availability

Following the Best Practices for Preservation and Replicability (Schuster et al., 2022), we make available the code and instructions to replicate our results. the system for atmospheric modeling (SAM) is free software and can be obtained from `http://rossby.msrc.sunysb.edu/~marat/SAM.html`. The version used in this work together with modified source code, initialization profiles, namelists and data analysis scripts are hosted on Zenodo and can be found with the digital object identifier (DOI) `10.5281/zenodo.6978839`(Ramírez Reyes and Yang, 2022a). The data was analyzed using the Julia Programming Language (Bezanson et al., 2017) available under MIT license at www.julialang.org, with the Images.jl package available with MIT license at `https://github.com/JuliaImages/Images.jl`. Figures were created using the Makie.jl package (Danisch and Krumbiegel, 2021) available under MIT license at `https://github.com/JuliaPlots/Makie.jl`.

Appendix

On the importance of the SGS parameterization at a grid spacing of 2 km

This experiment consists of one run that differs from Control only by turning off the horizontal mixing of water vapor fields from the SGS parameterization. This simulation will be referred to as NoSGS. In this study, we use a grid spacing of 2 km. At this resolution, we would expect a significant part of the entrainment and detrainment from clouds still depends on the SGS parameterization (Bryan et al., 2003; Craig and Dörnbrack, 2008; Tompkins and Semie, 2017). By turning off the SGS parameterization, we remove the unresolved portion of eddy transports, specifically the entrainment and detrainment, allowing us to directly evaluate the hypothesis that a reduction of detrainment and entrainment of clouds would inhibit TC genesis (also consistent with (Zhao et al., 2012). However, we discovered that spontaneous TC genesis still occurs in this setup. When taking

a close look at the moisture fields, Figures 2.1 and 2.2 show that turning off the horizontal mixing of water vapor by the SGS parameterization does not have a strong effect on the standard deviation of water vapor. This could imply that SAM has substantial horizontal mixing at a grid spacing of 2 km, rendering the contribution of the SGS parameterization less important. The mixing could come from resolved flows or the numerical implementation of SAM. SAM uses the finite difference method, which might be diffusive and act as an effective way of mixing water vapor. All the cited works used different numerical models. Therefore, our finding does not directly oppose theirs. We consider that the representation of mixing processes in CRMs and how these processes depend on the resolution is a problem worth revisiting in future studies.

Acknowledgments

Argel Ramírez Reyes was supported by a CONACYT-UCMexus fellowship. Da Yang was supported by Laboratory Directed Research and Development (LDRD) funding from Berkeley Lab, provided by the Director, Office of Science, of the U.S. Department of Energy under Contract DE-AC0205CH11231, and the U.S. Department of Energy, Office of Science, Office of Biological and Environmental Research, Climate and Environmental Sciences Division, Regional and Global Climate Modeling Program under Award DE-AC0205CH11231. Da Yang was also supported by a Packard Fellowship for Science and Engineering, and the France-Berkeley Fund. Argel Ramírez Reyes thanks Matthew R. Igel, Adrian Tompkins, and Chis Davis for their useful input in this work.

Chapter 4 Organization of convection in a GPU-friendly shallow water model

4.1 Abstract

Some aspects of moist convection and its organization in the Earth's tropics are still poorly represented in comprehensive models. This poor representation clouds our understanding and hinders the capacity of comprehensive models to answer important questions about convection. For example, those related to the genesis and intensification of TCs or the prediction of storm systems like the Madden-Julian oscillation. To improve our understanding of the behavior of convection, and apply this improvements to convective parameterization, simple models offer an economic and valuable resource. Here, we implement a convective parameterization into a shallow water model with GPU capabilities. We aim to build an easy-to-use, reproducible workflow using open software tools. We find that this system permits economic simulations of convective systems. We show that this model is capable of reproducing features of organized convection observed in much more complex 3D models. We further show that simple scaling arguments can predict some geometric characteristics of the organized steady state, showcasing the usefulness of simple models to improve our understanding of tropical convection.

4.2 Introduction

In Earth's tropics, deep thunderstorms tend to organize in different scales (ranging from the tens to thousands of kilometers). Some forms of organized convection are notable due to their societal impacts. For example, tropical cyclones (TCs), which intensify rapidly and continue to cost lives, and the Madden-Julian oscillation (MJO), which modulates thunderstorms in a large portion of the globe. These phenomena have been studied for decades, but major challenges remain in the

representation and prediction of some of their features in physically-based models of increasing complexity which are, in many regards, outperformed by statistical models. Some of the lacking features include the frequency of TCs in the present and future climate (Lee et al., 2020) and the onset and evolution of the MJO with more than 1-month lead time (Kim et al., 2021). Because most of these models are run at resolutions of the order of 100 km, the effects of convection are not explicitly resolved. Instead, they are parameterized. Some studies have proposed that improving the representation of convection in these models is required to improve their simulation of organized systems (Ma and Tan, 2009; Mohandas and Ashrit, 2014; Villafuerte et al., 2021; Yang and Ingersoll, 2013). Therefore, inquiring about the fundamental processes that organize convection and how they interact is fundamental to improving our understanding and bringing those improvements to the ever-more-comprehensive models.

The confluence of diverse mechanisms (e.g., radiation, phase changes, gravity waves, surface fluxes, etc) in a wide span of spatial and temporal scales in the organization of convection makes it difficult to quantify the role of certain processes in causing or maintaining the organization of convection. Recent research on simplified modeling setups has helped clarify some of these processes. Particularly, simulations of radiative-convective equilibrium (RCE, a state where radiative cooling is balanced by convective heating and has been used as a model for the tropical atmosphere) in cloud-permitting models and global circulation models have highlighted the role of the interactions between radiation and moisture in promoting self-aggregation of convection (Muller and Held, 2012; Wing et al., 2018) and TC genesis (Muller and Romps, 2018; Wing et al., 2016), which has been confirmed in the more complex real atmosphere (Ruppert et al., 2020). Similar RCE studies have successfully studied the role of evaporatively driven cold pools (Jeevanjee and Romps, 2013), Coriolis parameter (Nolan et al., 2007b; Zhou et al., 2013), sea surface temperatures (Khairoutdinov and Emanuel, 2013), and the moisture-convection feedback, which is enough to create TCs in rotating RCE but not self-aggregation in the non-rotating case (Ramírez Reyes and Yang, 2022a) (note that in the preceding list, we have mentioned studies of both, non-rotating self-aggregation and spontaneous TC genesis, recognizing that the same mechanisms may be important to both phenomena.)

While the RCE framework in cloud-resolving and global circulation models has yielded many insights about convection, it has some drawbacks. For example, both CRMs and GCMs are expensive to run on large domains or for long times, which causes, among other things, RCE studies to be constrained to case studies for the lack of large, statistical samples. At least two avenues are open to alleviate the computational expense while still gaining scientific insight. First, exploring conceptually simpler models capable of producing atmospheric-like dynamics in the presence of convection is a good avenue to pursue. A conceptually-simple model allows for studying convection and its organization analytically tractably. The second avenue suggests profiting from modern computer architectures. Accelerating suitable parts of the models using state-of-the-art hardware has become a growing necessity to make scientific inquiry more efficient and affordable.

On the use of modern computer architectures for computer models, the usage of general-purpose graphics processing units (GPUs) has gained relevance in the last decades. By March of 2023, 7 of the 10 highest-rated supercomputers have GPUs as one of their main computing hardware (Top500, 2022). A GPU is a processing unit that performs parallel workflows (Besard et al., 2019b). Scientific workflows, including hydrodynamical simulations, can benefit from this hardware, making simulations faster and more cost-effective (Ramadhan et al., 2020) compared to their CPU-only equivalents. Additionally, general-purpose GPUs are currently available even in consumer-grade laptops, increasing the applicability range of GPU-capable scientific software.

Regarding the avenue related to conceptually simpler models, a suitable starting point is the shallow water model (Vallis, 2016). The shallow water model is among the simplest models that can produce atmospheric-like dynamics. It has successfully explained some of the features of the tropical atmosphere variability. Notably, Matsuno (Matsuno, 1966) analyzed the wave dynamics of the Shallow Water equations and obtained the relations between frequency and wavenumber (dispersion relation) that tropical waves had to satisfy. It was later observed that most of the tropical convective activity occurs along the phase relations predicted by Matsuno (Wheeler and Kiladis, 1999), highlighting the importance of simple models. Following the success of the "dry" shallow water system of equations, it has been extended to consider some of the thermodynamic effects of moist convection in the tropical atmosphere. These studies have successfully represented

more features of tropical atmospheric variability. Gill (1980)'s pioneering work is the canonical example of this kind of model. More recently, shallow water models have been used to study the Madden-Julian oscillation (Yang and Ingersoll, 2013, 2014), convective self-aggregation in one dimension (Yang, 2021), and TC-like vortices (Lahaye and Zeitlin, 2016).

In particular, (Yang, 2021)'s model represents convection as a triggered process that can be interpreted as an accumulation of convective available potential energy that is released over a finite duration. This way of viewing convection as a triggered process (different from the convective quasi-equilibrium view (Arakawa and Schubert, 1974; Emanuel et al., 1994)) has proven to be useful in global circulation models, where it successfully represents some forms of convective organization, like the MJO (Hung et al., 2013; Yang and Ingersoll, 2013, 2014). Yang (2021)'s model is a 1-dimensional linear shallow water model with parameterized convection representing the planetary boundary layer. However, with minimal changes, it can be interpreted as representing the tropical free troposphere (Yang and Ingersoll, 2013). In Yang's model, there are no interactive radiation or interactive surface fluxes, but convection aggregates into one or more patches after starting from a random state. This highlights the importance of boundary layer processes in the aggregation of convection observed in three-dimensional CRM models. The simplicity of the one-dimensional model that produced convective self-aggregation allowed deriving a simple scaling law that predicts the spacing between different convective aggregates, which added to previous theories of the size of convective self-aggregation (Arnold and Putman, 2018; Wing and Cronin, 2016). However, because of its only dimension and linear dynamics, this simple model could not explore some other features of convective self-aggregation. Among the questions that arise from Yang's studies are: will the equivalent 2-D model produce self-aggregation? If adding rotation, will it produce TCs? Will a non-linear version of the model produce other forms of aggregation?

In this work, we build on Yang (2021)'s Shallow Water model. We aim to implement a parameterized convection scheme to a two-dimensional non-linear shallow water model to be able to run large-domain, long simulations of RCE while profiting from GPU-accelerated computers. We will show that in the steady state, this model can give rise to convective self-aggregation despite its simplicity, which may open the door for new simplified studies of the atmosphere. The implementation

of this model will pave the way to answer questions like:

1. Can a 2D non-linear Shallow water model with parameterized convection produce convective self-aggregation?
2. If yes, what sets the geometrical characteristics of the aggregates?
3. Are these processes relevant to the real atmosphere?
4. Can TCs *spontaneously* emerge in shallow-water f plane simulations?

And we will show our advances toward answering these questions. Because a wide exploration of the parameter space in the shallow water model requires a large number of simulations, this work focuses on implementing the shallow water model in a high-performance, portable, and flexible way that allows us to run hundreds of simulations with limited computational and time resources. Additionally, the main goal of this work is to answer our questions in a reusable, transparent, reproducible, and extensible manner that can be extended by others in the scientific community, following the precepts of open science (Mullendore et al., 2021).

The chapter first introduces the shallow water model and its convective parameterization. In section section 4.3, we discuss the implementation of the parameterization using the Julia language. In section section 4.4, we explore some of the parameter space accessible to this model and simulation results, which are then discussed in section section 4.5.

4.3 Methods

4.3.1 The shallow water model

The shallow water model, including the convective parameterization from (Yang and Ingersoll, 2013) consists of the following equations:

$$\frac{\partial u}{\partial t} + u\frac{\partial u}{\partial x} + v\frac{\partial u}{\partial y} - fv = -g\frac{\partial h}{\partial x} - \frac{u}{\tau_d} \tag{4.1}$$

$$\frac{\partial v}{\partial t} + u\frac{\partial v}{\partial x} + v\frac{\partial v}{\partial y} + fu = -g\frac{\partial h}{\partial y} - \frac{v}{\tau_d} \tag{4.2}$$

$$\frac{\partial h}{\partial t} + \nabla \cdot (\mathbf{u}h) = \sum_i Q_i(x, y, t, t_i) + F_{ls} - \frac{h - h_0}{\tau_d}, \tag{4.3}$$

where u and v are the components of the velocity and h is the height of the model, f is the Coriolis parameter, τ_d is a timescale of damping, g is the acceleration of gravity, F_{ls} a large scale forcing that is constant in time and space, and $\sum_i Q_i(x, y, t, t_i)$ is the representation of the aggregated effects of individual convective events $Q_i(x, y, t, t_i)$ centered at point (x_i, y_i) that was triggered at time $t = t_i$, for i identifying all the convective points active at a given time in the domain. We first discuss the terms without the representation of convection. The left-hand side is the time tendency, the advection, and the Coriolis terms of the typical shallow water system (see, e.g., (Vallis, 2017)) with rotation. The first term on the right of 4.1 and 4.2 is the pressure gradient force, and the last term of the right of all equations is a linear damping term. A linear damping with the same damping constant in all three terms has been used before in shallow water studies, for example (Gill, 1980; Lindzen and Nigam, 1987; Neelin, 1989; Yang, 2021). In this model, damping in the momentum equations could be interpreted as damping due to surface friction. F_{ls} is a positive term that is homogeneous in space and constant in time. It represents the aggregated effect of surface fluxes and radiative cooling. Each individual convective heating acts as a mass sink given by

$$Q_i(x, y, t) = \begin{cases} -\frac{q_0}{\pi r_c^2 \tau_c}\left[1 - \left(\frac{\Delta t_i - \tau_c/2}{\tau_c/2}\right)^2\right]\left(1 - \frac{r_i^2}{r_c^2}\right) & \text{when a convective event is active at point}(x_i, y_i) \\ 0, & \text{otherwise.} \end{cases} \tag{4.4}$$

In Equation 4.4, q_0 (units of length to the third power), τ_c (units of time), and r_c (units of length) are the magnitude, duration, and radius of each convective event, Δt_i is the time that has passed since the last convective event centered at point $i = (x_i, y_i)$ started, and r_i is the distance between (x, y) and (x_i, y_i). A convective event is triggered at point (x_i, y_i) when h_i (the height field

at that point) exceeds a certain threshold h_c. These convective events represent a mass sink with a finite duration τ_c.

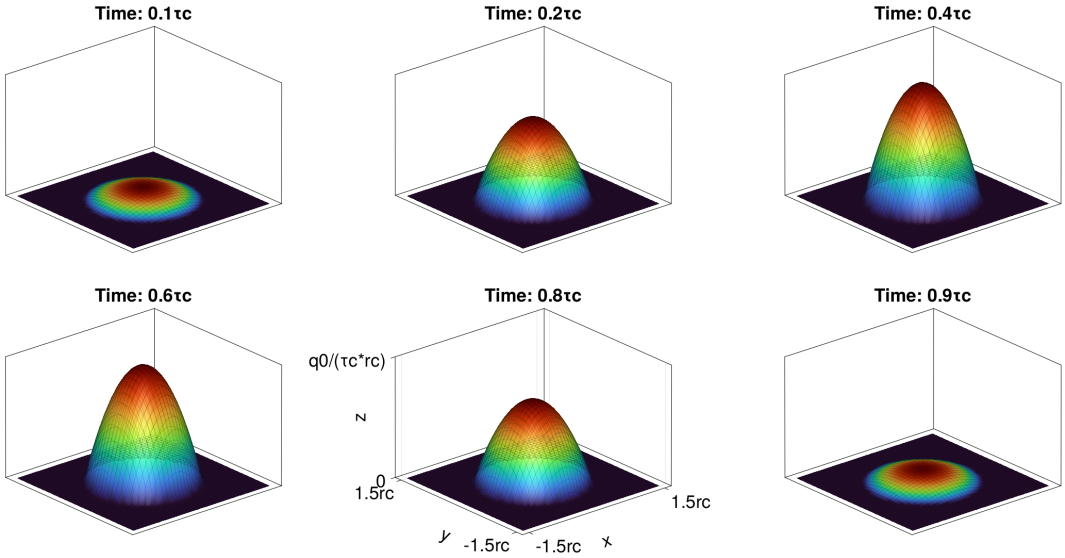

Figure 4.1: The shape of one convective event for different times

Each convective event removes mass in a circular area around its center. The amount of mass removed is higher at the center and at half of the convective period of length τ_c. It decreases with the radius until r_c, where it becomes zero. An illustration of one convective event at different times since its triggering can be observed in Figure 4.1. Averaged over time and in the whole domain, F_{ls} (a mass source) will balance the aggregated action of all the convective events in the domain, giving rise to a "radiative-convective equilibrium" steady state. In this state, the average number of convective events per unit time per unit area is proportional to $S_c = 3\frac{F_{ls}}{S_q}$. We call this number the number density of convective events.

Table 4.1 shows a summary of the tunable parameters of the model, including the convective parameterization.

4.3.2 Implementation of convective parameterization in a GPU-friendly way

This section will describe the model's implementation and a scalability benchmark for CPU and GPU implementation. The code is hosted on `https://github.com/aramirezreyes/RamirezReyes_`

Symbol	Name	Units
f	Coriolis parameter	1/s
g	gravitational acceleration	m/s^2
F_{ls}	Large-scale forcing	m/s
τ_d	Damping timescale	s
q_0	Amplitude of convection	m^3
r_c	Radius of convection	m
τ_c	Convection timescale	s
L_z	Initial height of the model	m
h_0	Relaxation height	m

Table 4.1: List of tunable parameters of the shallow water model

`ShallowWaterInFPlane` and designed with the reproducibility of experiments as one of the core principles.

We extend the shallow water model in Oceananigans.jl (Ramadhan et al., 2020). Oceananigans.jl is written in the Julia programming language (Bezanson et al., 2017), a high-level, dynamically typed, compiled language emphasizing technical computing. The shallow water model is solved using a finite volume discretization, with a fifth-order WENO advection scheme (e.g., (Lunet et al., 2017) and the integration in time uses the fourth-order Adams-Brashforth scheme. Oceananigans.jl allows the model to run on a system with Nvidia GPUs. The Julia language represents an ideal choice for our purposes. Julia contains infrastructure to emit code for different hardware platforms, which means that code written in Julia can be run on GPUs or CPUs with minimal modifications (Besard et al., 2019a,b). Finally, Oceananigans.jl counts with a well-documented and extension-friendly code base.

Because Oceananigans.jl's shallow water model already solves the non-linear, rotating, shallow water equations, we need only extend the solvers to add the convective forcing (first term on the right-hand side of Equation 4.3), the damping terms (last term on the right-hand side of Equation 4.1, Equation 4.2 and Equation 4.3), and the large-scale forcing (second term in the right-hand side of Equation 4.3).

One complication with our convective scheme is that its effects are nonlocal: once a convective event is triggered, it affects its surrounding points immediately within a radius R_c. This implies

that $n \sim R_c/\Delta x$ points will be affected in each direction at each timestep for each convective point. If one point is within reach of more than one convective event, it will simultaneously receive the contribution of all of them. Designing a parallelization strategy entails possible data race conditions: in a naive parallel implementation, two points could read from and write to the same point simultaneously if such a point is within reach of two distinct convective events. Considering this, we design the algorithm to imply more read/write operations but allow for a greater degree of parallelism. We describe the implementation in the following, and the code referenced can be found at `https://github.com/aramirezreyes/RamirezReyes_ShallowWaterInFPlane`.

First, let us assume that the height and velocity fields at each time step are stored in two-dimensional arrays of size $n \times m$, where n and m are the numbers of points in the x and y directions, respectively. In our implementation, we use two auxiliary arrays of the same size: **convection_triggered_time**, which stores floating point numbers indicating at what time the most recent convective event started in each point of the domain, and **isconvecting** which stores a boolean value indicating if this point was convecting during the previous timestep. Both auxiliary arrays are necessary due to two features of the representation of convection: first, the convective parameterization is nonlocal in time (the finite duration of convection implies that a convective event lasts for a predefined period even if the conditions to trigger convection disappear early in the life of the convective event), and second, it is nonlocal in space. Therefore we need two arrays to store "the memory" of the convective system. The parameterization is then comprised of two functions: one which updates the auxiliary arrays after the dynamical fields have been updated (**update_convective_events**) and one that applies the convective heating (**convec_heating**) to the height field.

We first explore **update_convective_events**. This function performs the operations described in Algorithm 1. In this part of the procedure, the value that the auxiliary arrays will receive in each index (i, j), depends on the value of other fields only at the same position (i, j). Therefore this function is trivially parallelizable (no more than one task, process, or work unit will read or write to the same index simultaneously). On the other hand, the function that applies the heating takes the form shown in Algorithm 2.

Algorithm 1 update_convective_events

input/output : isconvecting, convection_triggered_time :: Matrix{Float64}
input: h :: Matrix{Float64}
input: t, τ_c, h_c :: Float64

procedure UPDATE_CONVECTIVE_EVENTS(isconvecting,convection_triggered_time,h,t,τ_c,h_c)
    for all indices (i,j) **do**
        time_convecting ← t - convection_triggered_time
        needs_to_convect_by_time ← isconvecting **and** time_convecting $\leq \tau_c$
        needs_to_convect_by_height ← h $\geq h_c$
        will_start_convecting ← needs_to_convect_by_height **and** not(needs_to_convect_by_time)
        isconvecting ← needs_to_convect_by_time **or** needs_to_convect_by_height
        if will_start_convecting **then**
            convection_triggered_time ← t ▷ Only update time if is new convective event
        end if
    end for
end procedure

Algorithm 2 heat

input/output : isconvecting, convection_ triggered_ time :: Matrix{Float64}
output: heat :: Float64

procedure HEAT(isconvecting,convection_triggered_time) Parallel:
    for all indices (i,j) **do**
        for all indices ii,jj between - $R_c/\Delta x$ and $R_c/\Delta x$ **do**
            if isconvecting[i + ii, j + jj] **then**
                $distance_{sq} \leftarrow \Delta x^2(ii^2 + jj^2)$
                if $distance_{sq} < R_{sq}$ **then**
                $h[i,j] \leftarrow h[i,j] + q(distance, t, \tau_c)$
                end if
            end if
        end for
    end for
end procedure

In this case, to prevent race conditions, each processing thread takes care of computing the total heating that one point (i, j) will receive at the time, and all the points in the domain are covered, even if no convective events affect it, in which case the function returns zero. Each process iterates the whole neighborhood of its assigned point in the domain and collects the contributions of each neighboring event to its current index. This implies that each process will read and write only to its own assigned index, avoiding race conditions and making the problem embarrassingly parallel (with no needed communication between tasks) (Wikipedia contributors, 2023). Unfortunately, in this approach, all of the points must be visited in the outer loop of Algorithm 2, even if they are not in the neighborhood of any convective event. This could lead to slowdowns because if there are only a few convective points of the domain, the result of most of the evaluations will be zero, implying that many operations were unnecessary. The slowdown effect may be more noticeable if only a few convective points exist in the domain. An alternative approach consists in first identifying the convective points. Then each task could add the contributions of one convective event to their surroundings. This approach avoids doing computations for points that will not be affected but convection in a given time step. However, it leads to race conditions and is not easily parallelizable for the aforementioned reasons. Finally, if all the points were convecting simultaneously, both approaches would incur the same number of tasks accessing the same memory indices. They thus would be equivalent in terms of duration. Our selected approach offers good performance improvements due to parallelization; thus, it is deemed a good option (see section 4.5).

We set up **update_convective_events** as a "callback" function, an arbitrary function that is called between time steps. Finally, we embed the heat function as a "forcing" in the h field, to which we append the large scale forcing and the relaxation terms (Algorithm 3). This function will be called by Oceananigans.jl when solving the time evolution of the h field. The damping on the u and v fields is implemented similarly, but the only term on that forcing is the relaxation (without including the heating or the large-scale forcing).

Finally, these two algorithms were implemented using CUDA.jl functions to ensure their usability on GPUs, and regular Julia code for CPU-only operations. This allows us to compare the CPU and GPU implementations' performance and increases our code's usability. The CPU version uses

Algorithm 3 forcing

input: isconvecting, convection_ triggered_ time :: Matrix{Float64}
input: $\tau_c, i, j, h0, \tau_d, f_{ls}$
output: forcing :: Float64
1: $forcing \leftarrow heat(i,j) - (h - h0)/\tau_d - f_{ls}$

two forms of parallelization: vectorization and multi-threading. This is consistent with other parts of Oceananigans.jl. In the future, it is desirable to migrate the design to use KernelAbstractions.jl. KernelAbstractions.jl allows one to write some functions in a hardware-agnostic way, allowing one to write the code once and being able to run it on CPUs and multiple GPUs, including manufacturers such as NVIDIA, AMD, Intel, and Apple. An approach like this would require little time investment, but we let it for future work.

4.3.3 Benchmark simulation design

To benchmark the performance and behavior of our model, we design the following simulation as a reference experiment for this work:

Ly,Lx	f	h_c	τ_c	τ_d	c	q_0	F_{ls}	S_q	Length	Δt	# points	boundaries
48e6 m	0.0 s^{-1}	40 ms^{-1}	4 hours	0.8 day	20 ms^{-1}	5.0×10^7 m^3	3.73×10^{-7} ms^{-1}	7.46×10^{-15} $m^{-2}s^{-1}$	200 day	40 s	$(6000)^2$	periodic

Table 4.2: Parameters used in the reference experiment

We selected the parameters in Table 4.2 for the following considerations. First, the domain is large enough to be comparable to the earth's circumference in the tropics, which helps us benchmark the model in the largest domains that could be relevant for earth-like dynamics. It has many points that help us test the advantages of our GPU implementation and compare it with a CPU run. Our reference simulation also has an earth-like gravity wave speed and similar damping timescales as those used in previous studies of earth tropics (Yang, 2021; Yang and Ingersoll, 2013), which serves as a stepping stone for work relevant for Earth's tropics. The grid spacing is equal in both spatial dimensions $\Delta x = Lx/\#points = 8km$, which allows us to have $44 \text{ points} = \frac{\pi r_c^2}{\Delta x^2}$ points per convective point. The timestep is too conservative when the forcing is small (e.g., in this case, with

a wind velocity of $1m/s$, the Courant-Friedrichs-Lewy number is $CFL = U\frac{\Delta t}{\Delta x} = 0.05$, however, this timestep will allow us to vary the magnitude of the forcings q_0 and F_{ls} and the convective timescale τc without occupying ourselves with adjusting the timestep. Oceananigans.jl counts with infrastructure to use an adaptive time-step, but we have not used this functionality yet.

4.3.4 Expectations from the reference experiment

We can expect that Equation 4.1 - Equation 4.3 will give rise to gravity waves with a phase speed of $c = \sqrt{g\bar{h}}$ if the forcing is small so that the dynamics can be considered linear (Vallis, 2017; Yang, 2021) where $\bar{h}$ is the mean height of the model. Then, we can identify some characteristic length scales from our list of parameters. In comparing them, we can learn how the system will behave in different regions of the parameter space. A more formal analysis based on Buckingham's Pi theorem can be realized (Yang, 2021; Yang and Ingersoll, 2014), but for the time being, a simple analysis will suffice to gain some expectations of how our model will behave.

4.3.5 Characteristic length scales of the system

Here, we introduce some characteristic length scales that can be built by combining the parameters of the model:

- $l_d \coloneqq c\tau_d$ is the distance a gravity wave can travel before its amplitude is reduced by a factor of e (Euler's constant) by damping.
- $L_R \coloneqq c/f$ is the Rossby radius of deformation (the distance over which rotation may affect the movement). When the rotation rate is zero, this quantity becomes infinite and irrelevant.
- $L_c \coloneqq c\tau_c$ is the length traversed by a gravity wave during the lifecycle of a typical convective event.
- $l_{mfp} \coloneqq (c/Sq)^{\frac{1}{3}}$ can be interpreted as the "mean free path" or the average distance a gravity wave can travel without encountering a convective event (Yang, 2021; Yang and Ingersoll, 2013, 2014).

From here, we can identify some regions of the parameter space:

1. If $l_d >> l_c$ and $l_c > L$, the gravity waves created by one convective event can interact with the same event due to the periodic boundary conditions. This regime may be of little interest to the real atmosphere. However, it can give rise to interesting phenomena like resonance.

2. On the other hand, if $l_d >> l_c$, $l_d > l_{mfp}$ and $l_c < L$, this means that the gravity waves generated by one convective event can interact with other convective events but not with themselves. We consider that this part of the parameter space may be interesting for atmospheric phenomena.

For our reference simulation, the characteristic length scales take the following values:

Ly,Lx	L_R	l_d	l_{mfp}	l_c	R_c
48×10^6	∞	1.3824×10^6	138.9×10^3	288×10^3	30×10^3
m	m	m	m	m	m

Table 4.3: Characteristic lengths in the experiment

This implies that the simulation is in the second regime from the preceding list.

4.3.6 Parameter exploration

To better quantify relations between the behavior of the simulations and its parameters, we design simulations in which we keep some parameters constant but we vary another parameter. We list these simulations in the following table.

Table 4.4: Summary of simulation parameters in the sensitivity experiments.

Name	Parameter changed	Base configuration	Description of change	Simulation length
Var_{nx}	N_x	Reference	$N_x \in \{3000, 1500, 750, 375, 250, 125, 62, 60\}$	200 days
Var_c	L_z	Reference	$L_z \in \{40, 80, 160, 240, 320\}$	200 days
Var_f	f	Reference	$f \in \{1^{-5}\}$	200 days

4.3.7 Detection and characterization of aggregates

We use the convective heating field of the output to detect independent aggregates. Our reference simulation has $6000 \times 6000 = 36 \times 10^6$ points. To avoid using memory unnecessarily, we only read the data every 5 indices in each direction, ending with an array of 1200×1200 points for each timestep. In our tests, this array works well to identify the aggregates, and the whole output is unnecessary. We first apply a two-dimensional Gaussian filter to a snapshot of the convective heating field to eliminate some of the noise caused by individual peaks. Then we "mask" the points with values smaller than $-q_0/2$. At this point, we have an array of boolean values. Because we are using doubly periodic boundary conditions, some of the aggregates are simultaneously in two distant places (half of it adjacent to one border and half adjacent to the opposite border). We replicate the image in an "extended domain": a 3×3 grid that we will use temporarily to identify each aggregate only once finally. At this point, we have 9 copies of the image. We then use the function *label_components* from the package ImageMorphology.jl to identify individually connected regions of convection (in our case, the convecting aggregates). For each region, we compute the cartesian indices corresponding to its centroid by taking the average of all x and y positions that are inside the aggregate. Finally, to avoid double counting, we drop all the aggregates whose centroids are outside of the original domain but inside the "extended domain". This effectively gives us a list of the centroids of each individual aggregate at one timestep. We then can repeat this process for all the desired timesteps to have a list of all the aggregates and their positions vs. time.

4.4 Results

The GPU implementation achieves important performance improvements with respect to the CPU implementation. Figure 4.2 compares the run-time of the Var_{nx} simulation using a CPU node in the Cheyenne supercomputer with 72 CPU threads vs. using 1 GPU in a GPU node of the Casper supercomputer, both at NCAR. The speedup is larger for very small domains (higher than 10x for domains with less than half a million points). Then it decreases, presumably in a region where a larger workload offsets the cost of launching different CPU threads. Then it increases again to

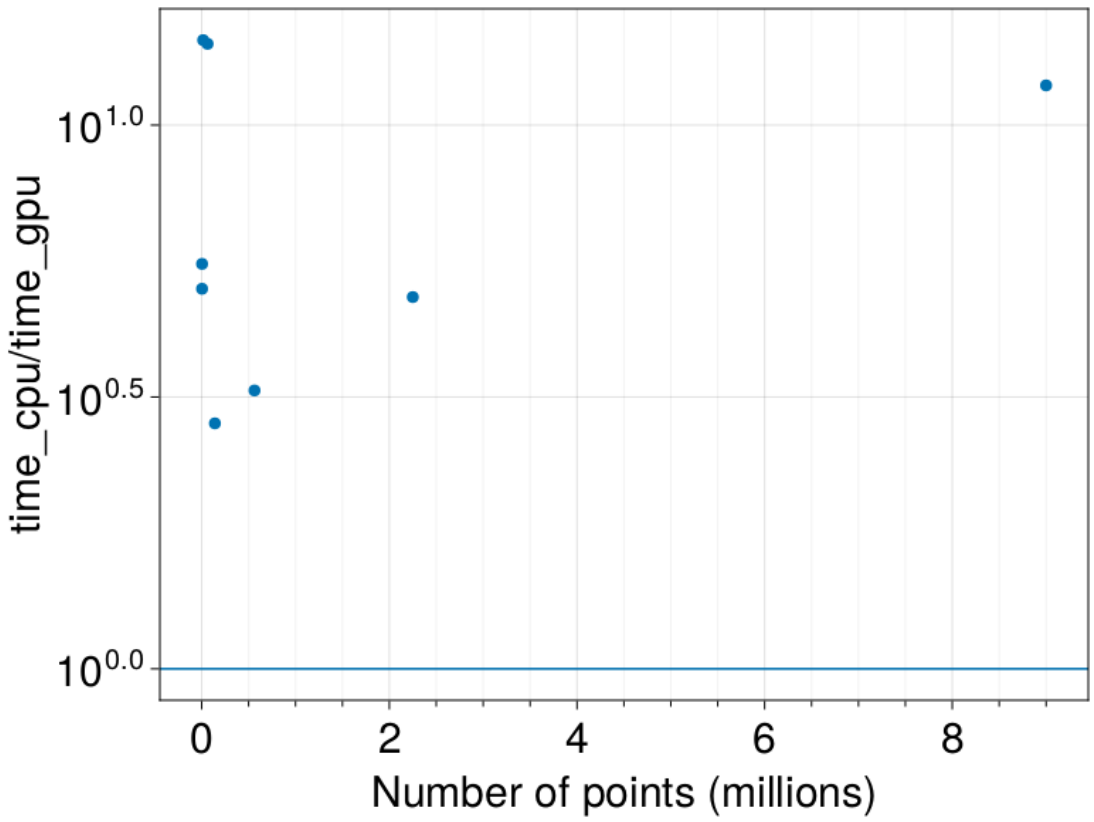

Figure 4.2: Speedup of the GPU vs the CPU implementation

larger than 10 for very large domains (larger than 10 million points). There is no clear methodology to compare performance gains between a CPU and a GPU model because both architectures are substantially different and, thus, difficult to compare. Here we compare them in terms of cost in a fashion that resembles the methodology of (Ramadhan et al., 2020). In our case, we consider the time needed for one computing node of the same supercomputing center to solve the same problem in both approaches. This makes sense, considering that some supercomputing centers charge usage per node-hour, making our comparison useful to estimate distinct costs. This methodology is not perfect, but it is useful as an illustration. Another important point is that a typical GPU node has more than 1 GPU. In our tests, at least 4 simulations can be run simultaneously for a full load in a node. Therefore, the speedups shown in Figure 4.2 could arguably be increased by a factor of 4.

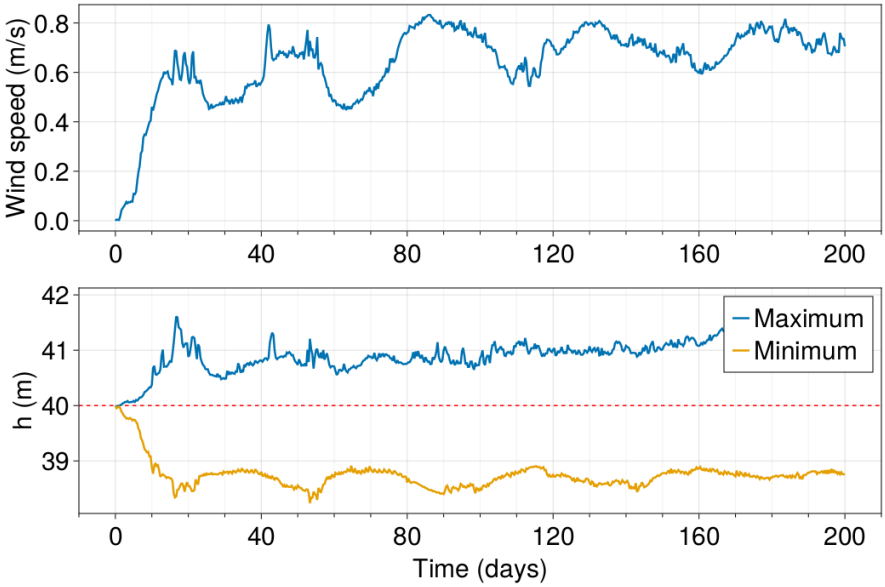

Figure 4.3: Time evolution of maximum wind speed (upper panel) in the domain, maximum height and minimum height (lower panel). The red line indicates the convective threshold h_c

Figure 4.3 shows the time evolution of maximum wind speed in the domain and the extrema of h. In our reference simulation, the wind speed increases from zero (the starting condition) when convection starts acting. It increases until day 30, when it reaches around 0.6m/s. After, it decreases and increases again. After day 80, it oscillates around a value of 0.7ms^{-1}, in what appears to be a steady state. The height field starts from random noise around $h = 39.9$m. It starts varying

when convection is triggered for the first time. After day 40, the variations in maximum height reach around $\pm 1m$, which is around 2.5% of its mean value. With this, we expect the dynamics to be linear in the reference simulation. When we decreased the forcings (F_{ls} and q_0) by a factor of 10, we found the time evolution of wind speed and height to evolve similarly to the reference simulation seems to confirm the linearity of the dynamics in this regime.

Convective events occur in a region of "low pressure" (low height in our model) when observing the slow-varying components of the fields. Although convection is triggered by anomalously high pressure ($h - \bar{h} > 0$ in the model), the points of high local pressure are embedded in a larger-scale region of low-pressure when observed in a time-smoothed field. Figure 4.4 shows a snapshot of a region that is rich in convection. The left-hand panels show a snapshot (upper) and a 5-day moving average (lower) of height, and the right-hand side shows the corresponding convective heating field. We can see that while the snapshot shows positive and negative height anomalies, the smoothed field shows all negative height anomalies in the region that coincides with the convective heating, showing that convective heating occurs in a slow-changing region of low pressure.

Convection self-aggregates into one or two regions of convection surrounded by a large space devoid of convection. Figure 4.5 shows snapshots of the reference simulation's days 2, 6, 13, and 73. The upper panels show convective heating, and the lower panels show wind speed. On day 2, convection is randomly distributed through the domain. By day 6, convective heating is concentrated in long filaments, and the wind speed has increased around the regions of convective heating. By day 13, the convective heating is concentrated in large-scale blobs of around 5000km on each side, and the wind speed has continued increasing. Finally, by day 73, only two convective regions remain. These convective regions are long, with a length of around 12000km and a width of the order of 2000km. The convecting aggregates comprise small-scale convective events and gravity wave activity visible on the lower panels and in Figure 4.6. Gravity waves propagate away from the aggregates, which travel in the domain at a velocity of around 10ms^{-1}, which is about one-half of the gravity wave speed in the reference experiment. The wind speed is smaller in the center of the aggregates and larger toward the edges, reaching wind speeds of 1ms^{-1}.

Convective aggregates displace along the diagonal directions at a speed that is approximately

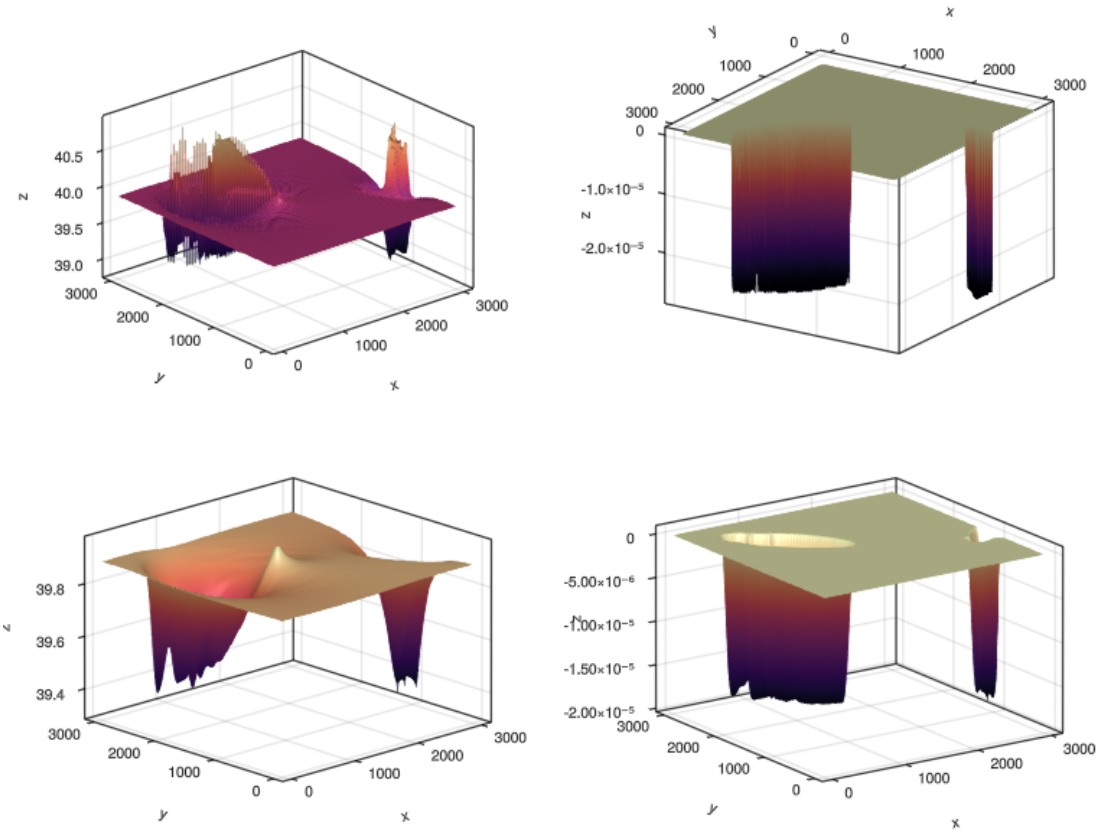

Figure 4.4: A convective event and its smoothed picture

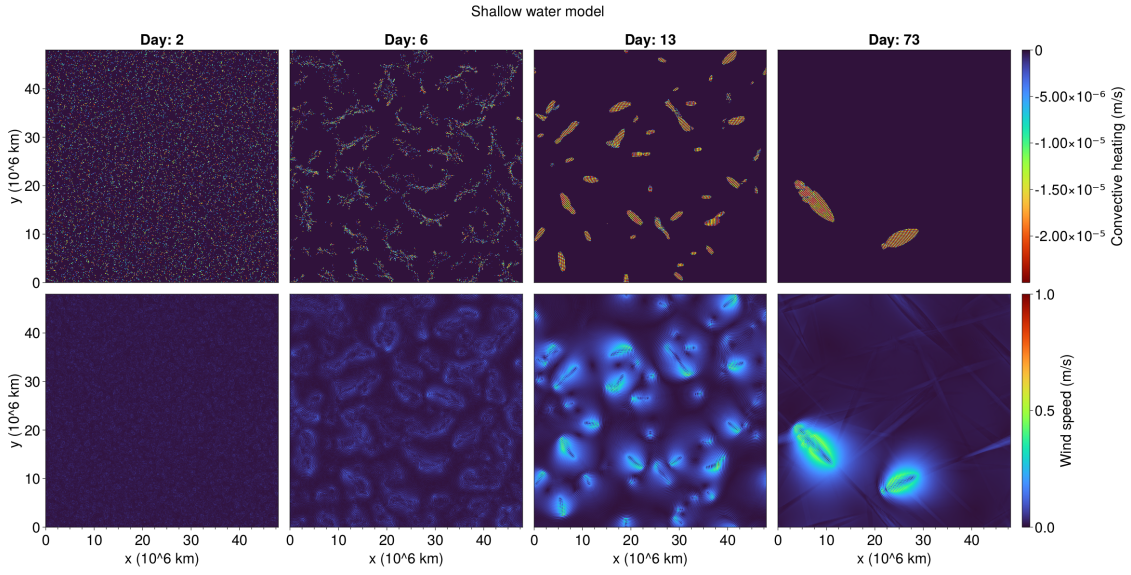

Figure 4.5: Snapshots of wind speed and convective heating fields for four different times.

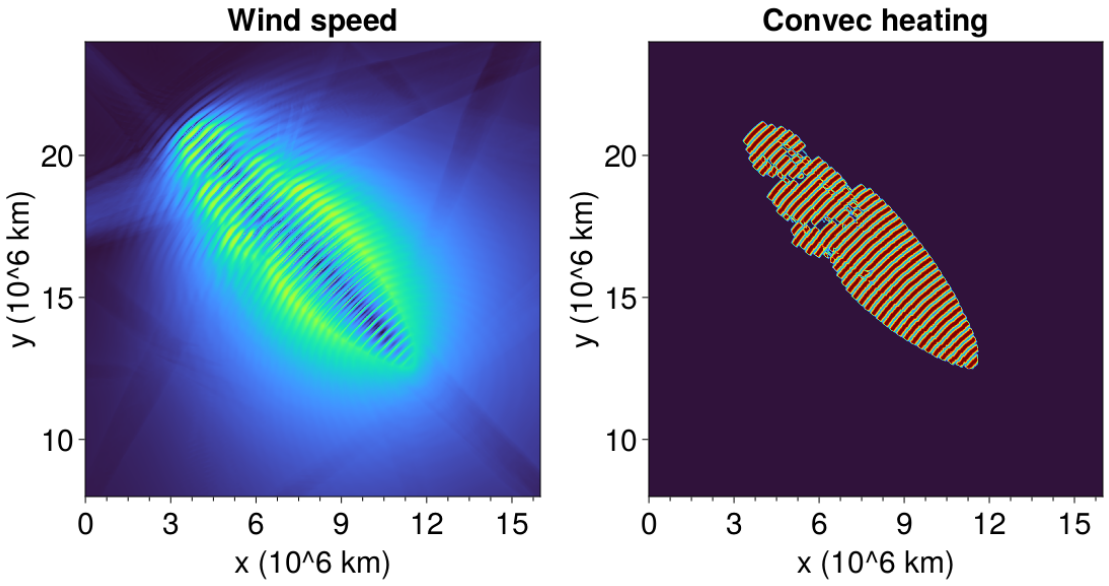

Figure 4.6: Closeup of wind speed and convective heating fields at day 73.

half that of the dry gravity wave speed c. This displacement velocity remains 0.5c when varying the gravity wave speed, as shown by the set of simulations with the same parameters as in the reference experiment but varying the initial height of the model L_z (Var_c, see Table 4.4). Figure 4.7 shows Hovmöller diagrams of the convective heating. To build the Hovmöller diagram, we rotated a snapshot by 45 deg. Therefore, the x-axis in Figure 4.7 is the distance along the domain's main or secondary diagonal (selected by the eye according to the direction of motion of the largest aggregate in the second half of the simulation). Because the domain is double periodic, we obtained a new squared domain with each side as long as the original diagonals while rotating the snapshot. In this rotated image, the largest aggregate moves horizontally. We then take the average of the selected field along the vertical direction of this rotated field. This gives us a line plot for each snapshot. By repeating the process for each timestep and stacking the results, we obtain the Hovmöller diagram. The lines that appear to move in the vertical direction of this Hovmöller diagram could correspond to aggregates that are moving along the other diagonal direction, but in the averaging, any information about its velocity is lost. Figure 4.7 also shows a line representing one-half of the gravity wave speed c (red) and the 0.5c (yellow). In all the simulations, the aggregates move with a

velocity closer to 0.5c, and this relation holds when such gravity wave speed is varied. Additionally, we can observe that for the cases with larger gravity wave speeds, the aggregates disappear after around 100 days. After this, the whole domain slowly relaxes to the triggering height, and then all of the domain convects uniformly for a brief time (horizontal red lines in the two latest panels). What may be happening is that a very fast gravity wave speed can efficiently remove all height anomalies, making the domain uniform. This period results in uninteresting physics, so we do not explore it further.

The spatial scale of the aggregates increases with τ_d. Figure Figure 4.8 shows the spatial scale of the aggregates, computed as the domain area divided by the average number of aggregates in the last 50 days of simulation for the experiments varying τ_d vs τ_d (or equivalently ld). This result is consistent with (Yang, 2021), which showed that the space between the center of aggregates depends on this quantity. Physically, τ_d sets the extent to which one convective event influences its environment via gravity waves.

4.4.1 The system in an f-plane

This work is part of a broader exercise trying to investigate the minimal set of ingredients that can form a TC. In this regard, the authors have explored this question from within the RCE framework, observing differences and similarities between the non-rotating RCE framework and RRCE, which is capable of supporting the spontaneous genesis of TCs (Ramírez Reyes and Yang, 2021, 2022b). This work has shown that convective-self aggregation can appear in our very simple model that does not represent explicitly components of the real atmosphere like interactive radiation, surface fluxes, or moisture. This seems consistent with previous literature (Yang, 2021). However, to this date and in several parameter regimes, we have not observed that spontaneous TC genesis exists in the shallow water model with parameterized convection. This possibility also seems consistent with the results of Ramírez Reyes and Yang (2022b), who showed that in the absence of surface flux and radiative feedback, the presence of moisture-convection feedback was needed for spontaneous TC genesis to occur. Therefore, while not a strong conclusion, it does not seem likely that this model will produce spontaneous TC genesis.

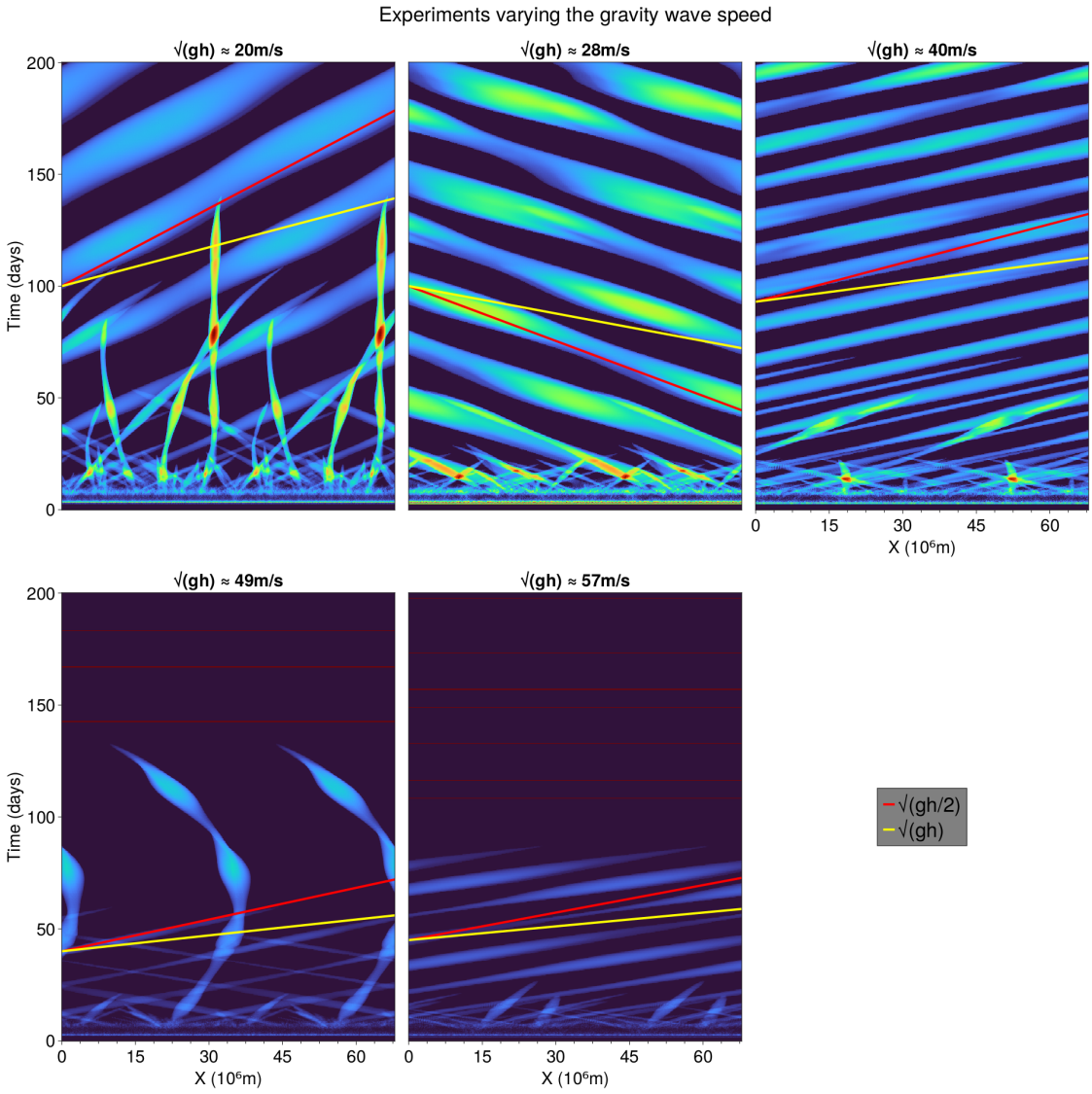

Figure 4.7: Hovmöller diagrams of the convective heating field in the simulations that vary the gravity wave speed

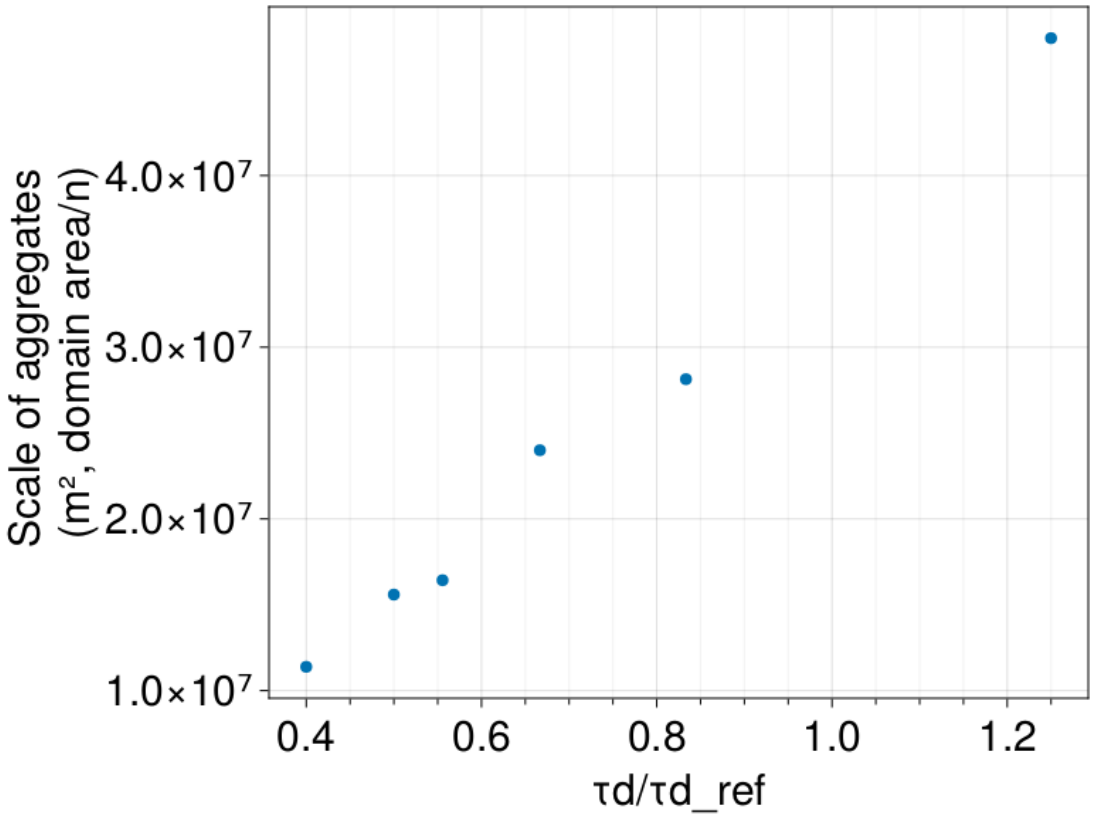

Figure 4.8: Spatial scale vs damping timescale

4.5 Discussion and conclusions

In this work, we implemented a very simple convective parameterization in a CPU/GPU-capable model. Because most new supercomputing facilities (e.g. supercomputing centers or cloud-computing service providers) currently include GPU-accelerated nodes, an implementation that can profit from this technology to accelerate scientific discovery is highly desirable. However, not everybody has access to the most modern architecture. Therefore, the possibility of having a performant implementation that can also run on CPUs permits the exploration of scientific questions in different settings. The GPU implementation allows substantial speedups with respect to the CPU implementation, allowing for extensive parameter exploration and statistical analysis. Although the results presented in this chapter do not showcase this power, in work leading to it, we successfully performed thousands of simulations, whose analysis is still underway.

We showed that the Shallow Water model with Yang (2021)'s representation of convection could produce convective self-aggregation in two dimensions. By running a very simple scaling analysis, we showed that features such as the gravity wave speed and the damping time scale strongly influence the behavior of convective aggregates.

The simplicity of the Shallow Water model allows for an analytical examination, which opens the doors for answering more questions related to convection. Apart from the architecture and dimensionality, our model adds to Yang (2021)'s possibility of running nonlinear experiments. While accessing a non-linear regime of motion may difficult the analytical tractability of the system, it may give rise to more interesting phenomena of convection.

However, the question arises as to whether this model can produce spontaneous TC genesis. Our current work does not allow us to answer this question categorically. However, previous literature suggests this may be impossible due to the lack of certain feedbacks, like moisture-convection feedback or surface-flux feedback. In either case, our model is flexible enough to allow rotating and non-rotating experiments with similar ease. Which we hope will provide an exciting tool to continue the search for answers to questions about convection.

Data and software availability

Following the Best Practices for Preservation and Replicability (Schuster et al., 2022), we make the code and instructions available to replicate our results. Oceananigans.jl (Ramadhan et al., 2020) is free software under the MIT license and can be obtained at `https://github.com/CliMA/Oceananigans.jl/`. The version used in this work and modified source code and instructions can be found at `https://github.com/aramirezreyes/RamirezReyes_ShallowWaterInFPlane/tree/arr_dissertation`. We analyzed the data using the Julia Programming Language (Bezanson et al., 2017) available under MIT license at `www.julialang.org`, with the Images.jl package available with MIT license at `https://github.com/JuliaImages/Images.jl`. We used the Makie.jl package (Danisch and Krumbiegel, 2021) available under MIT license at `https://github.com/JuliaPlots/Makie.jl` to create the figures shown in this work. We employed DrWatson.jl(Datseris et al., 2020) to manage our simulation experiments and submission scripts. DrWatson.jl is free software published under the MIT license and can be obtained in `https://github.com/JuliaDynamics/DrWatson.jl/`

Appendix

User interface

In Table 4.6, we show the parameters needed to run a simulation. These parameters must be stored in a **Dict** structure of Julia. Assuming we use a dictionary of parameters called *params*, Table 4.5 shows the basic script needed to run a simulation is composed of. However, the user should refer to the README in `https://github.com/aramirezreyes/RamirezReyes_ShallowWaterInFPlane/tree/arr_dissertation` for instructions to set up a working environment.

```
parameters = Dict(
    "architecture" => "GPU",
    "output_filename" => "one_convecting_point_bl_GPU",
    "f" => 0.0,# coriolis parameter5e-4 #5e-4
    "g" => 0.0,#gravitational acceleration 9.8
    "convection_timescale" => 1000.0, #convective time scale
    "convection_critical_height" => 40.0, #convection_triggering height
    "heating_amplitude" => 1.0e9,#convective heating 1.0e9 #originally 9 for heating, -8
    ↪  for cooling convective heating
    "large_scale_forcing" => 0.0,#radiative cooling rate
    "convective_radius" => 10_000, #convective radius
    "relaxation_parameter" => 0.0, #relaxation timescale
    "relaxation_height" => nothing, #height to relax to, if nothing, h relax to its mean
    "Lx" => 30000, #domain
    "Ly" => 30000,
    "Lz" => 40.0,
    "Nx" => 100,
    "Ny" => 100,
    "boundary_layer" => true,
    "initialization_style" => "one_convecting_point",
    "initialization_amplitude" => 1,
    "simulation_length_in_days" => 2000 / 86400,
    "output_interval_in_seconds" => 20,
    "timestep_in_seconds" => 20,
    "restart" => false,
    "checkpoint_interval_in_seconds" => Inf,
)

using RamirezReyes_ShallowWaterInFPlane

run_shallow_simulation(parameters)
```

Table 4.5: Basic script to run a simulation

Parameter	Possible values	Type	Notes/Units
architecture	CPU,GPU	String	
output_filename	Not constrained or nothing	Union{String,Nothing}	If nothing, name is autogenerated
f	Not constrained	Real	s^{-1}
g	Not constrained	Real	ms^{-2}
convection_timescale	Not constrained	Real	s
convection_critical_height	Not constrained	Real	m
heating_amplitude	Not constrained	Real	m^3
large_scale_forcing	Not constrained	Real	ms^{-1}
convective_radius	Not constrained	Real	m
relaxation_parameter	Not constrained	Real	τ_d^{-1}
relaxation_height	Not constrained or nothing	Union{Real,Nothing}	When nothing, relax to mean height
Lx	Not constrained	Real	Length of domain (m)
Ly	Not constrained	Real	Width of domain (m)
Lz	Not constrained	Real	Height of domain
Nx	Not constrained	Int	Number of grid points on x
Ny	Not constrained	Int	Number of grid points on y
boundary_layer	true, false	Bool	Changes sign of forcings
initialization_style	"gaussian", "rand", "one_convecting"	String	
initialization_amplitude	Not constrained	Real	Amplitude of perturbations in height (m)
gaussian_sigma_x	Not constrained	Real	Standard deviation with gaussian initialization style
gaussian_sigma_y	Not Constrained	Real	Standard deviation with gaussian initialization style
gaussian_rotation	Not constrained	Real	Angle of rotation of gaussian with gaussian initialization style (rad)
restart	true, false	Bool	Is this a restart run?
checkpoint_interval_in_seconds	Not constrained	Real	s
simulation_length_in_days	Not constrained	Real	day
output_interval_in_seconds	Not constrained	Real	s
timestep_in_seconds	Not constrained	Real	s

Table 4.6: User-facing parameters

Chapter 5 Main contributions and conclusions

In this work, we have explored the organization of convection in very idealized settings and its relation to Tropical Cyclone genesis.

In chapter 2, we showed that TCs can self-emerge in RRCE simulations even in the absence of a pre-existing disturbance, or feedback mechanisms between the atmospheric circulation and enthalpy fluxes from the ocean, or between radiative cooling and moisture, which had been considered essential ingredients for spontaneous TC genesis in previous studies. We also showed that despite these missing ingredients, TCs could evolve to similar intensities as with them and that TC genesis and intensification are associated with an increase in available potential energy (APE) lead by APE production by a release of latent heating that coincides with positive temperature anomalies.

In chapter 3, we showed that a feedback between moisture and convection is enough to create a moistening tendency that promotes convective events in regions with recent convective events. This tendency is enough to allow TCs to emerge, and it explains the origin of TC genesis in chapter 2. The moisture-entrainment feedback acts in two different ways: First, a fast component with a time scale of a few hours. This time scale relates to the time scale in which mixing between deep convective clouds and their environment occurs (which we call the detrainment timescale). This result may allow for benchmarks of deep convection parameterization in GCMs. The second time scale is longer and is related to the drying by subsidence time scale. In our simulations, this process impacts the ability of TCs to intensify. Because of the long timescale that characterizes this process, it is possible that the long time scale is not relevant for real Earth's TC intensification, in which moisture gradients are dominated by faster processes.

Finally, in chapter 4 we built a convective parameterization in an easy-to-use Shallow Water model using the Oceananigans.jl package and the Julia programming language as a base. This

flexible framework allows us to do a wide parameter exploration of RCE states that mimic the tropical atmosphere efficiently using different computer architectures. Using our shallow water model, we reproduced some results from more complex 3D models: we observed the self-aggregation of convection and how some simulation parameters could control the geometry and movement. More extensive work is needed to show that this form of convective organization represents real states of the tropical atmosphere, but the reusability of our code sets the path to answer important questions about convection. Our promise is that once a user installs the Julia programming language in their system, they can launch our example simulations in less than 10 minutes.

5.1 Interesting avenues to pursue

In the following lines, I explore some things that interested me during the development of this dissertation. These research ideas may be useful and directly applicable, or they may "only" be interesting from a curiosity-driven point of view.

5.1.1 Future work: Spontaneous TC genesis in RRCE

What sets the time to genesis, and how is it relevant for the real atmosphere? It is known that "spontaneous" TC genesis needs a long time to occur. Depending on the simulation details, this can range from 10 to 40 days. This characteristic is often cited as proof of the irrelevance of spontaneous TC genesis to the understanding of TC genesis on Earth: "If the typical sequence of events leading to TC genesis happens in timescales of around one week, why should we concern ourselves with processes that take 5 times that in the most ideal of circumstances?". In this author's opinion, the answer is that the time needed from the start of a simulation until TC genesis is not directly relevant to TC genesis. The relevant time frame may be from the first time a midlevel vortex exists until a TC is well formed (Davis, 2015). However, what sets the average time to this first vortex and its departures from the mean (this quantity can have a significant spread, as seen in Figure 2.2) is an interesting question that has not received enough attention. If TCs appear and disappear, this quantity could give insight into the frequency of genesis, which was one of our motivating questions. Research idea: trying to model the time to genesis as a stochastic process may help develop some

insight.

How is the detrainment timescale represented in GCM parameterizations, and how do their changes influence the rates of genesis? In chapter 3, we showed that the moistening effect of extinct convective events is fundamental for spontaneous TC genesis when other organizing feedbacks are absent. Because we turned off other feedbacks, we could study the timescale in which moistening by convection helps genesis. We posit that this relation may be important to aid TC genesis even when other feedbacks are present. Following recent literature about moisture effects in TC genesis and intensification in high-resolution models (Martinez et al., 2020; Ocasio et al., 2021), it is desirable to explore how well is this moisture-convection coupling represented in convective parameterizations in GCMs.

5.1.2 Future work: The shallow water model

The work presented in this chapter is part of a larger project to understand Tropical Cyclone genesis. In pursuing this goal, we have explored the phenomenon of convective self-aggregation. The argument connecting both phenomena is that, in many cases, the processes that lead to non-rotating self-aggregation of convection also lead to the spontaneous emergence of TCs in RCE or help the development of a TC from a pre-existing disturbance in the real atmosphere. However, our shallow water model has not observed spontaneous TC genesis. This does not mean that our effort has been futile, however. For example: What can the Shallow water model tell us about the vortical hot tower route to TC genesis? The phenomena are distinct: spontaneous TC genesis is not only convective self-aggregation plus rotation. For example, the studies of (Ramírez Reyes and Yang, 2021, 2022a) show that in a rotating setup, the moisture-convection feedback is sufficient to create a tropical cyclone. Still, without rotation, the same setup does not show convective self-aggregation. Therefore, a good idea is to inquire if the shallow water model can create one or more rotating vortices whose behavior could lead to improving our understanding of tropical cyclones. The author believes the most promising avenue is to study convective-scale processes. Early results with our shallow water model show that it produces regions of increased vorticity around convective events. This increased vorticity remains after the convective event has disappeared. This resembles

realistic examples of the interaction of convection and vorticity (e.g., figure 5 in Davis, 2015) and also some ingredients for the so-called vortical hot-tower route to TC genesis (Montgomery et al., 2006). How the physics of the shallow water model corresponds to that of real vortical hot towers, deserves some further examination.

Adding an "organization agent"

According to Chapters 2 and 3, Spontaneous TC genesis requires the presence of at least one organizing "feedback" to occur. This feedback can be picked between surface-flux, radiative, or moisture-convection feedback. This feedback must act as an organizing agent. This means that regions with convection must become increasingly likely to convect until they organize into a convecting cluster of a spatial scale comparable with the Rossby radius of deformation (see e.g., Ooyama, 1982). In our shallow water model, we still have not concluded that spontaneous TC genesis will not occur. However, this is possible, considering none of the three feedbacks is present. An interesting avenue to pursue, then, is to add an "organizing agent", or some kind of interactivity that strengthens the organizing tendency of the convection in the shallow water model and leads to spontaneous TC genesis.

5.2 Final thoughts: Are we closer to solving the mysteries of TCs?

In chapter 1, we motivated working on simplified models to gather an understanding of both of the processes that help a tropical disturbance to become a TC in the tropical atmosphere, and also to look for an insight into what are the quantities that, in a given climate, determine the frequency of TCs. We have definitely made advances in one sense. We found that feedback between moisture and convection may be enough to organize convection into a TC without needing a pre-existing disturbance. We quantified how fast this interaction needs to be to help genesis. The fact that TCs remain in the domain makes it difficult to infer how often this genesis process would occur if the TCs died with time. However, we now have new tools to help progress toward the answers. For example, the Shallow Water model could allow longer simulations or larger domains where TC exists.

Reference

Alland, J. J., Tang, B. H., and Corbosiero, K. L.: Effects of Midlevel Dry Air on Development of the Axisymmetric Tropical Cyclone Secondary Circulation, Journal of the Atmospheric Sciences, 74, 1455–1470, doi: 10.1175/JAS-D-16-0271.1, 2017.

Andersen, J. A. and Kuang, Z.: A Toy Model of the Instability in the Equatorially Trapped Convectively Coupled Waves on the Equatorial Beta Plane, Journal of the Atmospheric Sciences, 65, 3736–3757, doi: 10.1175/2008JAS2776.1, 2008.

Anthes, R. A. and Johnson, D. R.: Generation of Available Potential Energy in Hurricane Hilda (1964), Monthly Weather Review, 96, 291–302, doi: 10.1175/1520-0493(1968)096⟨0291:GOAPEI⟩2.0.CO;2, 1968.

Arakawa, A. and Schubert, W. H.: Interaction of a Cumulus Cloud Ensemble with the Large-Scale Environment, Part I, Journal of the Atmospheric Sciences, 31, 674–701, doi: 10.1175/1520-0469(1974)031⟨0674:IOACCE⟩2.0.CO;2, 1974.

Arnold, N. P. and Putman, W. M.: Nonrotating Convective Self-Aggregation in a Limited Area AGCM, Journal of Advances in Modeling Earth Systems, 10, 1029–1046, doi: 10.1002/2017MS001218, 2018.

Arnold, N. P. and Randall, D. A.: Global-Scale Convective Aggregation: Implications for the Madden-Julian Oscillation, Journal of Advances in Modeling Earth Systems, 7, 1499–1518, doi: 10.1002/2015MS000498, 2015.

Bartels, D. L. and Maddox, R. A.: Midlevel Cyclonic Vortices Generated by Mesoscale Convective Systems, Monthly Weather Review, 119, 104–118, doi: 10.1175/1520-0493(1991)119⟨0104:MCVGBM⟩2.0.CO;2, 1991.

Besard, T., Churavy, V., Edelman, A., and Sutter, B. D.: Rapid Software Prototyping for Heterogeneous and Distributed Platforms, Advances in Engineering Software, 132, 29–46, doi: 10.1016/j.advengsoft.2019.02.002, 2019a.

Besard, T., Foket, C., and De Sutter, B.: Effective Extensible Programming: Unleashing Julia on GPUs, IEEE Transactions on Parallel and Distributed Systems, 30, 827–841, doi: 10.1109/TPDS.2018.2872064, 2019b.

Bezanson, J., Edelman, A., Karpinski, S., and Shah, V. B.: Julia: A Fresh Approach to Numerical Computing, SIAM Review, 59, 65–98, doi: 10.1137/141000671, 2017.

Bister, M. and Emanuel, K. A.: Dissipative Heating and Hurricane Intensity, Meteorology and Atmospheric Physics, 65, 233–240, doi: 10.1007/BF01030791, 1998.

Bister, M. and Emanuel, K. A.: Low Frequency Variability of Tropical Cyclone Potential Intensity 1. Interannual to Interdecadal Variability, Journal of Geophysical Research: Atmospheres, 107, ACL 26–1–ACL 26–15, doi: 10.1029/2001JD000776, 2002.

Bretherton, C. S.: INSTABILITY — Wave-CISK, in: Encyclopedia of Atmospheric Sciences, edited by Holton, J. R., pp. 1019–1022, Academic Press, Oxford, doi: 10.1016/B0-12-227090-8/00177-9, 2003.

Bretherton, C. S., Blossey, P. N., and Khairoutdinov, M. F.: An Energy-Balance Analysis of Deep Convective Self-Aggregation above Uniform SST, Journal of the Atmospheric Sciences, 62, 4273–4292, doi: 10.1175/JAS3614.1, 2005.

Bryan, G. H., Wyngaard, J. C., and Fritsch, J. M.: Resolution Requirements for the Simulation of Deep Moist Convection, Monthly Weather Review, 131, 2394–2416, doi: 10.1175/1520-0493(2003)131⟨2394:RRFTSO⟩2.0.CO;2, 2003.

Carstens, J. D. and Wing, A. A.: Tropical Cyclogenesis From Self-Aggregated Convection in Numerical Simulations of Rotating Radiative-Convective Equilibrium, Journal of Advances in Modeling Earth Systems, 12, e2019MS002 020, doi: 10.1029/2019MS002020, 2020.

Chavas, D. R. and Emanuel, K. A.: Equilibrium Tropical Cyclone Size in an Idealized State of Axisymmetric Radiative–Convective Equilibrium, Journal of the Atmospheric Sciences, 71, 1663–1680, doi: 10.1175/JAS-D-13-0155.1, 2014.

Chavas, D. R. and Reed, K. A.: Dynamical Aquaplanet Experiments with Uniform Thermal Forcing: System Dynamics and Implications for Tropical Cyclone Genesis and Size, Journal of the Atmospheric Sciences, 76, 2257–2274, doi: 10.1175/JAS-D-19-0001.1, 2019.

Chavas, D. R., Lin, N., and Emanuel, K.: A Model for the Complete Radial Structure of the Tropical Cyclone Wind Field. Part I: Comparison with Observed Structure, Journal of the Atmospheric Sciences, 72, 3647–3662, doi: 10.1175/JAS-D-15-0014.1, 2015.

Chavas, D. R., Lin, N., Dong, W., and Lin, Y.: Observed Tropical Cyclone Size Revisited, Journal of Climate, 29, 2923–2939, doi: 10.1175/JCLI-D-15-0731.1, 2016.

Collins, W., Rasch, P., Boville, B., McCaa, J., Williamson, D., Kiehl, J., Briegleb, B., Bitz, C., Lin, S.-J., Zhang, M., and Dai, Y.: Description of the NCAR Community Atmosphere Model (CAM 3.0), Tech. rep., UCAR/NCAR, doi: 10.5065/D63N21CH, 2004.

Craig, G. C. and Dörnbrack, A.: Entrainment in Cumulus Clouds: What Resolution Is Cloud-Resolving?, Journal of the Atmospheric Sciences, 65, 3978–3988, doi: 10.1175/2008JAS2613.1, 2008.

Craig, G. C. and Mack, J. M.: A Coarsening Model for Self-Organization of Tropical Convection, Journal of Geophysical Research: Atmospheres, 118, 8761–8769, doi: 10.1002/jgrd.50674, 2013.

Cronin, T. and Chavas, D. R.: Dry and Semi-Dry Tropical Cyclones, 2018.

Cronin, T. W. and Chavas, D. R.: Dry and Semi-Dry Tropical Cyclones, Journal of the Atmospheric Sciences, doi: 10.1175/JAS-D-18-0357.1, 2019.

Danisch, S. and Krumbiegel, J.: Makie.Jl: Flexible High-Performance Data Visualization for Julia, Journal of Open Source Software, 6, 3349, doi: 10.21105/joss.03349, 2021.

Datseris, G., Isensee, J., Pech, S., and Gál, T.: DrWatson: The Perfect Sidekick for Your Scientific Inquiries, Journal of Open Source Software, 5, 2673, doi: 10.21105/joss.02673, 2020.

Davidson, N. E., Holland, G. J., McBride, J. L., and Keenan, T. D.: On the Formation of AMEX Tropical Cyclones Irma and Jason, Monthly Weather Review, 118, 1981–2000, doi: 10.1175/1520-0493(1990)118⟨1981:OTFOAT⟩2.0.CO;2, 1990.

Davis, C. A.: The Formation of Moist Vortices and Tropical Cyclones in Idealized Simulations, Journal of the Atmospheric Sciences, 72, 3499–3516, doi: 10.1175/JAS-D-15-0027.1, 2015.

de Rooy, W. C., Bechtold, P., Fröhlich, K., Hohenegger, C., Jonker, H., Mironov, D., Pier Siebesma, A., Teixeira, J., and Yano, J.-I.: Entrainment and Detrainment in Cumulus Convection: An Overview, Quarterly Journal of the Royal Meteorological Society, 139, 1–19, doi: 10.1002/qj.1959, 2013.

Deardorff, J. W.: Stratocumulus-Capped Mixed Layers Derived from a Three-Dimensional Model, Boundary-Layer Meteorology, 18, 495–527, doi: 10.1007/BF00119502, 1980.

Dunkerton, T. J., Montgomery, M. T., and Wang, Z.: Tropical Cyclogenesis in a Tropical Wave Critical Layer: Easterly Waves, Atmos. Chem. Phys., p. 61, 2009.

Emanuel, K.: The Relevance of Theory for Contemporary Research in Atmospheres, Oceans, and Climate, AGU Advances, 1, e2019AV000 129, doi: 10.1029/2019AV000129, 2020.

Emanuel, K. A.: An Air-Sea Interaction Theory for Tropical Cyclones. Part I: Steady-State Maintenance, Journal of the Atmospheric Sciences, 43, 585–605, doi: 10.1175/1520-0469(1986)043⟨0585:AASITF⟩2.0.CO;2, 1986.

Emanuel, K. A.: Atmospheric Convection, Oxford University Press, New York, 1994.

Emanuel, K. A.: Tropical Cyclones, Annual Review of Earth and Planetary Sciences, 31, 75–104, doi: 10.1146/annurev.earth.31.100901.141259, 2003.

Emanuel, K. A.: 100 Years of Progress in Tropical Cyclone Research, Meteorological Monographs, 59, 15.1–15.68, doi: 10.1175/AMSMONOGRAPHS-D-18-0016.1, 2018.

Emanuel, K. A., Neelin, J. D., and Bretherton, C. S.: On Large-Scale Circulations in Convecting Atmospheres, Quarterly Journal of the Royal Meteorological Society, 120, 1111–1143, doi: 10.1002/qj.49712051902, 1994.

Frisius, T.: Surface-Flux-Induced Tropical Cyclogenesis within an Axisymmetric Atmospheric Balanced Model, Quarterly Journal of the Royal Meteorological Society, 132, 2603–2623, doi: 10.1256/qj.06.03, 2006.

Fritz, C. and Wang, Z.: Water Vapor Budget in a Developing Tropical Cyclone and Its Implication for Tropical Cyclone Formation, Journal of the Atmospheric Sciences, 71, 4321–4332, doi: 10.1175/JAS-D-13-0378.1, 2014.

Gill, A. E.: Some Simple Solutions for Heat-Induced Tropical Circulation, Quarterly Journal of the Royal Meteorological Society, 106, 447–462, doi: 10.1002/qj.49710644905, 1980.

Grabowski, W. W. and Moncrieff, M. W.: Moisture–Convection Feedback in the Tropics, Quarterly Journal of the Royal Meteorological Society, 130, 3081–3104, doi: 10.1256/qj.03.135, 2004.

Gray, W. M.: GLOBAL VIEW OF THE ORIGIN OF TROPICAL DISTURBANCES AND STORMS, Monthly Weather Review, 96, 669–700, doi: 10.1175/1520-0493(1968)096⟨0669:GVOTOO⟩2.0.CO;2, 1968.

Halperin, D. J., Penny, A. B., and Hart, R. E.: A Comparison of Tropical Cyclone Genesis Forecast Verification from Three Global Forecast System (GFS) Operational Configurations, Weather and Forecasting, 35, 1801–1815, doi: 10.1175/WAF-D-20-0043.1, 2020.

Held, I. M. and Zhao, M.: Horizontally Homogeneous Rotating Radiative–Convective Equilibria at GCM Resolution, Journal of the Atmospheric Sciences, 65, 2003–2013, doi: 10.1175/2007JAS2604.1, 2008.

Hsieh, T.-L., Vecchi, G. A., Yang, W., Held, I. M., and Garner, S. T.: Large-Scale Control on the Frequency of Tropical Cyclones and Seeds: A Consistent Relationship across a

Hierarchy of Global Atmospheric Models, Climate Dynamics, 55, 3177–3196, doi: 10.1007/s00382-020-05446-5, 2020.

Hung, M.-P., Lin, J.-L., Wang, W., Kim, D., Shinoda, T., and Weaver, S. J.: MJO and Convectively Coupled Equatorial Waves Simulated by CMIP5 Climate Models, Journal of Climate, 26, 6185–6214, doi: 10.1175/JCLI-D-12-00541.1, 2013.

Jeevanjee, N. and Romps, D. M.: Convective Self-Aggregation, Cold Pools, and Domain Size, Geophysical Research Letters, 40, 994–998, doi: 10.1002/grl.50204, 2013.

Khairoutdinov, M. F. and Emanuel, K. A.: Rotating Radiative-Convective Equilibrium Simulated by a Cloud-Resolving Model, Journal of Advances in Modeling Earth Systems, 5, 816–825, doi: 10.1002/2013MS000253, 2013.

Khairoutdinov, M. F. and Randall, D. A.: Cloud Resolving Modeling of the ARM Summer 1997 IOP: Model Formulation, Results, Uncertainties, and Sensitivities, Journal of the Atmospheric Sciences, 60, 607–625, doi: 10.1175/1520-0469(2003)060⟨0607:CRMOTA⟩2.0.CO;2, 2003.

Kiehl, T., Hack, J., Bonan, B., Boville, A., Briegleb, P., Williamson, L., and Rasch, J.: Description of the NCAR Community Climate Model (CCM3), doi: 10.5065/D6FF3Q99, 1996.

Kim, H., Ham, Y. G., Joo, Y. S., and Son, S. W.: Deep Learning for Bias Correction of MJO Prediction, Nature Communications, 12, 3087, doi: 10.1038/s41467-021-23406-3, 2021.

Klotzbach, P. J., Chan, J. C. L., Fitzpatrick, P. J., Frank, W. M., Landsea, C. W., and McBride, J. L.: The Science of William M. Gray: His Contributions to the Knowledge of Tropical Meteorology and Tropical Cyclones, Bulletin of the American Meteorological Society, 98, 2311–2336, doi: 10.1175/BAMS-D-16-0116.1, 2017.

Kuang, Z.: Modeling the Interaction between Cumulus Convection and Linear Gravity Waves Using a Limited-Domain Cloud System–Resolving Model, Journal of the Atmospheric Sciences, 65, 576–591, doi: 10.1175/2007JAS2399.1, 2008.

Kuang, Z. and Bretherton, C. S.: A Mass-Flux Scheme View of a High-Resolution Simulation of a Transition from Shallow to Deep Cumulus Convection, Journal of the Atmospheric Sciences, 63, 1895–1909, doi: 10.1175/JAS3723.1, 2006.

Lahaye, N. and Zeitlin, V.: Understanding Instabilities of Tropical Cyclones and Their Evolution with a Moist Convective Rotating Shallow-Water Model, Journal of the Atmospheric Sciences, 73, 505–523, doi: 10.1175/JAS-D-15-0115.1, 2016.

Laing, A. G. and Fritsch, J. M.: Mesoscale Convective Complexes over the Indian Monsoon Region, Journal of Climate, 6, 911–919, doi: 10.1175/1520-0442(1993)006⟨0911:MCCOTI⟩2.0.CO;2, 1993.

Lee, C.-Y., Camargo, S. J., Sobel, A. H., and Tippett, M. K.: Statistical–Dynamical Downscaling Projections of Tropical Cyclone Activity in a Warming Climate: Two Diverging Genesis Scenarios, Journal of Climate, 33, 4815–4834, doi: 10.1175/JCLI-D-19-0452.1, 2020.

Lindzen, R. S. and Nigam, S.: On the Role of Sea Surface Temperature Gradients in Forcing Low-Level Winds and Convergence in the Tropics, Journal of the Atmospheric Sciences, 44, 2418–2436, doi: 10.1175/1520-0469(1987)044⟨2418:OTROSS⟩2.0.CO;2, 1987.

Lorenz, E. N.: Available Potential Energy and the Maintenance of the General Circulation, Tellus, 7, 157–167, doi: 10.1111/j.2153-3490.1955.tb01148.x, 1955.

Lorenz, E. N.: Available Energy and the Maintenance of a Moist Circulation, Tellus, 30, 15–31, doi: 10.1111/j.2153-3490.1978.tb00815.x, 1978.

Lucas, C., Zipser, E. J., and Lemone, M. A.: Vertical Velocity in Oceanic Convection off Tropical Australia, Journal of the Atmospheric Sciences, 51, 3183–3193, doi: 10.1175/1520-0469(1994)051⟨3183:VVIOCO⟩2.0.CO;2, 1994.

Lunet, T., Lac, C., Auguste, F., Visentin, F., Masson, V., and Escobar, J.: Combination of WENO and Explicit Runge–Kutta Methods for Wind Transport in the Meso-NH Model, Monthly Weather Review, 145, 3817–3838, doi: 10.1175/MWR-D-16-0343.1, 2017.

Ma, L.-M. and Tan, Z.-M.: Improving the Behavior of the Cumulus Parameterization for Tropical Cyclone Prediction: Convection Trigger, Atmospheric Research, 92, 190–211, doi: 10.1016/j.atmosres.2008.09.022, 2009.

Mapes, B. E.: Convective Inhibition, Subgrid-Scale Triggering Energy, and Stratiform Instability in a Toy Tropical Wave Model, Journal of the Atmospheric Sciences, 57, 1515–1535, doi: 10.1175/1520-0469(2000)057⟨1515:CISSTE⟩2.0.CO;2, 2000.

Martinez, J., Nam, C. C., and Bell, M. M.: On the Contributions of Incipient Vortex Circulation and Environmental Moisture to Tropical Cyclone Expansion, Journal of Geophysical Research: Atmospheres, 125, e2020JD033 324, doi: 10.1029/2020JD033324, 2020.

Matsuno, T.: Quasi-Geostrophic Motions in the Equatorial Area, Journal of the Meteorological Society of Japan. Ser. II, 44, 25–43, doi: 10.2151/jmsj1965.44.1_25, 1966.

McBride, J. L. and Zehr, R.: Observational Analysis of Tropical Cyclone Formation. Part II: Comparison of Non-Developing versus Developing Systems, Journal of the Atmospheric Sciences, 38, 1132–1151, doi: 10.1175/1520-0469(1981)038⟨1132:OAOTCF⟩2.0.CO;2, 1981.

Merlis, T. M. and Held, I. M.: Aquaplanet Simulations of Tropical Cyclones, Current Climate Change Reports, 5, 185–195, doi: 10.1007/s40641-019-00133-y, 2019.

Merlis, T. M., Zhou, W., Held, I. M., and Zhao, M.: Surface Temperature Dependence of Tropical Cyclone-Permitting Simulations in a Spherical Model with Uniform Thermal Forcing, Geophysical Research Letters, 43, 2859–2865, doi: 10.1002/2016GL067730, 2016.

Mlawer, E. J., Taubman, S. J., Brown, P. D., Iacono, M. J., and Clough, S. A.: Radiative Transfer for Inhomogeneous Atmospheres: RRTM, a Validated Correlated-k Model for the Longwave, Journal of Geophysical Research: Atmospheres, 102, 16 663–16 682, doi: 10.1029/97JD00237, 1997.

Mohandas, S. and Ashrit, R.: Sensitivity of Different Convective Parameterization Schemes on

Tropical Cyclone Prediction Using a Mesoscale Model, Natural Hazards, 73, 213–235, doi: 10.1007/s11069-013-0824-6, 2014.

Montgomery, M. T.: Recent Advances in Tropical Cyclogenesis, in: Advanced Numerical Modeling and Data Assimilation Techniques for Tropical Cyclone Prediction, edited by Mohanty, U. C. and Gopalakrishnan, S. G., pp. 561–587, Springer Netherlands, Dordrecht, doi: 10.5822/978-94-024-0896-6_22, 2016.

Montgomery, M. T. and Smith, R.: Paradigms for Tropical Cyclone Intensification, Australian Meteorological and Oceanographic Journal, 64, 37–66, doi: 10.22499/2.6401.005, 2014.

Montgomery, M. T., Nicholls, M. E., Cram, T. A., and Saunders, A. B.: A Vortical Hot Tower Route to Tropical Cyclogenesis, Journal of the Atmospheric Sciences, 63, 355–386, doi: 10.1175/JAS3604.1, 2006.

Mullendore, G. L., Mayernik, M. S., and Schuster, D. C.: Open Science Expectations for Simulation-Based Research, Frontiers in Climate, 3, 2021.

Muller, C. J. and Bony, S.: What Favors Convective Aggregation and Why?, Geophysical Research Letters, 42, 5626–5634, doi: 10.1002/2015GL064260, 2015.

Muller, C. J. and Held, I. M.: Detailed Investigation of the Self-Aggregation of Convection in Cloud-Resolving Simulations, Journal of the Atmospheric Sciences, 69, 2551–2565, doi: 10.1175/JAS-D-11-0257.1, 2012.

Muller, C. J. and Romps, D. M.: Acceleration of Tropical Cyclogenesis by Self-Aggregation Feedbacks, Proceedings of the National Academy of Sciences, 115, 2930–2935, doi: 10.1073/pnas.1719967115, 2018.

Neelin, J. D.: On the Intepretation of the Gill Model, Journal of the Atmospheric Sciences, 46, 2466–2468, doi: 10.1175/1520-0469(1989)046⟨2466:OTIOTG⟩2.0.CO;2, 1989.

Nolan, D. S.: What Is the Trigger for Tropical Cyclogenesis?, Australian Meteorological Magazine, 56, 241–266, 2007.

Nolan, D. S., Moon, Y., and Stern, D. P.: Tropical Cyclone Intensification from Asymmetric Convection: Energetics and Efficiency, Journal of the Atmospheric Sciences, 64, 3377–3405, doi: 10.1175/JAS3988.1, 2007a.

Nolan, D. S., Rappin, E. D., and Emanuel, K. A.: Tropical Cyclogenesis Sensitivity to Environmental Parameters in Radiative–Convective Equilibrium, Quarterly Journal of the Royal Meteorological Society, 133, 2085–2107, doi: 10.1002/qj.170, 2007b.

Ocasio, K. M. N., Brammer, A., Evans, J. L., Young, G. S., and Moon, Z. L.: Favorable Monsoon Environment over Eastern Africa for Subsequent Tropical Cyclogenesis of African Easterly Waves, Journal of the Atmospheric Sciences, 78, 2911–2925, doi: 10.1175/JAS-D-20-0339.1, 2021.

Ooyama, K. V.: Conceptual Evolution of the Theory and Modeling of the Tropical Cyclone, Journal of the Meteorological Society of Japan. Ser. II, 60, 369–380, doi: 10.2151/jmsj1965.60.1_369, 1982.

Patricola, C. M., Saravanan, R., and Chang, P.: The Response of Atlantic Tropical Cyclones to Suppression of African Easterly Waves, Geophysical Research Letters, 45, 471–479, doi: 10.1002/2017GL076081, 2018.

Pierrehumbert, R. T.: Principles of Planetary Climate, Cambridge University Press, Cambridge ; New York, 2010.

Ramadhan, A., Wagner, G. L., Hill, C., Campin, J.-M., Churavy, V., Besard, T., Souza, A., Edelman, A., Ferrari, R., and Marshall, J.: Oceananigans.Jl: Fast and Friendly Geophysical Fluid Dynamics on GPUs, Journal of Open Source Software, 5, 2018, doi: 10.21105/joss.02018, 2020.

Ramírez Reyes, A. and Yang, D.: Spontaneous Cyclogenesis without Radiative and Surface-Flux Feedbacks, Journal of the Atmospheric Sciences, 78, 4169–4184, doi: 10.1175/JAS-D-21-0098.1, 2021.

Ramírez Reyes, A. and Yang, D.: The Moisture-Entrainment-Convection Feedback Can Be Suf-

ficient to Cause Spontaneous Tropical Cyclone Genesis, Zenodo, doi: 10.5281/zenodo.6978839, 2022a.

Ramírez Reyes, A. and Yang, D.: The Moisture-Entrainment-Convection Feedback Can Lead to Spontaneous Tropical Cyclone Genesis, doi: 10.48550/arXiv.2208.11160, 2022b.

Randall, D. A. and Huffman, G. J.: A Stochastic Model of Cumulus Clumping, Journal of the Atmospheric Sciences, 37, 2068–2078, doi: 10.1175/1520-0469(1980)037⟨2068:ASMOCC⟩2.0.CO;2, 1980.

Randall, D. A. and Wang, J.: The Moist Available Energy of a Conditionally Unstable Atmosphere, Journal of the Atmospheric Sciences, 49, 240–255, doi: 10.1175/1520-0469(1992)049⟨0240:TMAEOA⟩2.0.CO;2, 1992.

Raymond, D. J. and López Carrillo, C.: The Vorticity Budget of Developing Typhoon Nuri (2008), Atmospheric Chemistry and Physics, 11, 147–163, doi: 10.5194/acp-11-147-2011, 2011.

Raymond, D. J., Sessions, S. L., and Fuchs, Ž.: A Theory for the Spinup of Tropical Depressions, Quarterly Journal of the Royal Meteorological Society, 133, 1743–1754, doi: 10.1002/qj.125, 2007.

Reed, K. A. and Chavas, D. R.: Uniformly Rotating Global Radiative-Convective Equilibrium in the Community Atmosphere Model, Version 5, Journal of Advances in Modeling Earth Systems, 7, 1938–1955, doi: 10.1002/2015MS000519, 2015.

Romps, D. M.: An Analytical Model for Tropical Relative Humidity, Journal of Climate, 27, 7432–7449, doi: 10.1175/JCLI-D-14-00255.1, 2014.

Romps, D. M.: MSE Minus CAPE Is the True Conserved Variable for an Adiabatically Lifted Parcel, Journal of the Atmospheric Sciences, 72, 3639–3646, doi: 10.1175/JAS-D-15-0054.1, 2015.

Rousseau-Rizzi, R., Rotunno, R., and Bryan, G.: A Thermodynamic Perspective on Steady-State Tropical Cyclones, Journal of the Atmospheric Sciences, 78, 583–593, doi: 10.1175/JAS-D-20-0140.1, 2021.

Ruppert, J. H., Wing, A. A., Tang, X., and Duran, E. L.: The Critical Role of Cloud–Infrared Radiation Feedback in Tropical Cyclone Development, Proceedings of the National Academy of Sciences, p. 202013584, doi: 10.1073/pnas.2013584117, 2020.

Satoh, M., Stevens, B., Judt, F., Khairoutdinov, M., Lin, S.-J., Putman, W. M., and Düben, P.: Global Cloud-Resolving Models, Current Climate Change Reports, 5, 172–184, doi: 10.1007/s40641-019-00131-0, 2019.

Schreck, C. J., Knapp, K. R., and Kossin, J. P.: The Impact of Best Track Discrepancies on Global Tropical Cyclone Climatologies Using IBTrACS, Monthly Weather Review, 142, 3881–3899, doi: 10.1175/MWR-D-14-00021.1, 2014.

Schuster, D., Mayernik, M., and Mullendore, G. L.: Products Developed through the "What About Model Data?, Determining Best Practices for Preservation and Replicability, EarthCube Research Coordination Network" Project, doi: 10.5065/G936-Q118, 2022.

Scorer, R. S. and Ludlam, F. H.: Bubble Theory of Penetrative Convection, Quarterly Journal of the Royal Meteorological Society, 79, 94–103, doi: 10.1002/qj.49707933908, 1953.

Seeley, J. T. and Romps, D. M.: Why Does Tropical Convective Available Potential Energy (CAPE) Increase with Warming?, Geophysical Research Letters, 42, 10,429–10,437, doi: 10.1002/2015GL066199, 2015.

Seidel, S. D. and Yang, D.: The Lightness of Water Vapor Helps to Stabilize Tropical Climate, Science Advances, 6, eaba1951, doi: 10.1126/sciadv.aba1951, 2020.

Shi, X. and Bretherton, C. S.: Large-Scale Character of an Atmosphere in Rotating Radiative-Convective Equilibrium, Journal of Advances in Modeling Earth Systems, 6, 616–629, doi: 10.1002/2014MS000342, 2014.

Skamarock, C., Klemp, B., Dudhia, J., Gill, O., Liu, Z., Berner, J., Wang, W., Powers, G., Duda, G., Barker, D., and Huang, X.-y.: A Description of the Advanced Research WRF Model Version 4.3, doi: 10.5065/1dfh-6p97, 2021.

Smith, R. K.: On the Theory of Cisk, Quarterly Journal of the Royal Meteorological Society, 123, 407–418, doi: 10.1002/qj.49712353808, 1997.

Smith, R. K., Montgomery, M. T., Kilroy, G., Tang, S., and Müller, S. K.: Tropical Low Formation during the Australian Monsoon: The Events of January 2013, Australian Meteorological and Oceanographic Journal, 65, 318–341, doi: 10.1071/es15023, 2015.

Sobel, A. H., Wing, A. A., Camargo, S. J., Patricola, C. M., Vecchi, G. A., Lee, C.-Y., and Tippett, M. K.: Tropical Cyclone Frequency, Earth's Future, 9, e2021EF002 275, doi: 10.1029/2021EF002275, 2021.

Tang, B. H., Fang, J., Bentley, A., Kilroy, G., Nakano, M., Park, M.-S., Rajasree, V. P. M., Wang, Z., Wing, A. A., and Wu, L.: Recent Advances in Research on Tropical Cyclogenesis, Tropical Cyclone Research and Review, 9, 87–105, doi: 10.1016/j.tcrr.2020.04.004, 2020.

Thompson, G., Field, P. R., Rasmussen, R. M., and Hall, W. D.: Explicit Forecasts of Winter Precipitation Using an Improved Bulk Microphysics Scheme. Part II: Implementation of a New Snow Parameterization, Monthly Weather Review, 136, 5095–5115, doi: 10.1175/2008MWR2387.1, 2008.

Tompkins, A. M.: Organization of Tropical Convection in Low Vertical Wind Shears: The Role of Water Vapor, Journal of the Atmospheric Sciences, 58, 529–545, doi: 10.1175/1520-0469(2001)058⟨0529:OOTCIL⟩2.0.CO;2, 2001.

Tompkins, A. M. and Craig, G. C.: Radiative–Convective Equilibrium in a Three-Dimensional Cloud-Ensemble Model, Quarterly Journal of the Royal Meteorological Society, 124, 2073–2097, doi: 10.1002/qj.49712455013, 1998.

Tompkins, A. M. and Semie, A. G.: Organization of Tropical Convection in Low Vertical Wind Shears: Role of Updraft Entrainment, Journal of Advances in Modeling Earth Systems, 9, 1046–1068, doi: 10.1002/2016MS000802, 2017.

Top500: ORNL's Exaflop Machine Frontier Keeps Top Spot, New Competitor Leonardo Breaks the Top10 — TOP500, https://www.top500.org/news/ornls-exaflop-machine-frontier-keeps-top-spot-new-competitor-leonardo-breaks-the-top10/, 2022.

Vallis, G. K.: Geophysical Fluid Dynamics: Whence, Whither and Why?, Proceedings of the Royal Society A: Mathematical, Physical and Engineering Sciences, 472, 20160 140, doi: 10.1098/rspa.2016.0140, 2016.

Vallis, G. K.: Atmospheric and Oceanic Fluid Dynamics: Fundamentals and Large-Scale Circulation, Cambridge University Press, Cambridge New York, NY Port Melbourne Delhi Singapore, 2nd edition edn., 2017.

Veiga, J. A. P., Pezza, A. B., Simmonds, I., and Dias, P. L. S.: An Analysis of the Environmental Energetics Associated with the Transition of the First South Atlantic Hurricane, Geophysical Research Letters, 35, doi: 10.1029/2008GL034511, 2008.

Velasco, I. and Fritsch, J. M.: Mesoscale Convective Complexes in the Americas, Journal of Geophysical Research: Atmospheres, pp. 9591–9613, doi: 10.1029/JD092iD08p09591@10.1002/(ISSN)2169-8996.RAINFALL1, 2012.

Villafuerte, M. Q., Lambrento, J. C. R., Hodges, K. I., Cruz, F. T., Cinco, T. A., and Narisma, G. T.: Sensitivity of Tropical Cyclones to Convective Parameterization Schemes in RegCM4, Climate Dynamics, 56, 1625–1642, doi: 10.1007/s00382-020-05553-3, 2021.

Waite, M. L. and Khouider, B.: The Deepening of Tropical Convection by Congestus Preconditioning, Journal of the Atmospheric Sciences, 67, 2601–2615, doi: 10.1175/2010JAS3357.1, 2010.

Wang, B., Liu, F., and Chen, G.: A Trio-Interaction Theory for Madden–Julian Oscillation, Geoscience Letters, 3, 34, doi: 10.1186/s40562-016-0066-z, 2016.

Wang, Z.: Thermodynamic Aspects of Tropical Cyclone Formation, Journal of the Atmospheric Sciences, 69, 2433–2451, doi: 10.1175/JAS-D-11-0298.1, 2012.

Wang, Z.: Characteristics of Convective Processes and Vertical Vorticity from the Tropical Wave to Tropical Cyclone Stage in a High-Resolution Numerical Model Simulation of Tropical Cyclone Fay (2008), Journal of the Atmospheric Sciences, 71, 896–915, doi: 10.1175/JAS-D-13-0256.1, 2014a.

Wang, Z.: Role of Cumulus Congestus in Tropical Cyclone Formation in a High-Resolution Numerical Model Simulation, Journal of the Atmospheric Sciences, 71, 1681–1700, doi: 10.1175/JAS-D-13-0257.1, 2014b.

Wang, Z., Montgomery, M. T., and Dunkerton, T. J.: Genesis of Pre–Hurricane Felix (2007). Part I: The Role of the Easterly Wave Critical Layer, Journal of the Atmospheric Sciences, 67, 1711–1729, doi: 10.1175/2009JAS3420.1, 2010.

Wheeler, M. and Kiladis, G. N.: Convectively Coupled Equatorial Waves: Analysis of Clouds and Temperature in the Wavenumber–Frequency Domain, Journal of the Atmospheric Sciences, 56, 374–399, doi: 10.1175/1520-0469(1999)056⟨0374:CCEWAO⟩2.0.CO;2, 1999.

Wikipedia contributors: Embarrassingly Parallel, Wikipedia, 2023.

Wing, A. A. and Cronin, T. W.: Self-Aggregation of Convection in Long Channel Geometry, Quarterly Journal of the Royal Meteorological Society, 142, 1–15, doi: 10.1002/qj.2628, 2016.

Wing, A. A., Camargo, S. J., and Sobel, A. H.: Role of Radiative–Convective Feedbacks in Spontaneous Tropical Cyclogenesis in Idealized Numerical Simulations, Journal of the Atmospheric Sciences, 73, 2633–2642, doi: 10.1175/JAS-D-15-0380.1, 2016.

Wing, A. A., Emanuel, K. A., Holloway, C. E., and Muller, C. J.: Convective Self-Aggregation in Numerical Simulations: A Review, in: Shallow Clouds, Water Vapor, Circulation, and Climate Sensitivity, edited by Pincus, R., Winker, D., Bony, S., and Stevens, B., Space Sciences Series of ISSI, pp. 1–25, Springer International Publishing, Cham, doi: 10.1007/978-3-319-77273-8_1, 2018.

Wong, K. C., Tailleux, R., and Gray, S. L.: The Computation of Reference State and APE Production by Diabatic Processes in an Idealized Tropical Cyclone: Reference State and APE Production in a Tropical Cyclone, Quarterly Journal of the Royal Meteorological Society, 142, 2646–2657, doi: 10.1002/qj.2854, 2016.

Wu, L., Su, H., Fovell, R. G., Dunkerton, T. J., Wang, Z., and Kahn, B. H.: Impact of Environmental Moisture on Tropical Cyclone Intensification, Atmospheric Chemistry and Physics, 15, 14 041–14 053, doi: 10.5194/acp-15-14041-2015, 2015.

Yang, D.: Boundary Layer Diabatic Processes, the Virtual Effect, and Convective Self-Aggregation, Journal of Advances in Modeling Earth Systems, 10, 2163–2176, doi: 10.1029/2017MS001261, 2018a.

Yang, D.: Boundary Layer Height and Buoyancy Determine the Horizontal Scale of Convective Self-Aggregation, Journal of the Atmospheric Sciences, 75, 469–478, doi: 10.1175/JAS-D-17-0150.1, 2018b.

Yang, D.: Convective Heating Leads to Self-Aggregation by Generating Available Potential Energy, Geophysical Research Letters, 46, 10 687–10 696, doi: 10.1029/2019GL083805, 2019.

Yang, D.: A Shallow-Water Model for Convective Self-Aggregation, Journal of the Atmospheric Sciences, 78, 571–582, doi: 10.1175/JAS-D-20-0031.1, 2021.

Yang, D. and Ingersoll, A. P.: Triggered Convection, Gravity Waves, and the MJO: A Shallow-Water Model, Journal of the Atmospheric Sciences, 70, 2476–2486, doi: 10.1175/JAS-D-12-0255.1, 2013.

Yang, D. and Ingersoll, A. P.: A Theory of the MJO Horizontal Scale, Geophysical Research Letters, 41, 1059–1064, doi: 10.1002/2013GL058542, 2014.

Yang, D. and Seidel, S. D.: The Incredible Lightness of Water Vapor, Journal of Climate, 33, 2841–2851, doi: 10.1175/JCLI-D-19-0260.1, 2020.

Yano, J.-I.: Basic Convective Element: Bubble or Plume? A Historical Review, Atmospheric Chemistry and Physics, 14, 7019–7030, doi: 10.5194/acp-14-7019-2014, 2014.

Zarzycki, C. M.: Sowing Storms: How Model Timestep Can Control Tropical Cyclone Frequency in a GCM, Journal of Advances in Modeling Earth Systems, 14, e2021MS002 791, doi: 10.1029/2021MS002791, 2022.

Zhao, M., Held, I. M., and Lin, S.-J.: Some Counterintuitive Dependencies of Tropical Cyclone Frequency on Parameters in a GCM, Journal of the Atmospheric Sciences, 69, 2272–2283, doi: 10.1175/JAS-D-11-0238.1, 2012.

Zhou, W., Held, I. M., and Garner, S. T.: Parameter Study of Tropical Cyclones in Rotating Radiative–Convective Equilibrium with Column Physics and Resolution of a 25-Km GCM, Journal of the Atmospheric Sciences, 71, 1058–1069, doi: 10.1175/JAS-D-13-0190.1, 2013.

Zhou, W., Held, I. M., and Garner, S. T.: Tropical Cyclones in Rotating Radiative–Convective Equilibrium with Coupled SST, Journal of the Atmospheric Sciences, 74, 879–892, doi: 10.1175/JAS-D-16-0195.1, 2017.